

DEVELOPMENT OF A SCREENING TOOL TO ASSESS THE FEASIBILITY OF
SOLAR-TO-STEAM APPLICATION FOR THE PURPOSE OF ENHANCED OIL
RECOVERY

A THESIS SUBMITTED TO
THE BOARD OF GRADUATE PROGRAMS
OF
MIDDLE EAST TECHNICAL UNIVERSITY, NORTHERN CYPRUS CAMPUS

BY
ALFRED EJIRO ABUKUBU

IN PARTIAL FULFILLMENT OF THE REQUIREMENTS
FOR
THE
DEGREE OF MASTER OF SCIENCE
IN
THE
SUSTAINABLE ENVIRONMENT AND ENERGY SYSTEMS PROGRAM

SEPTEMBER 2020

Approval of the Board of Graduate Program

Prof. Dr. Gürkan Karakaş

I certify that this thesis satisfies all the requirements as a thesis for the degree of Master of Science

Asst. Prof. Dr. Ceren İnce
Derogar
Program Coordinator

This is to certify that we have read this thesis and that in our opinion it is fully adequate, in scope and quality, as a thesis for the degree of Master of Science.

Asst. Prof. Dr. Onur Taylan

Supervisor

Assoc. Prof. Dr. Emre Artun

Co-Supervisor

Examining Committee Members:

Asst. Prof. Dr. Onur Taylan
Mechanical Engineering Dept., METU NCC

Assoc. Prof. Dr. Emre Artun
Petroleum and Natural Gas Engineering Dept., Istanbul Technical University

Asst. Prof. Dr. Doruk Alp
Petroleum and Natural Gas Engineering Dept., METU NCC

Assoc. Prof. Dr. Murat Fahrioglu
Electrical and Electronics Engineering Dept., METU NCC

Asst. Prof. Dr. Serhat Canbolat
Petroleum and Natural Gas Engineering Dept., Near East University

I hereby declare that all information in this document has been obtained and presented in accordance with academic rules and ethical conduct. I also declare that, as required by these rules and conduct, I have fully cited and referenced all material and results that are not original to this work.

Name, Last name:

Signature:

ABSTRACT

DEVELOPMENT OF A SCREENING TOOL TO ASSESS THE FEASIBILITY OF SOLAR-TO-STEAM APPLICATION FOR THE PURPOSE OF ENHANCED OIL RECOVERY

Abukubu, Alfred Ejiro
M.S., Sustainable Environment and Energy Systems
Supervisor: Assist. Prof. Dr. Onur Taylan
Co-Supervisor: Assoc. Prof. Dr. Emre Artun

SEPTEMBER 2020, 127 Pages

Enhanced oil recovery (EOR) involves the implementation of various techniques for increasing oil recovery, which typically involves injection of an agent that help to increase the oil flow. Steam injection is a common method to increase the recovery from heavy-oil reservoirs, which contain oil that has very high viscosity that may not be produced at economic rates due to inability to flow by viscous forces. Using concentrating solar power (CSP) as a renewable-energy system is one means to attain this objective, with a reduction in CO₂ emissions and fuel usage in generating steam, and could be at a lower cost than burning natural gas. The objective of this study to develop a coupled solar-energy/steam-injection forecasting tool to understand the impact of certain designs and natural parameters on the process. The study would use an existing data driven screening tool (artificial neural network), trained with numerical-simulation results, to optimize the steam-injection efficiency. Then solar-energy and steam-injection models, are going to be integrated so that both models can communicate. In the entirety of the project, economic indicators such as steam cost, capital investments for solar system would be reflected amongst other operational parameters to present a more realistic analysis. Finally, integrated models will be organized in a graphical-user-interface (GUI) input/output type application to convert the coupled models into a user-friendly screening tool, easy to use and understand by an investor or an engineer.

Keywords: Genetic Algorithm, Optimization, Cyclic steam injection, Enhanced oil recovery, Solar-steam

ÖZ

GELİŞTİRİLMİŞ PETROL ÇIKARMA AMACIYLA GÜNEŞ ENERJİSİYLE BUHAR ÜRETME UYGULAMASININ FİZİBİLİTESİNİ DEĞERLENDİRMEK İÇİN BİR TARAMA ARACININ GELİŞTİRİLMESİ

Abukubu, Alfred Ejiro
Yüksek Lisans, Sürdürülebilir Çevre ve Enerji Sistemleri
Tez Yöneticisi: Dr. Öğr. Üyesi Onur Taylan
Ortak Tez Yöneticisi: Doç. Dr. Emre Artun

Eylül 2020, 127 sayfa

Geliştirilmiş petrol çıkarma yöntemleri, çıkarılan petrolü arttırmak amacıyla genellikle bir sıvının enjeksiyonunu içeren birtakım teknikleri kapsar. Buhar enjeksiyonu, çok yüksek viskozite nedeniyle, basınç farklılığına bağlı akışkanlığı çok düşük olan ağır petrolerin üretimini arttırmada sıklıkla kullanılan bir tekniktir. Karbon dioksit emisyonunu ve yakıt harcamalarını düşürmeye yarayan ve buhar üretmede doğalgaz kullanımından daha az masraflı olabilen bir yenilenebilir enerji türü olan güneş enerjisi, bu amacı gerçekleştirmede kullanılan yollardan biridir. Bu çalışmanın amacı, belirli tasarım parametrelerinin ve doğal değişkenlerin etkisini anlamaya yarayacak bağlaşıklık bir güneş-enerjisi/buhar-enjeksiyonu tahmin aracı geliştirmektir. Daha önce geliştirilmiş olan yapay sinir ağları ve sayısal model sonuçlarıyla oluşturulmuş bir veri-bazlı araç, buhar enjeksiyonu tasarımını optimize etmek için kullanılacaktır. Daha sonra güneş enerjisi üretimi tahmin modeli ile optimum buhar enjeksiyonu tasarımları birleştirilecektir. Buhar üretme masrafları, yatırım masrafları gibi parametreler tasarım özelliklerine yansıtılarak daha gerçekçi bir analiz yapılması sağlanacaktır. Oluşturulan model, bir arayüz aracılığıyla bir mühendis veya yatırımcı tarafından kolay şekilde kullanılabilecek hale getirilecektir.

Anahtar Kelimeler: Genetik Algoritma, Optimizasyon, Döngüsel buhar enjeksiyonu, Geliştirilmiş yağ geri kazanımı, Güneş buharı.

To Peace, Love, Common Ground and my “Family”

ACKNOWLEDGMENTS

I want to express my earnest gratitude to Asst. Prof. Dr. Onur Taylan and guru Assoc. Prof. Dr. Emre Artun for their guidance, advice, encouragements, insight and hardly wavering patience and understanding throughout this study.

I would like to also show appreciation to METU NCC and METU family at large for presenting me with this opportunity.

My gratitude is also extended to Dr. Doruk Alp, Dr. Salam Al-Rbaewi, Dr. Ceren Ince and to my colleagues.

I would like to also show my utmost appreciation to Tiger Omang, Kaguz, Ollie, Barongo, Simba, Fadex, Bob Norn, Tuğçe Alabuğa and others for their support during this thesis research and making this Cyprus experience splendid. You are all greatly appreciated.

I would like say special thanks to my own ‘Avengers’ Chief Alex Ojigho Dedjo, Chief Mrs. Agnes Dedjo, My lovely Mum Clara Abukubu, Clarita, Hanujay, Bella, Fejiro ‘Marine’, Eneyo, Rona, Alex ‘Uncle’ AKP and the rest of my wonderful clan. You all are nothing if not special and thanks for making life wonderful.

Finally, I would like to thank and congratulate Myself for coming through.

TABLE OF CONTENTS

ABSTRACT.....	v
ÖZ	vii
ACKNOWLEDGMENTS	ix
TABLE OF CONTENTS.....	x
LIST OF TABLES.....	xii
LIST OF FIGURES.....	xiv
LIST OF SYMBOLS	xvii
LIST OF ABBREVIATIONS	xix
CHAPTERS	
1. INTRODUCTION.....	1
2. LITERATURE REVIEW	8
2.1 Steam Injection.....	8
2.1.1 Steam flooding.....	8
2.1.2 Cyclic Steam Injection.....	9
2.2 Steam Injection Generation Methods	11
2.3 Concentrating Solar Power (CSP) Systems	12
2.4 SAM Solar Direct Steam Generation Model	25
2.5 Solar-Steam Generation.....	28
2.6 Genetic Algorithm Optimization	33
2.6.1 Structure and Mechanisms of Genetic Algorithm	34
3. PROBLEM STATEMENT	40
4. METHODOLOGY	41
4.1 Screening Model for the Cyclic Steam Injection (CSI) Process (Yalgin 2018).....	42
4.2 Optimization Tool Development	43
4.3 SAM Solar Model	46
4.4 Optical Performance Analysis	51
4.5 Thermal Performance Analysis.....	52
4.6 Solar Field Design.....	54
4.7 Integration of Optimized CSI and Solar Models	58
4.8 Economic Analysis.....	59

5.	RESULTS AND DISCUSSION	63
5.1	Optimization Performance and Results	63
5.2	Solar Field Performance	71
5.3	Economic Analysis	80
5.4	Sustainability	84
5.5	Cyclic Solar Steam Injection (CSSI) Screening Tool	88
6.	CONCLUSION	91
7.	RECOMMENDATIONS FOR FUTURE WORK	93
	REFERENCES	94
	APPENDICES	103
A.	Receiver Geometry Calculation and CIAT and SPT Tables	103
B.	Genetic Algorithm Optimization Code	105
C.	Solar Input Generation Code	108
D.	SAM SIPH Function Code	113
E.	CSI-SAM Combination Code	122
F.	CSSI Graphical Schematic	124

LIST OF TABLES

TABLES

Table 2.1 Summary of major solar EOR projects	30
Table 4.1 Obtained reservoir properties of Amal and Ikiztepe fields.....	44
Table 4.2 Calculated reservoir data for both fields	45
Table 4.2 Average values of reservoir parameters for optimization	45
Table 4.4 Typical Meteorological Year data for a location	47
Table 4.5 Incidence angle modifier coefficients for Φ_T and Φ_L directions	52
Table 4.6 Coefficients for steam temperature adjustment heat loss polynomial	53
Table 4.7 Coefficients for wind velocity adjustment heat loss polynomial	53
Table 4.8 Power cycle inputs modifications to minimize power cycle influence over the solar model performance (Turchi and Neises 2015).....	56
Table 4.9 Design input parameters for Solar field design	57
Table 4.10 Constant values for saturation pressure simplified model.....	58
Table 4.11 Economic Parameters for NPV analysis	61
Table 5.1 Results from Population and Generation Trial for Year 2	64
Table 5.2 Results from Population and Generation Trial for Year 10	65
Table 5.3 Optimized CSI Steam design parameter for Amal field	70
Table 5.4 Optimized CSI Steam design parameter for Amal field	70
Table 5.5 Input Values for collector and field	72
Table 5.6 Solar fraction of steam from CSI-SOL combination test for Amal Field ...	80
Table 5.7 Yearly oil recovery from CSI-SOL and revenues for NPV analysis	81
Table 5.8 Depreciation values for NPV analysis	82
Table 5.9 Depletion values for NPV analysis	82
Table 5.10 Tax and net cash flow after-tax values for NPV analysis	83
Table 5.11 NPV analysis for major economic parameters	84

Table 5.12 10-year analysis for environmental externalities and considerations to feasibility analysis	86
Table 5.11 Tax and net cash flow after-tax values for NPV analysis considering ITC	87
Table A.1 Typical Solar position and CIAT Table (Section A)	104
Table A.2 Typical Solar position and CIAT Table (Section B)	104

LIST OF FIGURES

FIGURES

Figure 1.1 Classification of EOR Methods (Jenkins et al, 2019)	2
Figure 2.2 Injection of steam and Production of oil via Steam Flooding (Shah et al, 2010)	9
Figure 2.3 Operational stages of CSI procedure: injection, soaking, and production (Yalgin, 2018)	9
Figure 2.4 A cycle of CSI procedure with all stages and ERL (Yalgin, 2018)	10
Figure 2.5 Solar tower or central receiver system: Coalinga California (Brightsource, 2011)	13
Figure 2.6 Parabolic dish collector system. (Curry, 2005).	14
Figure 2.7 Parabolic trough collector system “Solar Thermal Technology” (ADB,2013).	15
Figure 2.8 Linear Fresnel reflector system “Concentrated Solar Power” (Anonymous,2015).	16
Figure 2.9 Illustration of LF and PTC shape likeness (Singh, 2017).....	17
Figure 2.10 Daily collector tracking motion routine (Weiss & Rommel, 2008)	18
Figure 2.11 Trapezoidal cavity receiver (Singh, 2017)	19
Figure 2.12 Evacuated tube receiver with secondary reflector (Rycroft, 2017)	19
Figure 2.13 Standard vacuum absorber tube schematic (Eck et al, 2010)	20
Figure 2.14 Compact linear Fresnel reflector design (Kalogirou, 2014)	20
Figure 2.15 Heat flux distribution of an absorber tube at different zenith angles (Eck et al 2007).....	22
Figure 2.16 Novatec Solar design longitudinal and transversal plane IAM curves (Wagner, 2012).....	27
Figure 2.17 Schematic an enclosed trough solar-steam EOR plant (GlassPoint, 2017)	29
Figure 2.18 Flow path of Genetic algorithm optimization	38
Figure 5.1 Optimized CSI Efficiency per population of 1,10,50,100,500,1000 and 10000	64
Figure 5.2 Year 2 Fitness Value Evaluation for a population size of 10 and Generation of 300	65

Figure 5.3 Year 2 Fitness Value Evaluation for a population size of 100 and Generation of 300	66
Figure 5.4 Year 10 Fitness Value Evaluation for a population size of 100 and Generation of 300	66
Figure 5.5 Economic rate limit CSI efficiency variation for Year 2-10	67
Figure 5.6 Steam injection CSI efficiency variation for Year 2-10	67
Figure 5.7 Steam temperature CSI efficiency variation for Year 2-10.....	68
Figure 5.8 Injection time CSI efficiency variation for Year 2-10	68
Figure 5.9 Soaking time CSI efficiency variation for Year 2-10	69
Figure 5.10 Steam CSI quality efficiency variation for Year 2-10	69
Figure 5.13 Annual daily steam temperature profile for IPH and DSLF models.....	73
Figure 5.14 Annual Profile of Thermal and Collector optical efficiencies for DSLF and collector efficiency for IPH model.....	73
Figure 5.15 Annual steam mass flowrate profile for DSLF and IPH model	74
Figure 5.16 Hourly wind (top) and field outlet temperature (bottom) for IPH model	74
Figure 5.17 Hourly wind (top) and field outlet temperature (bottom) for DSLF model	75
Figure 5.18 Hourly wind (top) and irradiance (bottom) for Both models	75
Figure 5.19 Hourly optical efficiency (red) and wind speed (blue) in the IPH model	76
Figure 5.20 IPH Thermal power produced (red) and losses (dark) for available irradiance	77
Figure 5.21 DSLF Thermal power produced (dark green) and losses (light green) for available irradiance	77
Figure 5.22 Annual output of the IPH model for different collector azimuth angles Left (-90, -45, 0, 45, 90) Right.....	78
Figure 5.23 Optical efficiency at different collector azimuth angles (-90, -45, 0, 45, 90) (red) collector angle = 0.....	79
Figure 5.24 Thermal loss performance of the IPH model for varying collector length, longest (red) and shortest (blue).....	79
Figure 5.26 Sensitivity analysis of NPV to major economic parameters	83
Figure A.1 compound parabola geometry	103
Figure F.1 Schematic map of the reservoir tab of the CSSI screening tool graphical user interface	124

Figure F.2 Schematic map of the solar tab of the CSSI screening tool graphical user interface.....	125
Figure F.3 Schematic map of the economics tab of the CSSI screening tool graphical user interface	126
Figure F.4 Layout and plot options of the CSSI screening tool graphical user interface plot tab	127

LIST OF SYMBOLS

a	Constant of saturation pressure	
A_{SF}	Solar field Area	m^2
b	Constant of saturation pressure	
c	Constant of saturation pressure	
d	Constant of saturation pressure	
e	Constant of saturation pressure	
eff	CSI Efficiency	STB/STB
f_{solar}	Solar fraction of steam	fraction
$f_{geometry}$	Geometry effects	
f_{hl}	Heat loss factor	fraction
$f_{opticalerr}$	Optical error.	
$f_{reflectivity}$	Mirror reflectivity	
$f_{soiling}$	Mirror soiling	
$f_{tracking}$	Tracking error	
i	Frequency of hours	
L	Denotes Lower bound	
$L_{collector}$	Length of collector module	m
n	number of CSI cycle	
n_{Loops}	Number of loops	
N_p	Cumulative oil recovered	STB
q'_{hl}	Total Heat loss	W/m
$q'_{hl,i}$	Heat loss per module section	W/m
q_{steam}	Steam mass flowrate	$bb1/hr$
$Q_{thermal}$	Thermal	
RNL_{SM1}	Required number of loops for SM = 1	
S_{inj}	Cumulative injected steam	STB
T	Temperature	$^{\circ}C$
T_{cr}	Critical Temperature	$^{\circ}C$

$T_{\text{field, in}}$	Field inlet temperature	°C
$T_{\text{field, out}}$	Field outlet temperature	°C
T_r	Reduced Temperature	
$T_{\text{sf, average}}$	Solar field average temperature	°C
T_{steam}	Steam temperature	
U	Denotes Upper bound	
V_{wind}	Wind speed	m/s
ΔT	Change in Temperature	°C
Greek Letters		
α_s	Solar altitude	(°)
γ_s	Solar azimuth	(°)
$\eta_{\text{loop, optical}}$	Loop Optical efficiency	
$\eta_{\text{loop, thermal}}$	Loop Thermal efficiency	
$\eta_{\text{loop, total}}$	Total loop efficiency	
$\eta_{\text{piping, thermal}}$	Piping Thermal efficiency	
θ_z	Solar zenith angle	(°)
Φ_L	Longitudinal incidence angle	
Φ_T	Transversal incidence angle	

LIST OF ABBREVIATIONS

CIAT	Collector incidence angle table	
CLFR	Compact linear Fresnel reflector	
DSLFR	Direct steam linear Fresnel	
IAM	Incidence angle modifier	(°)
IPH	Industrial process heating	
LFR	Linear Fresnel reflector	
PTC	Parabolic trough collector	
RNL	Required number of loops	
SM	Solar multiple	
SPT	Solar position table	
TRA	Total required area	m ²

CHAPTER 1

INTRODUCTION

Enhanced oil recovery (EOR also referred to as tertiary oil recovery) is the adoption of different techniques or methods for increasing the amount of extractable crude oil from an oil field. According to Faergestad (2016), global oil resources are valued between 9 to 13 trillion barrels. Heavy oil accounts for about 70% of said global oil resources (estimated at about 6.3 to 9.1 trillion barrels) 1.7 trillion barrels of global oil resources are counted as reserves as illustrated in the 2017 BP Statistical review (BP Report, 2017). Recovery of heavy oil and other resources has become looked-for, due to both the increase in energy demand and depletion of available of light oil resource. Light oil resources are characterized by a high API gravity and a low viscosity; much easier to extract. In contrast, heavy oil or natural bitumen is burdensome to extract and characterized by low API and high viscosity ranging from 20 to 10 API and 100 to 10,000 cp, respectively. Given its aforementioned characteristics of a high viscosity and low API, mobility of heavy oil is somewhat impaired in the reservoir and orthodox production procedures cannot be simply used. To overcome this challenge of mobility impairment, viscosity can be reduced by the utilization of enhanced oil recovery (EOR) or tertiary recovery techniques.

EOR practices can be either non-thermal or thermal procedures and are of three major techniques: chemical injection, gas injection and thermal recovery. Amongst the non-thermal methods, miscible flooding has shown remarkable success, however with limited applicability due to accessibility and costs of solvents on a commercial scale. While chemical methods may perhaps have been in the previous times uneconomical, these methods still hold promising prospects. Immiscible gas injection techniques such as CO₂ flooding have been more effective than others for heavy oil. For thermal methods, steam-based techniques have been commercially more successful. The method of choice is dependent on the attributes of the reservoir of

interest. Thermal EOR in particular is generally considered as the most pertinent technique for improving recovery of heavy oil which accounts for the bulk of today's remaining reserves. There are several thermal EOR techniques such as hot water flooding, in-situ combustion, steam flooding, steam assisted gravity drainage (SAGD) and cyclic steam injection (CSI). Figure 1.1 shows the classification of all EOR methods.

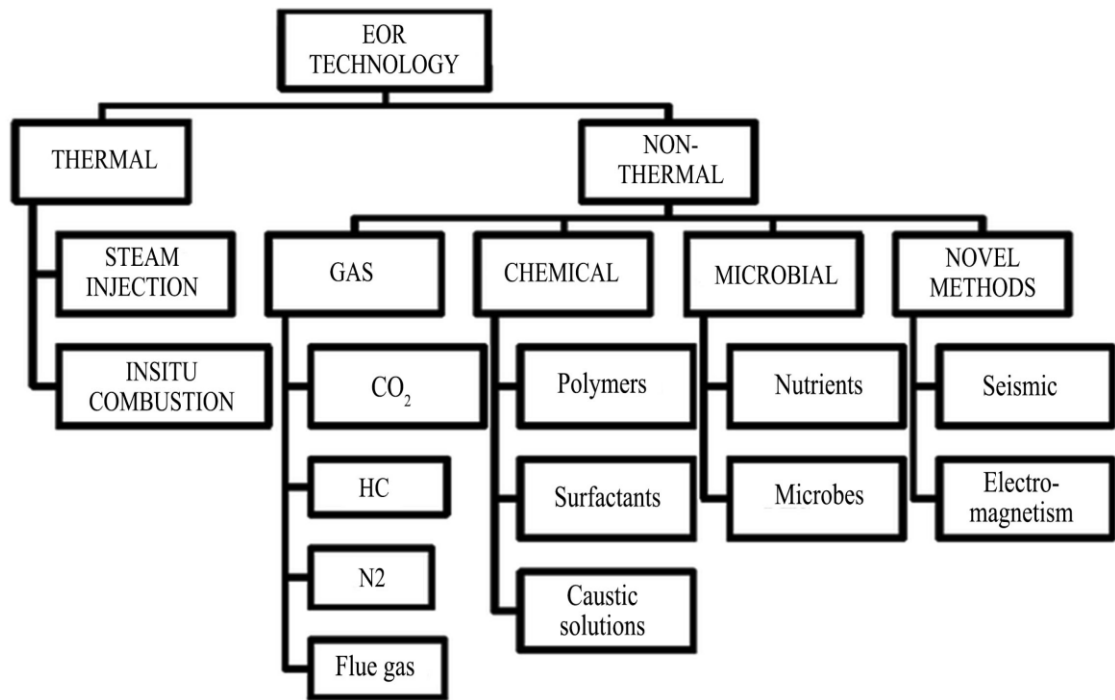


Figure 1.1 Classification of EOR Methods (Jenkins et al, 2019)

Steam injection is a very common technique to increase the heavy oil recovery; whereby injected steam thaws in oil, reducing the oil viscosity and consequently ameliorates the ability of the oil to flow and overall recovery. Over epochs, oil practices have necessitated using oil and natural gas for the heating of water to produce steam. In California, significant quantities of natural gas are burnt as per usage in thermal EOR. Burning natural gas in this day and age is becoming a very expensive source of energy around the world, in terms of energy demand, finance and as well as environment wise.

In the light of current global climate change challenge, there is an increasing global need for environmental sustainability by seeking alternative and renewable sources of energy beyond conventional fossil fuels. The utilization of renewable energy sources like wind, bio, hydro, solar, and geothermal energy is therefore pertinent in order to achieve sustainability goals globally. A gradual and assured way of using such resources whilst meeting the global energy demands is the inclusion via hybridization and innovation with current energy production schemes. One aspect where the possibility for such a technological undertaking presents itself is the steam generation for industrial processes with concentrating solar power systems (CSP). Photovoltaic (PV) cell tech might be well dominant in the solar power field; however, CSP creates a medium for the generation of steam at high temperatures for both electricity and industrial applications.

In addition, recent fluctuations in oil prices have negatively affected oilfield operations, mostly affected are oilfield operations requiring substantial investment. EOR operations suffer from such fluctuations, given its requirement for substantial investment for surface injection facilities and injection agents. Lower oil prices compel operating firms to reduce their associated costs of oilfield procedures and sometimes lead to the fostering of new technologies. As firms try to find new means to keep with the times and change of operations. Renewable energy offers a way of achieving such objective, by generating electricity or heat, at a lower cost than burning natural gas. A worthy example for this is on-site steam generation using solar energy, which has been either pilot tested or applied successfully in some fields around the world. In fact, there are a number of countries in different world regions which may be suitable for adoption of this application due to their favorable climate and heavy oil resources such as United States, Venezuela, Oman, Ecuador, Indonesia, Kuwait, Mexico, Colombia, Turkey, Angola, Madagascar, Chad.

Given the technology's somewhat infancy, there has not been any study conducted to develop a systematic methodology to identify whether a certain

geographic area would be a worthy candidate or not for such kind of a solar-to-steam application for the purpose of increasing heavy oil recovery. Although a number of studies focused on specific locations and assessed the lifecycle and feasibility, no study has been made which focuses on the screening and optimization aspects through a methodological framework. Therefore, this thesis intends to form a universal model applicable by practicing engineers to assess the feasibility of solar-to-steam application for the purpose of enhanced oil recovery in a practical manner. The model would require reservoir characteristics, steam injection design parameters and geographical solar-energy characteristics as inputs, and would output the expected efficiency in terms of a discounted efficiency parameter that takes into account income from additional oil recovery obtained and costs due to steam generation and steam injection.

This study aims to develop a tool that can provide guidance to investors and engineers to quickly assess the potential and feasibility of solar-to-steam applications for a heavy-oil reservoir in a given location. The tool involves a model optimized that uses a genetic algorithm (GA) to identify the optimum design parameters for cyclic steam injection (CSI): a thermal recovery method in which steam is injected into a well and subsequently placed back on production from the same well in cycles. The design parameters of interest include:

- Steam injection rate: This determines volume or rate at which steam is injected into the oil reservoir or formation. A key parameter in the injection process, higher injection rates reduces heat loss and spurs recovery (Yen et al, 1989). A steam injection rate range of (500-2000) bbl/d is used in this study.
- Steam injection time: This indicates the total time or period of steam injection per cycle for a CSI procedure prior to the soaking period, ranging from several days to weeks. An injection time range of (10-60) days is used in this study.
- Steam temperature: Is the temperature at which steam is injected; and has a reciprocal effect on the oil viscosity and mobility. Steam

temperature is related to pressure via the equation of state; higher temperature and pressure at constant injection rate and quality results in a higher recovery and water production (Ali et al, 2015). This can be set high enough to allow for good heat transfer between oil-steam and reduce the viscosity, steam temperature range of 450-700 °F is adopted in this study.

- Steam quality: The amount of the injected steam in the gas phase denoted either in fraction (0-1) or percentage (0-100%). The higher the value the higher amount of vapor content of the steam. Generally, slightly wet quality steam (<100%) is preferred for both steady temperature control and reduce scale deposition (De Leon et al, 1979). A steam quality range of (70%-100%) is set for this study.
- Soaking time: This determines the time period for which the well is shut in ranging from several days to weeks to allow even heat circulation for thinning the oil. Soaking time range of (10-30) days is used in this study.
- Economic rate limit: This indicates the minimum profitable production rate after the production phase is begun before the well is shut to restart a new cycle of the CSI procedure. In essence, it denotes the least acceptable rate of economic feasibility before restarting the process. A range of (5-25) bbl/d is used for the economic rate limit in this study

The CSI model was created and trained in an earlier study using an artificial neural network that is used to forecast process performance depending on the steam-injection design parameters such as; steam injection rate, injected steam temperature, steam quality, durations of steam injection and soaking, and economic rate limit. A solar model is built to estimate steam and heat generation of a system, by inputting weather conditions, ambient temperature, etc. using National Renewable Energy Laboratory, System Advisor Model software (NREL, SAM). SAM is a modeling software for techno-economic analysis that can be used to facilitate decision-making in regards to modeling renewable energy systems. Amongst its modeling options are Solar photovoltaics (PV), concentrated solar power (CSP), industrial process

heat for parabolic and linear Fresnel system, solar heating, geothermal power generation, etc.

SAM offers linear Fresnel reflector (LFR) modeling for steam flow configuration options of either recirculated (RC) or once-through (OT) steam flow in the solar field. Mostly used in current steam generator designs is the RC boiler designs, the water and steam exit the boiler section as a two-phase mixture. Steam quality is regulated at the desired value with a recirculation pump by varying the mass flow of dry steam. At the boiler outlet, dry steam is separated from the saturated liquid, the latter is returned to the boiler inlet and the dry steam is sent on to the super-heater or turbine sections. The main benefit of the RC flow configuration is the ability to maintain stable heat transfer from the absorber to the fluid, this prevents burn-out or local overheating. However, it requires a recirculation pump, separation equipment, and return piping presenting extra costs and parasitic consumption. An alternative design is the once-through, which heats water from a sub-cooled liquid state to a superheated steam phase with a single loop pass. Mass flow can be varied to meet the required outlet steam temperature. Eliminates the need for steam separation and transport equipment presenting no extra costs and parasitic consumption. However, the prospects of flow and heat transfer instabilities as well as control complexities are a possibility (Wagner and Zhu 2014).

Coupling this capability to model CSP with an optimized CSI steam model is the main focus of this study. An estimate is to be made whether the solar characteristics of given location of interest can lead to an efficient steam-generation plan for the coupled solar-energy model and a CSI data-driven forecasting tool. A graphical user interface is to be made available to provide guidance to users as forecasting/screening tool, and quickly assess potential and feasibility then makes a recommendation of utilizing this process in a given area. Through a number of economic input parameters, the tool can also output an expected net present value of a certain design scheme to quantify its feasibility. In addition, externalities of other aspects of feasibility is briefly incorporated with a feasibility analysis inclusive of the

environmental externalities and how incentives for environmental friendly energy sources and specifically adoption of solar-steam in thermal EOR can help improve feasibility of such projects and improve both climate and energy sustainability towards GHG emission reduction.

The primary target end-users of this tool is:

- 1) Employees of companies (engineers and geologists) who operate in oil fields where heavy oil is produced (in regions where this project may be feasible such as South-Eastern Turkey, Middle East, California/USA, some countries in South America and Africa).
- 2) Investors (solar-panel producers and solar-energy providers), who would like to propose the use of solar energy to efficiently produce heavy oil.

This thesis is organized into

- Chapter 2, gives a literature survey of steam injection, solar thermal systems solar-steam injection, and applications of genetic algorithm optimization.
- Chapter 3, explains the statement of the problem and workflow.
- Chapter 4 illustrates the principles of the genetic algorithm optimization process its structure and development of the optimization model, the construction of the solar system and integration of the optimized CSI model and solar model.
- Chapter 5, results of the optimization model, technical feasibility of the optimized designed parameters and solar model, and an economic assessment of the solar-CSI procedure is presented. The graphical user interface (GUI) application is also presented.

Chapter 6, gives a brief summary and key conclusions.

CHAPTER 2

LITERATURE REVIEW

2.1 Steam Injection

The benefits of steam injection into oil wells to boost petroleum production was first advocated in 1917 (Ali 1974). Extensive field tests for this practice began in the late 1950s with increased consideration in the early 1960s after Shell Oil Company's success with cyclic steam injection in California (Ali 1974). California oil fields have for long favored steam injection EOR methods, given their favorable reservoir and petroleum characteristics with the procedure applied to the majority of oil wells at least once (De Leon et al., 1979). Steam injection methods are generally of two main types: Steam flooding and Cyclic Steam Injection (CSI).

2.1.1 Steam flooding

Steam generated is injected into the reservoir by specially located injection wells and oil is produced from another well. Also referred to as steam drive or continuous steam injection; it employs two mechanisms to improve oil recovery. First, the oil is heated to higher temperatures to initiate a decrease in viscosity, aiding its flow towards the producing wells. The second mechanism is the physical displacement, as condensed hot water from the steam and the steam itself generate an artificial drive. Employing a behavior in resemblance to water flooding, that pushes oil towards the production wells. In addition, steam lessens the interfacial tension between paraffin and asphaltenes and rock surfaces during the steam distillation of crude oil light ends creating a small miscible solvent bank able to remove trapped oil and enhances oil production via this near-wellbore cleanup factor during the injection.

Fig 2.1 illustrates steam flooding with injection and production wells.

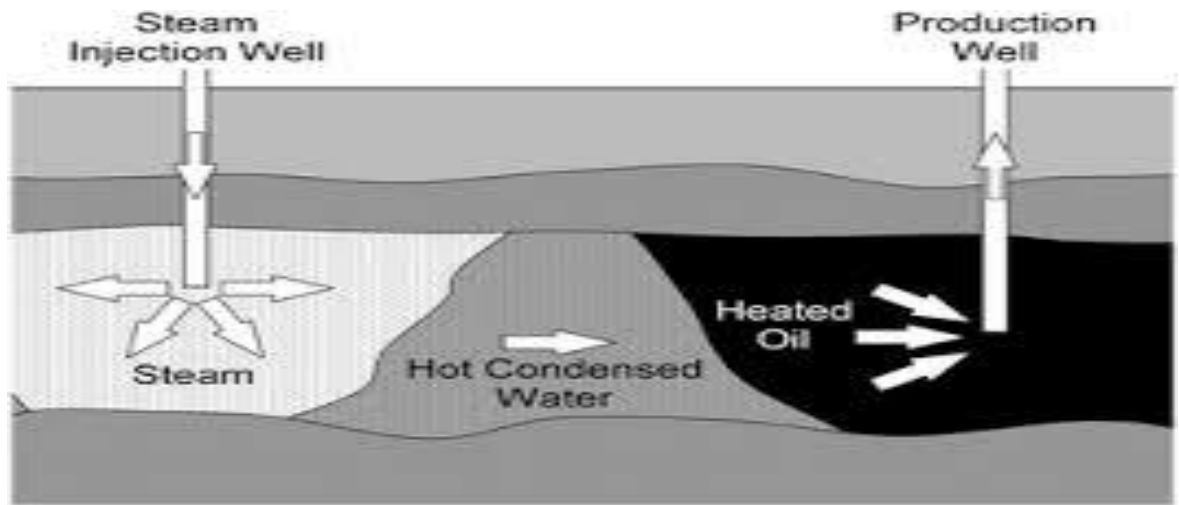


Figure 2.2 Injection of steam and Production of oil via Steam Flooding (Shah et al, 2010)

2.1.2 Cyclic Steam Injection

Correspondingly referred to as cyclic steam stimulation (CSS) or “huff and puff” steam injection. It’s a solitary well technique for heavy oil reservoirs, where a well is used for both injection and production. The objective is to increase the temperature around the wellbore with the steam energy and whilst decreasing heavy oil viscosity. There are three stages of operation in a cyclic process: injection, soaking, and production as shown in Figure 2.2.

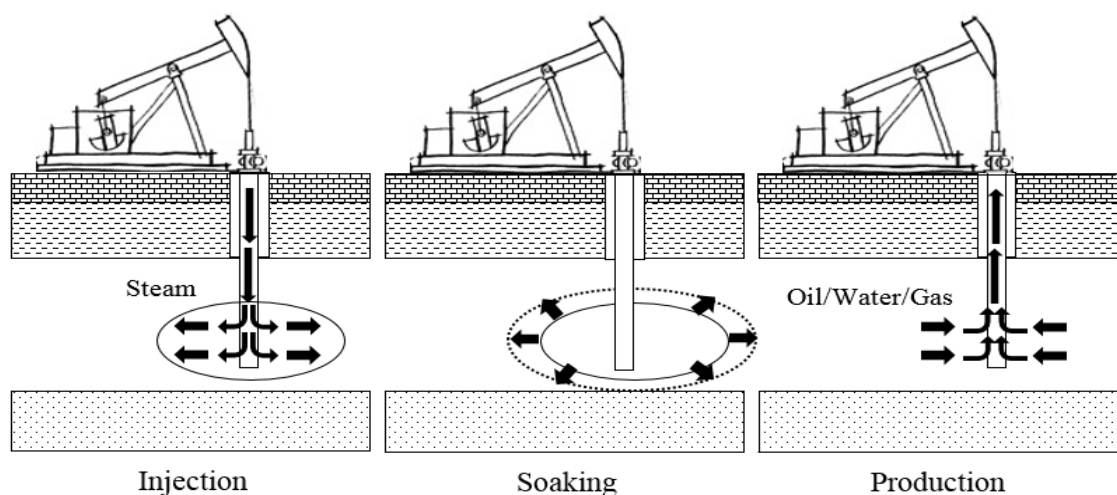


Figure 2.3 Operational stages of CSI procedure: injection, soaking, and production (Yalgin, 2018)

Injection Stage: As the name suggests, steam is injected into the reservoir to increase the reservoir temperature. Dependent on reservoir conditions, this stage generally lasts for a period of 3 to 4 weeks (Arpaci,2014).

Soaking Stage: When the injection stage is finished, the injected well is shut-in to allow steam diffusion into the formation. During this steam diffusion process, reservoir temperature increases, and consequently oil viscosity decreases. Also dependent on reservoir conditions, the duration of the soaking is generally between 2 to 3 weeks (Arpaci,2014). It is vital to select just the right suitable duration for this stage because too short a duration would lead to premature procedure and formation is not heated. However, too long a duration begets heat lost and the reservoir cools down again.

Production Stage: Upon achieving the desired viscosity, the well is placed back on production until the economic rate limit (ERL) for the procedure is reached. At which point the well is shut-in and the next cycles of injection-soaking-production are repeated until the least achievable feasible rates. Hence the name of the procedure cyclic steam injection (CSI). Figure 2.3 illustrates the cycle of a CSI procedure.

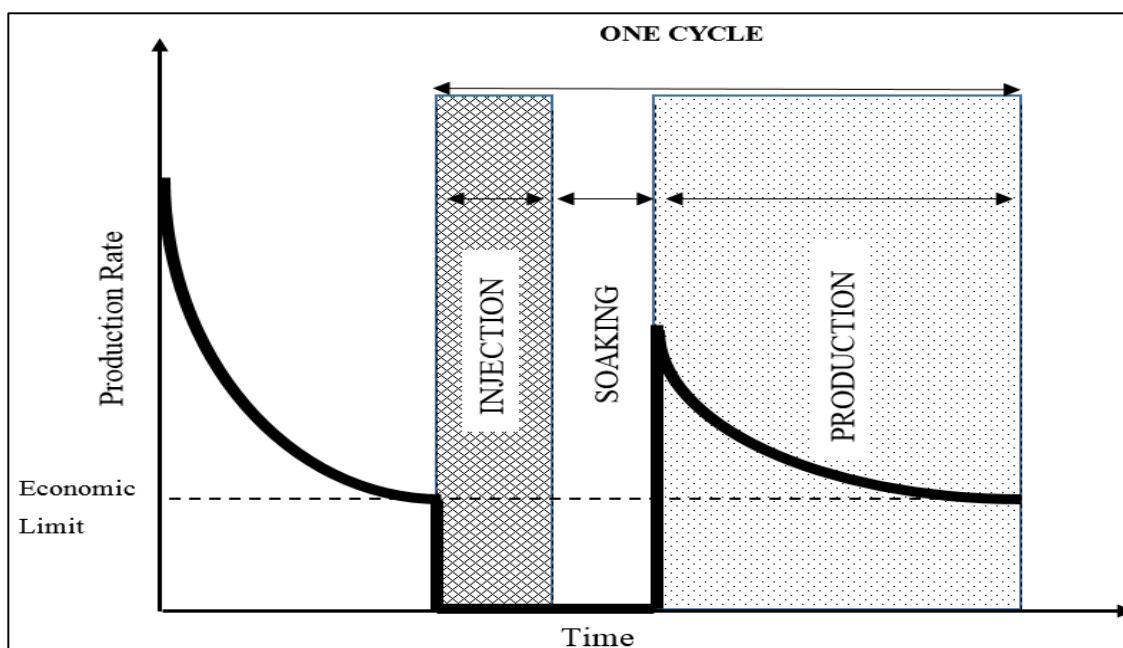


Figure 2.4 A cycle of CSI procedure with all stages and ERL (Yalgin, 2018)

It is recommended to start the next cycle when the oil rate is about one-third of the rate at the beginning of the cycle, so the pressure and rate are high enough to maintain good performance of the subsequent cycles (Sheng,2013). The number of steam stimulation cycles recommended for economical and effective is 6-7 and a maximum of 10 cycles (Liu, 1997). Oil rates peak in the second and third cycles, with sharp decrease during the fourth to sixth cycles and decreases slowly in the seventh cycle (Sheng,2013).

2.2 Steam Injection Generation Methods

For steam-injection operations in the oil field, there are typically three options for steam generation methods that can be considered (Chaar et al. 2015) namely:

Fuel-fired once-through steam generator (boiler)¹, Cogeneration using a power plant via a once-through heat-recovery steam generator ² and Solar steam generator by using concentrating solar power ³. Option 1 is operationally the most flexible and controllable option, also it involves low capital cost per ton of steam production and short construction time. However, it uses the direct burning of fuel to generate steam and heavily dependent on fuel costs. Option 2, uses “waste heat” via high-temperature flue gas released from a gas turbine to produce steam via a once-through heat-recovery steam generator. It also bodes a low capital cost per ton of steam production as well as increased system efficiency, especially for simple cycle power plants. This option, however, is linked directly to power generation, indirectly consumes natural gas, and involves a duct burning required to balance electrical and thermal energy that itself is dependent on fuel price. Option 3, been the option of interest uses mirrors to concentrate and harness the sun’s energy for the production of steam. While this option is capital intensive and dependent on location weather, it requires no fuel consumption and as results in far much-reduced greenhouse gas (GHG) emissions. It also presents an extendable field life.

Each of these options has different advantages and disadvantages with regard to its efficiency and cost that might favor its selection. For example, while

solar-energy requires a major CapEx, the reduction in both CO₂ emissions and fuel usage may favor this generation method. Though, solar radiation characteristics of a region or location are quite central to sustain steam capacity required for the reservoir under consideration.

2.3 Concentrating Solar Power (CSP) Systems

In the solar steam generation system, CSP systems capture suns energy and heat flowing water to produce steam for the injection procedure. The CSP systems used in steam or high-temperature applications are generally classified into line focusing and point focusing includes:

Solar tower: This point focusing system consists of a large number of huge dual-axis sun-tracking mirrors (heliostats) track the sun and absorbed by a central receiver on a tower. Focused sunlight heats a heat transfer fluid in the receiver, which itself heats the flowing feed-water to produce steam. This can steam can be used for needed industrial purposes or electricity generation. Solar tower systems can attain higher temperatures with high capacity factors, and very high concentration factors (IRENA Report, 2017). Operating temperatures up to 1000°C and high efficiencies are achievable and required very high investment costs (IRENA Report, 2017). Figure 2.5 shows a picture of a solar tower system.



Figure 2.5 Solar tower or central receiver system: Coalinga California
(Brightsource, 2011)

Parabolic dish collector: The dish engine is also a point focusing system which concentrates light onto a receiver positioned at the reflector focal point using a stand-alone parabolic-shaped reflector. The reflector using a dual-axis tracking system to track the Sun's motion. Unlike other CSP systems that use steam turbines for electricity generation, Dish collectors use a working fluid in a heat engine and are heated for power conversion (Buck et al., 2002). Operating temperatures up to 700°C is achievable. Figure 2.6 shows a picture of a parabolic dish collector system.



Figure 2.6 Parabolic dish collector system. (Curry, 2005).

Parabolic trough collector (PTC): This is a line focusing system that consists of linear trough-shaped reflectors, a receiver tube mounted along the reflectors focal line; to which light is concentrated. The receiver tube contains heat transfer fluid heated by concentrated solar energy and uses heat exchangers to produce superheated steam. The tracking system is along either the north-south or the east-west axis since the system is a single-axis tracking system. Operating temperatures of about 400°C are attainable. Figure 2.7 shows a schematic sketch of a parabolic trough collector system with the main part labeled.

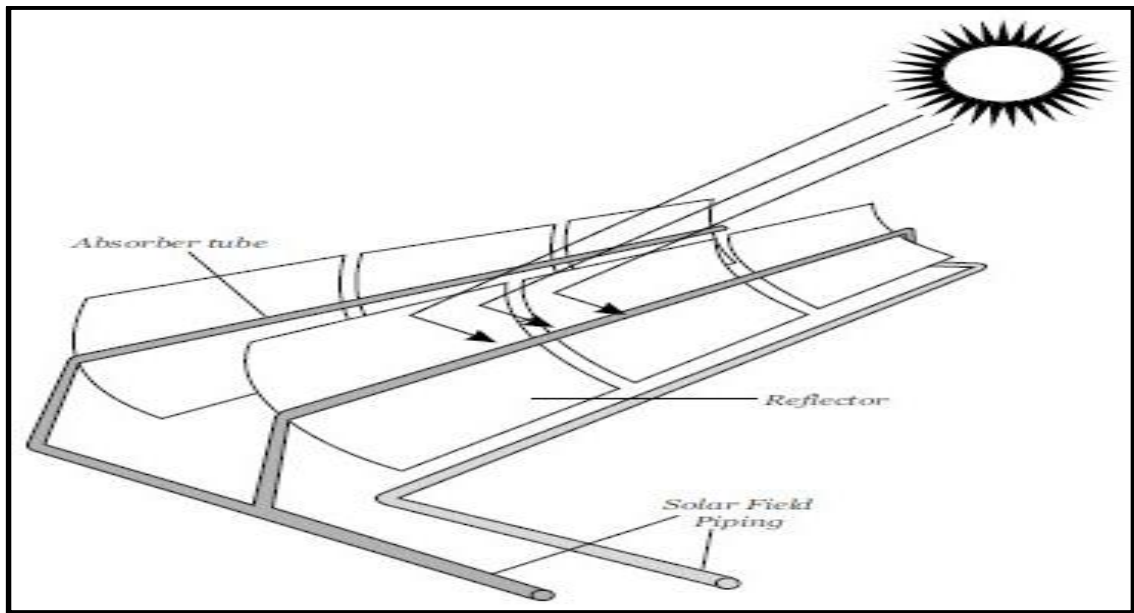


Figure 2.7 Parabolic trough collector system “Solar Thermal Technology” (ADB,2013).

Linear Fresnel Reflector (LFR): Named after the lighthouse Fresnel lens, developed by French physicist Augustin-Jean Fresnel. Linear Fresnel reflector (LFR) similar to parabolic trough as a line focusing system, but uses long, thin segments of flat or curved mirror strips mirrors to focus sunlight unto a fixed absorber located along a common elevated focal point of the reflectors. The absorber is fundamentally a set of parallel high-pressure steam pipes with water pumped in at one end; the water boils as it moves along the hot pipes, heated by the concentrated solar radiation focused on pipes. This enables the generation of steam at high pressures for power generation and industrial steam applications. Figure 2.8 shows a schematic photograph of a linear Fresnel reflector system with the main part labeled. Every line of mirrors is fitted with a single-axis tracking system and optimized to ensure sunlight concentration on the fixed receiver at all times (IRENA Report, 2017). The fixed nature of its receiver LF systems have fewer moving parts, providing a reduced need for steel and cement for reinforcement materials. In addition, a higher mirror surface per unit receiver and easier mass production of mirrors give an easier applicability and consequently cutting LF system costs. LF systems are suitable in locations with restricted

land availability, high wind loads, dual purposes such as simultaneously providing energy for heat or electricity generation and providing shade for farm animals, and parking space (Singh, 2017).



Figure 2.8 Linear Fresnel reflector system “Concentrated Solar Power”
(Anonymous,2015).

LFR mirror strips to mimic the parabolic (PTC) shape as illustrated in Figure 2.9. LF reflectors typically consist of several main components: mirrors (reflectors), receiver (absorber), and a tracking system; all of which are briefly explained. Also, depending on if used for electricity generation purposes a power block system is included to convert thermal energy.

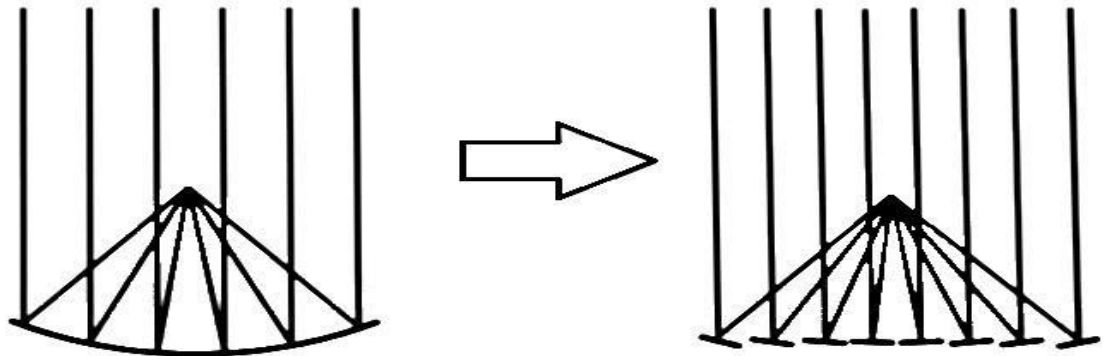


Figure 2.9 Illustration of LF and PTC shape likeness (Singh, 2017)

Reflectors: These are either flat or slightly curved glass mirrors with highly reflective capabilities. Curvature is added to increase the mirror concentration ratio and simpler receiver design and size (Galindo et al, 2019). Mirrors are aided a corrugated sheet with a special glue that provides mirrors support and prevent reflective paint from damages due to weather conditions (Singh, 2017). Then mounted to a galvanized iron tracking enabled truss framework.

Tracking System: Tracking system rotates and defocus mirrors to concentrate maximum solar radiation, control during extreme radiation, maintenance, or emergencies (Kalogirou, 2014). Restoration to initial position at the end of operational hours. The tracking mechanism are of two types dual-axis or single-axis. The former tracks the sun using altitude and azimuth but holds better tracking efficiency and higher costs. But the single-axis method tracks the sun in either latitudinal or longitudinal directions depending on the orientation of the reflectors. Both mechanisms are controlled either mechanically or preferably electronically. Where the latter, uses sensors and motors to measure solar radiation and turn mirrors or computer-controlled system connected to solar flux sensors on receivers. Figure 2.10 depicts a daily collector tracking motion

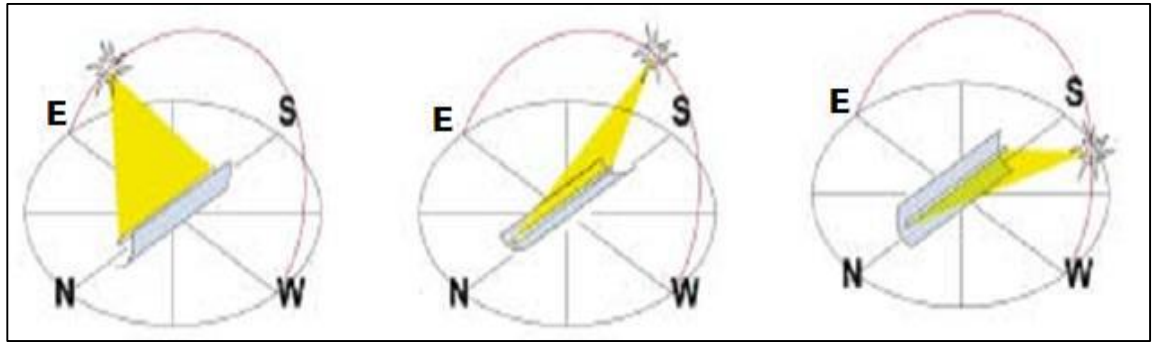


Figure 2.10 Daily collector tracking motion routine (Weiss & Rommel, 2008)

Receivers: As suggested by its name receives or absorbs the reflect solar energy. Consists of an insulated cover, an absorber tube, and support frameworks. Today several receiver types are commercially available such as evacuated linear receivers with lesser heat loss, good performance at high temperatures; however, weathering influences and unfavorable climatic conditions reduce performance severely (Kalogirou, 2014). Evacuated tube receivers have a secondary reflector that to mitigates the unavoidable optical inaccuracy of the Fresnel mirrors to improve optical efficiency; it is formed by the intersection of parabolas. Singh (2017) defined parabola shape for max concentration ratio for a receiver with radius r and a half acceptance angle θ_c using findings by Kalogirou (2014). Showed that the profile generated is an elongated parabola which is uneconomical and as such the profile is slightly truncated at its ends. Flatter-shaped secondary reflectors usage has been suggested for performance improvement, but studies show reduced manufacturing and maintenance costs from the use of large absorbers with evacuated tube replacing secondary reflectors (Wagner et al 2014). These equations can be seen in Appendix A. Non-evacuated absorber tubes trapezoidal cavity receivers with larger absorber surface areas have a high heat loss capacity and best suitable for processes with low-temperature requirements (180-300°C) (Morin et al 2012). Figures 2.11 and 2.12 respectively illustrate an evacuated tube receiver and a trapezoidal cavity receiver. The stainless steel tube absorber has a selective coating of high absorbance and low emittance capacities. Absorbers have a casing of insulating materials (glass wool), steel supports for wind loads, and vacuum

cover (envelope) that reduces heat losses. The typical absorber schematic is depicted in Figure 2.13

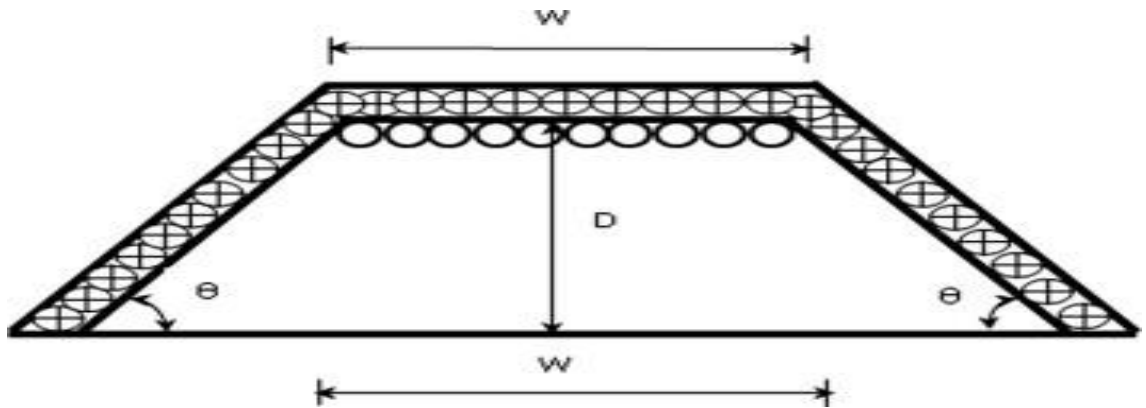


Figure 2.11 Trapezoidal cavity receiver (Singh, 2017)

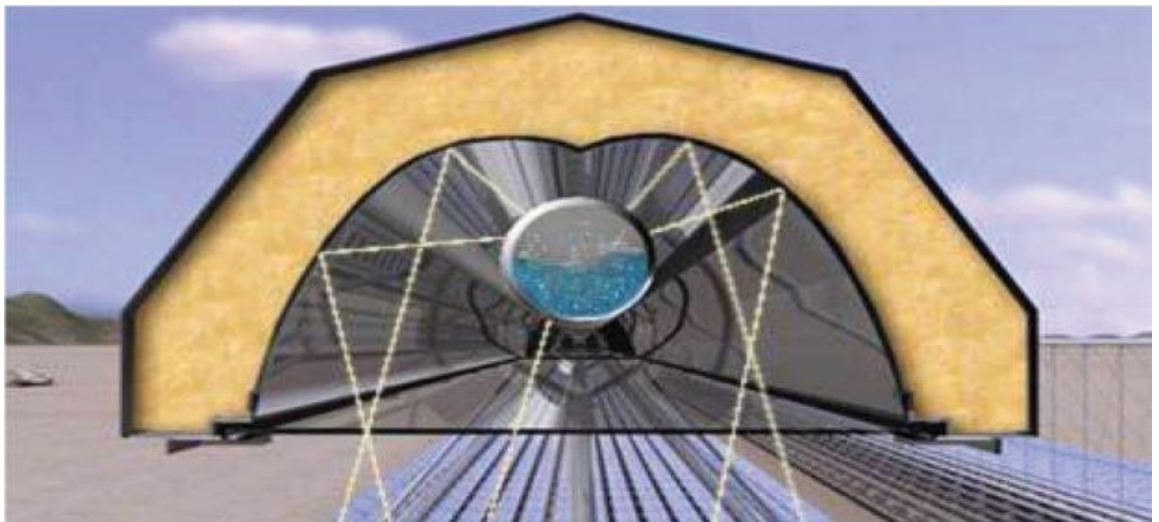


Figure 2.12 Evacuated tube receiver with secondary reflector (Rycroft, 2017)

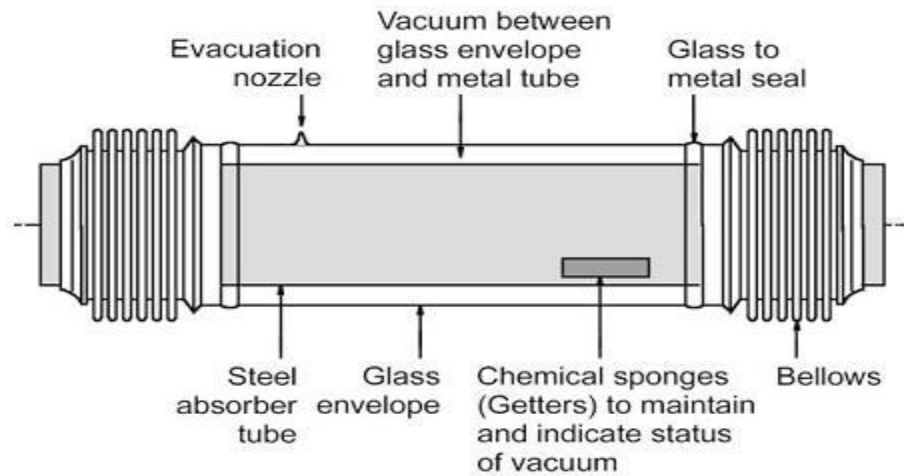


Figure 2.13 Standard vacuum absorber tube schematic (Eck et al, 2010)

A variation of LFR to combat efficiency losses and increased spacing resulting in shading and blocking between adjacent mirrors is the Compact Linear Fresnel reflector (CLFR). The adjacent elements are closely interleaved to avoid shading and oriented to direct radiation to at least two towers. This enables high reflector densities, low receiver height, lesser land use, and cost. Suitable for projects located with land availability restrictions. A typical CLFR design is shown in Figure 2.14.

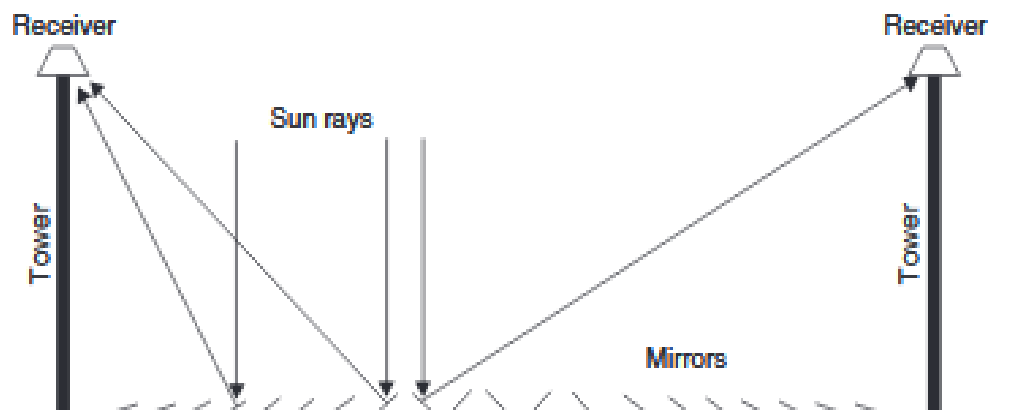


Figure 2.14 Compact linear Fresnel reflector design (Kalogirou, 2014)

CSP systems operate using either of two fluid systems; heat transfer fluid (synthetic oils) or direct steam generation (DSG) for heating water directly by a solar system to generate steam. This has been applied in both electricity

generation and solar industrial process heat applications. With the latter presenting a large avenue for DSG innovations and technologies. A major plus of this method is that DSG reduces cost by eliminating, the need for heat exchangers and heat transfer fluid. Direct steam generation with LFR are of several examples the Novatec, Supernova plant (Mertins, et al. 2011) and Areva Solar (Morin et al, 2011). High temperatures and pressures are required to attain the needed steam, LFRs are easier to obtain high pressures than PTC due to the fixed nature of piping. However, pressures drop might be faced due to the long length of plants over long distances. Eck et al (2007) determine optimum lengths of preheater, evaporator, and superheater sections with estimated pressure drop. To reduce pressure drop, total length required can be partitioned into parallel lines segments for every section. Pye (2008) states that a two-phase heat transfer inside the absorber tubes improves heat transfer and reduces solar field heat loss given the removal of heat exchangers. To obtain high temperatures accurate tracking, curved mirrors, and secondary reflectors are recommended to improve flux distribution or concentration of solar radiation. This can be problematic in the superheater section where thermal stress might be induced as the steam has a lesser heat transfer in this section causing unbalanced heating between lower and upper parts of the absorber tube (Eck et al, 2007). As illustrated by the flux distribution in Figure 2.15. Thence, Eck et al (2007) recommends absorber temperatures not greater than 500°C or defocusing mirrors to avoid degradation. In this study, DSG-LFR is used for modeling a solar steam generation system. With the study more inclined towards saturated steam so this issue presents minimal cause for concern in the system's design.

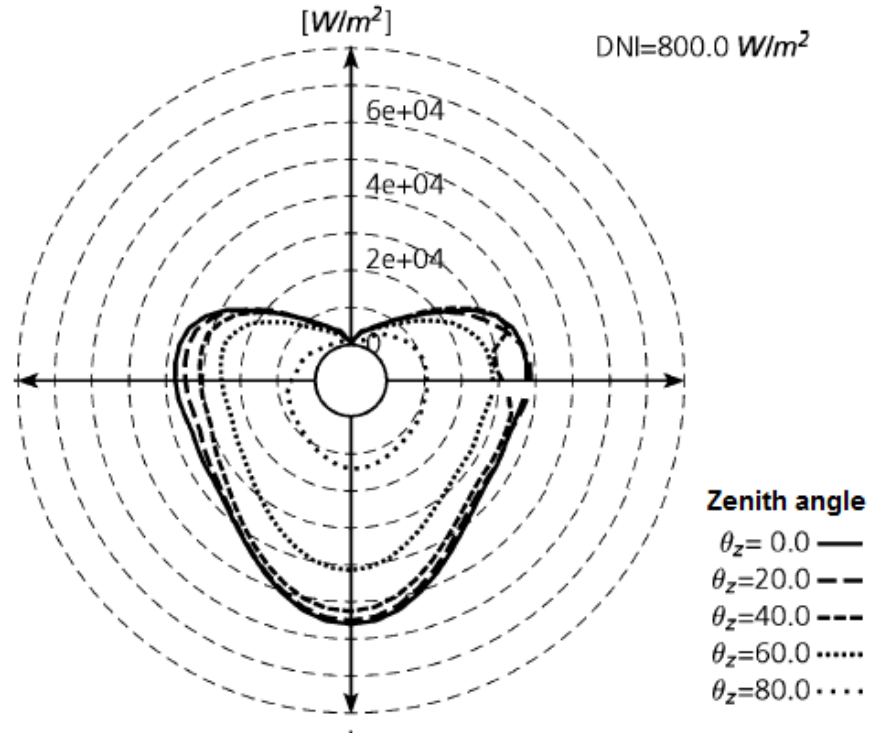


Figure 2.15 Heat flux distribution of an absorber tube at different zenith angles (Eck et al 2007)

A feasibility study to evaluate the total efficiency of a power plant with direct steam generation and energy storage by means of a steam accumulator, and compare it to the efficiency of the same plant with an organic Rankine cycle (Schlaifer 2012). Singh et al. (1999) studied the overall efficiency of an optimized LFR design with simulation developed for an LFR model using a variable number of mirror stripes. They evaluated an LFR system using 10, 15, and 20 mirrors reflectors. Results indicated a decrease in overall collector efficiency with an increase of reflective surface. The study also estimates s optimum mirror number in the range of 10-15 at an optimum width between 10 and 12 cm.

Badia et al (2013) design and test a method to assess the optical quality of solar concentrators. Huang et al. (2014) performed an optical study of an LF reflector azimuth tracking with an analytical model and SolTrace ray-tracing software. The model estimated an LFR overall efficiency of 61%, greater than

PTC working at similar conditions. In addition, it was observed that as height was increased, so did shading and blocking effects, and receiver width significantly affected heat loss. While Song et al (2015) established a mathematical model to compute optical losses (cosine, end, blocking, and shading losses), that was used to study the effect of design parameters such as receiver height, reflectors width, and row gap. The study indicated that increasing row spacing decreases shading, and wider sized mirrors cause higher shading and blocking effect which lessens optical efficiency. It also stated that for receiver heights below 3m., losses due to receiver's shadow were substantial; and thus, recommended heights above 3m.

Chemisana et al. (2013) used an absorber reflection method in designing and testing a method to measure the optical quality of solar concentrators and validated by the dual-axis LFR system. Showed that several factors ranging from bending, twisting, sagging and stresses affect optical quality. Performance analysis of an LFR prototype with ray-tracing model on both flat and curved mirrors using a multi-tube trapezoidal cavity receiver determined that slightly curved reflectors give about four times higher concentration ratios than flat mirrors (Abbas et al. 2013).

Mills and Morrison (2000) presented a study investigating LFR configurations with an evacuated tube receiver assembly comparable to receivers used in solar hot water applications. Although, limited to Mills & Morrison receivers and solar field configurations. Results from this study apply to systems with only boilers operations and no option for superheating. And included in the *TRNAus* library; for use with LFR systems in TRNSYS simulator for solar hot water (Wagner 2012). A study examined receiver thermal performance dependency on solar radiation using a simple heat model of the carrier fluid temperature at the collector outlet. The study showed similar concentration efficiencies achieved by the LFR and the PTC systems until a threshold temperature of the carrier fluid. To add with, heat carrier fluid flow in series by receiver tubes, comparatively high thermal efficiencies are achievable (Abbas et al 2012). (Goswami, et al 1990, Reynolds 2004, Pye 2008, Facao

et al 2009, Abbas et al 2012, Flores-Larsen et al 2012) developed concentrators and receiver performance prediction models. These studies established the thermal performance of LF receivers and collectors.

Patil et al. (2014) used CFD to design optimization of a non-evacuated receiver. Considering the non-uniformity temperature distribution, defined by sinusoidal and square wave functions. Results show both functions simulated lesser heat losses for a non-evacuated receiver with a non-uniform temperature distribution than uniform temperature distributions. In addition, an increase in heat losses with an hour angle increase for a fixed absorber temperature and increasing non-uniformity observed. Thus, a collector design to facilitate a large concentration of radiation at the receiver bottom is suggested. Another numerical study by Patil et al (2014) on non-evacuated receiver heat loss to define its temperature and flux distribution. Results exhibited an inverse reciprocation of different heat losses as convection heat losses increased for wind velocity change from 0 to 10 m/s by 140%, but a 71% decline in radiation losses. Therefore, the total heat loss increase was less considerable to convection losses. Also, the heat loss difference of 1.5% between uniform and non-uniform temperature distributions was estimated.

Several comparison studies have been done on the performance of Linear Fresnel and other CSP technologies using annual energy production codes (Haberle et al. 2002, Gharbi et al. 2011, Giostri et al. 2011, Morin et al. 2011). Montes et al, 2012 performed a comparison study between (LFR) and compact linear Fresnel reflector (CLFR). With results showing a decrease in losses due to shading and blocking in CLFRs but reduced incident radiation on the receiver and reduced overall efficiency in comparison to LFR. This is a result of beam spread as mirrors are positioned farther away from the receiver in CLFR. Another comparative study by Abbas et al (2016) on the optical performance of LFR and PTC systems. Used two receiver types (multi-tube receiver and a secondary reflector receiver). The study settles that a North-

South orientation to be most efficient for PTC, but performance was similar in both orientations for LFR.

Walker (2013) showed the capability for LFR to replace existing thermal sources in regards to process heat and power generation. Ray-trace simulation models used to analyze optical performance to make a sensitivity analysis for parameters like receiver width and height, number of mirrors, and mirror gaps. Several modeling and simulation environments (TRNSYS, Thermoflex, and Octave) have been used to predict the performance DSG solar power plant. This study enables a user to select the best amongst the lot. From this study, TRNSYS is considered the most suitable for dealing with transient periods of radiation studies that have been done for heat loss, optical, solar concentration (Ravelli et al. 2016).

Forristall (2008) did a comprehensive thermal study of an evacuated tube receiver using one and two-dimensional heat transfer models. Comparisons with laboratory test results showed excellent results between theoretical and experimental surface temperatures. In another study by Burkholder and Kutscher (2008) experimentally tested two Schott PTR70 receivers to estimate heat loss for temperature ranges between 100°C and 500°C. Results were found to give similar estimates as a one-dimensional heat loss model. Heat loss correlations of both studies are applied in commercial software like System Advisor Model (SAM). SAM models are used to develop a DSG-LFR model in this study and incorporates TRNSYS simulation tools.

2.4 SAM Solar Direct Steam Generation Model

To estimate solar-steam production for a location, the System Advisor Model (SAM) was used to develop an hourly solar performance prediction model. SAM model is capable of developing various renewable transient system estimation models. Solar models for the direct steam generation with linear Fresnel (LF) concentrating solar plant CSP collector technology developed based on Novatec Solar Boilers were used for solar-steam models. LF reflectors (LFR) are emerging as an alternative to solar towers, and troughs

technologies for steam production in heat industrial processes and power generation (Walker, 2013). SAM performs solar radiation calculations in with the value of reference DNI and the midday position of the sun on the summer solstice (June 21 and December 21; north and south of the equator correspondingly) (Wagner and Gilman, 2011).

SAM allows the creation of direct steam generation based on two:

Process Heat Linear Direct Steam Model (IPH): Models performance of a DSG plant for the production of saturated steam at a specified temperature and pressure for industrial thermal applications. The DSG SIPH model can model PTC and LFR systems, by changing the optical characteristics, pumping power, and heat loss of the collector (Kurup et al 2017).

Direct Steam Linear Fresnel System (DSLRF): Models performance of a DSG plant for the production of saturated steam at specified temperature and pressure, mainly for the design of power generation systems. The DSLRF model represents all key accompanying subsystems included in the solar field of direct steam plants; a steam Rankine power cycle, an optional supplementary fossil backup system, feedwater pumps, a heat rejection system, and a control system.

Besides slight differences in modeling a power cycle for thermal-electrical energy conversion and plant-parasitic for a DSLRF model, both models are fairly similar.

Enables modeling configurations and depiction options of various technologies for flexible and precise performance analysis. The performance of either system is dependent on the optical and thermal efficiencies of its collector and receiver respectively.

LFR optical performance is modeled either of three ways:

- Solar Position Table (SPT): Allows specifying solar field optical efficiency as a function of solar azimuth γ_s and zenith θ_z angles for a specific collector orientation. The model calculates the solar position

angles and interpolates within the table to determine the optical efficiency for each simulation time step via SAM. (NREL, SAM)

- Collector Incidence Angle Table (CIAT): Similar to a solar position table, expressed in terms of transversal Φ_T and longitudinal Φ_L collector incidence angles. This is a commonly used method for specifying optical performance than SPT. SPT and CIAT tables are shown in Appendix A.
- Incidence Angle Modifier (IAM) Polynomials: Uses polynomial equation to calculate transversal and longitudinal IAM values to calculate the final optical efficiency modifier. IAM is dependent on collector and receiver geometry and optical properties, Figure 6.8 of the system based design shows the common trends observed (Singh, 2017). It is apparent that less orthogonality of sun angle yields a high IAM factor.

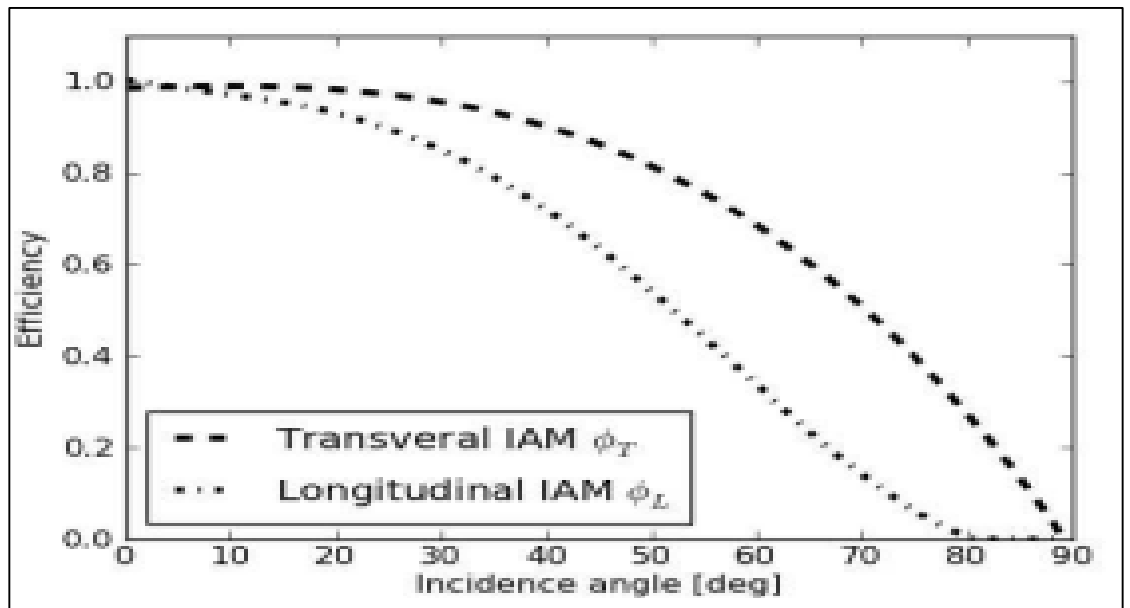


Figure 2.16 Novatec Solar design longitudinal and transversal plane IAM curves (Wagner, 2012)

The receiver thermal losses are modeled using either a polynomial model heat loss model expressed as a function of the difference between ambient temperature, steam temperature, and wind velocity; or with high performance

evacuated tube receivers applicable for high temperature suitable for superheated steam applications (Wagner and Zhu, 2012). Evacuated tube systems have a superior heat loss capacity, but poor shading effects might supersede heat loss superiority (Lubkoll, 2011). Thus, since saturated steam is generally preferred for EOR steam injection applications, the polynomial model is selected as the option for measuring and analyzing thermal performance.

Solar field design for both models follows similar but slightly different paths. DSLF models use this parameter to compute the required space area to run the power cycle at its full design capacity and estimate the heat transfer fluid mass flow rate for sizing the header pipe. In the IPH model, the design point direct normal irradiance (DNI) determines the number of heliostats. An increase in DNI indicates that fewer heliostats are required to attain target power rating, however reducing this DNI has a contradictory effect. DNI value at the design-point should stipulate the plant DNI to achieve the target power rating, including thermal and piping losses (Wagner and Gilman 2011).

The solar model permits a parametric analysis of different inputs and output combinations to analyze the field performance designed. These results combine with the optimization results of the design steam parameters to the same duration basis to investigate this technical feasibility of solar DSG steam generation.

2.5 Solar-Steam Generation

Solar steam EOR as explained harnesses the sun energy to produced steam, replacing the burning natural gas which could be in short supply in many oil fields. According to a study by XENERGY Inc. (2001), the oil and gas industry is one of the biggest steam consuming industries globally. Thus making this industry a prime candidate for solar thermal. In regions with oil reserves far greater than gas reserves, solar steam for enhanced oil recovery befits a valuable key to overcome issues of gas shortage.

In 1983, Atlantic Richfield Company (ARCO) developed using a central tower technology a solar-steam generation pilot plant in Taft, California (Ramesh et al, 2019). Ensuing in the development of a 1 MW thermal energy at peak operating conditions. Although not cost-effective, it exhibited technical feasibility and for the first time the applicability of solar steam to facilitate heavy oil recovery. In 2011, GlassPoint commissioned the first commercial solar EOR project; which was a 300kWt plant with approximately 1 acre and 1MMBTU/hr. in area and production respectively (Bierman, et al, 2013). Chevron partnered with BrightSource energy to build a solar tower 29 MWt plant in 2011, which was then the largest solar steam project for EOR spanning 100 acres of 3,822 mirrors or heliostats of 10-ft. by 7-ft. mirrors attached on a 6-ft. toughen pole directing sunlight on a 327-ft solar tower (IEA Report, 2014). GlassPoint solar steam generation system is an enclosed trough system, that uses a glasshouse as protection against the harsh environmental conditions (dust, humidity, sand, and wind) prevalent in oilfields. This presents an advantage in regions with higher soiling rates and greater average wind speeds, eliminating (12-30) percentage weekly drop in solar collection in between washes for (Bierman et al., 2013). Figure 2.9 depicts a typical representation of GlassPoint enclosed trough solar steam generation for EOR.

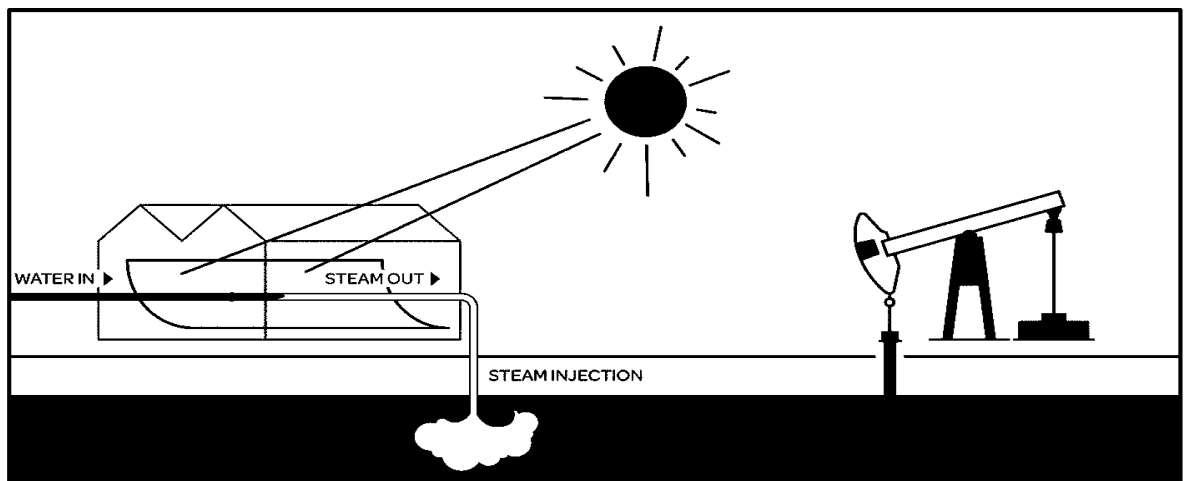


Figure 2.17 Schematic an enclosed trough solar-steam EOR plant (GlassPoint, 2017)

GlassPoint has undertaken other projects of similar nature since then with 7MWt and 1GWt solar plants commissioned in 2013 and 2018 respectively for oil fields in Oman in conjunction with Petroleum Development Oman (PDO). A summary of a number of solar EOR projects is illustrated in Table 2.1.

Table 2.1 Summary of major solar EOR projects

Project	Kern County	Coalinga	Amal west	Miraah
Location	California USA	California USA	Oman	Oman
Technology Provider	GlassPoint	BrightSource	GlassPoint	GlassPoint
Date Commissioned	February 2011	October 2011	February 2013	February 2018
System Capacity	300kWt	29MWt	7MWt	1GWt
CSP Type	Enclosed trough	Solar Tower	Enclosed trough	Enclosed trough
Steam Production	-	-	50 tons/d	6000 tons/d

Several studies have been conducted that focus on different aspects of the solar-assisted steam injection process. Van Heel et al. (2010) studied the effect of injection on solar-energy assisted enhanced oil recovery with a simulation study that considers constant-injection-rate and variable-injection-rates for a steam-injection project in Oman. Their study showed that varying injection rates due to seasonal solar cycles hold no significant effect on the recovery. Their application to both fractured and non-fractured reservoirs provides confidence regarding the applicability of solar-energy in varying reservoir types.

A life cycle assessment study focusing on the San Joaquin Valley, Kern River Field in California was conducted by Sandler et al. (2012). The study

combined reservoir simulation with economic analysis and considered steam generation with solely solar energy and with solar energy backed up with natural gas. It was found that both generation schemes over a 27-year project life resulted in very similar net present values. Thus, favoring a completely solar-energy based steam scheme due to carbon emissions of natural gas. It was also observed that injection rate variations due to fluctuations in steam generation present no major effect on reservoir performance.

Process assimilation options for linking solar steam generators into current steam facilities, and the ensuing facilities costs, energy contribution (solar fraction), and net CO₂ credits generated were also reviewed for the projects in California (O'Donnell et al. 2015; Irani et al. 2018). A synthetic reservoir modeling study showed a higher net present value using 100% solar-generated-steam set-up vs. a hybrid solar-gas based generation, although better recovery was observed in hybrid set-up with continuous, stable steam injection (Yegane et al. 2016).

Agarwal and Kovscek (2013) presented a coupled modeling study that investigates the geomechanical effects of fluctuations in steam rate due to diurnal/nocturnal and seasonal variations. The study focused on the Tulare Sand steam injection project in California and showed solar-generated steam injection to be safe in relation to geomechanical aspects. As modeling results show no significant variation in pore pressure was observed that may cause compaction for up to 1000 bbls of injection per day while maintaining injection pressures much below the formation fracturing pressure.

Construction and performance of the first solar-based steam generation in the Amal Field in Oman was presented (Palmer and O'Donnell 2014; Wilson 2015) indicating that a once-through solar steam generator capable of producing 80% quality steam at 100 bar with almost 99% uptime of the solar field. With steam characteristics consistent with standard EOR requirements, relieving the burden of steam generation by natural gas. Thus, making the project successful for a country that consumes over 22% of its natural gas

production for power generation, steam generation, and gas injection. Potential application and technical integration of solar-energy assisted steam generation in Kuwait was presented by demonstrated that solar-steam EOR can economically replace 75% of the gas necessary for thermal recovery in Kuwait, (Palmer and O'Donnell 2015). Irani et al. (2018) studied the potential application and technical integration of solar-energy assisted steam generation in Iran, Iraq, Egypt, Qatar, Saudi Arabia, Syria, Turkey, and UAE.

Afşar and Akin (2016) presented a study on the solar-energy assisted steam-injection in a heavy oil field in South-East Turkey. They used continuous steam injection together with a standby natural gas system when direct normal insolation (DNI) is sporadic to preserve the required steam rate during difficult climatic, nights, and winter periods. The solar collector system was built in Transient System Simulation Tool (TRNSYS) and merged with the steam injection method which was modeled using a commercial reservoir simulator. Results showed that local DNI of the selected region was not high enough to sustain the continuous steam injection, requiring a natural gas system on standby which appeared to be uneconomic considering the costs and current oil price levels.

Studies mostly indicated favorable results but also it seems that each case is different and the applicability of solar energy differs, depending on a number of factors, including the geographical location, and reservoir characteristics. These factors affect the solar-radiation characteristics to use solar energy to generate steam efficiently and reservoir characteristics affect the steam requirements for the reservoir under consideration. Although a number of case studies from Turkey, California, Kuwait, and Oman were presented in the literature, there has not been a systematic approach or a generalized screening model that can be followed or used to understand the applicability to a given location and heavy-oil reservoir. In this project, to address this missing component, we aim to develop a coupled solar-energy/steam-injection forecasting tool to understand the impact of certain design and natural parameters on the process. Through a data-driven approach, we aim

to develop a tool that is fast and that can provide accurate estimations of the feasibility of the project.

2.6 Genetic Algorithm Optimization

Technological digital innovation has led to major transformations in the global industrialization, including the petroleum industry. Several technologies are available to acquire large volumes of data in much shorter timeframes. The real challenge faced by engineers becomes the development of appropriate methods for converting the collated data in a manner that is both methodological and reliable towards quicker decision making. (Artun 2016). By seeking avenues that overcome such challenges through the utilization of suitable knowledge management, data analysis, and integration practices that saves significant resources in terms of manpower, software, and hardware. The current paradigm in the evolution of science adopts advanced data analysis practices to synthesize empirical, experimental, and computational findings (Hey 2009; Mohaghegh 2011). Data-driven models or screening tools; with artificial intelligence systems such as neural networks, fuzzy rule-based systems, and optimization tools are among commonly used tools for analyzing and optimizing data to obtain useful information quickly on a plethora of scenarios in a very short time whilst minimizing the computational resources required.

Any process requires a set of inputs and a set of outputs values. Optimization problem-solving approaches try to make an already existing process perform at its best possible peak or improve on the overall process. Optimization processes try to find value(s) of inputs that yields the best possible “optimized” output value(s). Standard reservoir modeling can be an expensive and time-consuming procedure, especially with complex reservoirs that required a comprehensive portrayal of reservoirs’ characteristics and behaviors. Computational intelligence optimization tools solely or coupled with other data-driven model techniques that reduce time, energy, and cost

of simulation modeling. Optimization tools generally used include particle swarm optimization, mean variance mapping optimization (MVM0) and genetic algorithm. These tools can be used as standalone models or as hybrid neuro-genetic models to optimized processes.

Genetic algorithm (GA) is a search algorithm optimization tool based on the biological theory of evolution for problem-solving and information identification. GA is a robust evolutionary-based tool quite powerful, fast, and efficient tool for finding optimal solution from a pool possible solutions to a given problem. By using a natural selection to seek the best solutions in a space of possible solutions to a given problem. Obtained by means of mutation, crossover, and selection of candidate solutions in a generic population-based metaheuristic optimization process. GA entails a genetic depiction of the solution domain and its objective function to compute the solution domain. It uses a parallel search mechanism that minimizes entrapment in local maxima/minima. It combines randomly structured genetic operators with a survival of the fittest sense to reach a solution. First introduced in the 1960s by John H. Holland, and in 1975 showed for the first time the use of crossover and reproduction, mutation and selection for adaptive and artificial systems studies. To date, there have been several established variations of GA and a broad range of optimization problems have adopted its application (Vrajitoru, 2000).

The genetic algorithm optimization method is characterized as follows:

- i. The parameter set are coded, not the parameters themselves.
- ii. Initiates its examination from a populace of points, not a single point.
- iii. Use probabilistic evolution procedures and not deterministic rules.
- iv. Uses an objective function, not derivatives or supplementary knowledge.

2.6.1 Structure and Mechanisms of Genetic Algorithm

Genetic algorithms mimic biological evolution via the natural selection process. The idea resembles the human evolution theory of Charles Darwin

and Alfred R. Wallace, which states that in any population, the fittest survives and reproduces offspring for the next generation, according to the phenotype of individuals'. In the same way, GA selects the fittest individuals from a population crop of solutions for the reproduction of offspring for the next generation of solutions until it reaches an optimal solution. To understand the structure and methodology of GA, some key terms are explained:

Population: Analogous to the human population in a given society. This a set of possible solutions (chromosomes) to the problem. Chromosomes contain elements (genes) with values (allele) for each chromosome. This can be specified either in terms of population size or type. Large population sizes have a paradoxical effect, as it increases the GA solution space search for a global minimum.

Genotype and Phenotype: Genotype is the populace of the computation space, while phenotype is the populace of the real world solution space. In the computation space, solutions are represented in a manner easily comprehended and manipulated with a computing system.

Decoding and Encoding: Decoding transforms a solution from the genotype to the phenotype space, whereas encoding is vice versa. Decoding is usually quick since it is recurrently performed in a GA throughout the fitness value computation

Selection: Also termed Parent selection, the fittest individuals selected pass their genes to the next generation. Two pairs of individuals (parents) are selected based on their fitness scores. Individuals with high fitness have more chances to be selected for reproduction. Utmost care needed to maintain good population diversity and avoid premature convergence caused by the domination of the population by extremely fit individual is recommended for GA success.

Crossover: This is essentially the reproduction phase, selected parents pair are mated, and an offspring or more are produced with the parents' genetic material.

Mutation: This is used to introduce and keep diversity in the genetic population and is typically applied with a low probability. An adaptive feasible mutation option capable of adjusting to the success and failure of preceding generations is applied.

Survivor Selection: This determines individuals to be eliminated and which to retained in the next generation. It ensures the fitter individuals are not removed from the population, and simultaneously maintains population diversity. Using either age-based selection or fitness base selection methods.

Fitness Function: This receives solutions as inputs and gives the fitness of the solutions as outputs. It determines the ability of an individual to compete with other individuals (i.e. individual fitness). It determines selection probability-based on individual fitness value or score. An individual's fitness value is the fitness function value for that individual. Since MATLAB optimization is a minimization fitness function, the best fitness value is the smallest fitness value for any person in the population.

Termination: The algorithm terminates if the population converges (no reproduction significantly different from the previous generation). At this point, GA is considered to have provided a/set of optimized solution(s) to the problem.

To incorporate good diversity, prevent population domination and prevent premature convergence, several methods are suggested such as; increasing population size, using a uniform crossover method, segmenting, and altering similar individuals to optimality (Shyalika, 2019). In addition, the population size should not be too large to avoid slowing down the algorithm. However, a smaller population might not be enough for a good mating pool. Large

population sizes are thought to be of a superior choice than voluminous generations, as far as computational time and memory space permits it; however, a too small number of generations could influence results (Vrajitoru, 2000). Thus, an optimal populace size decision requires a trial and error (Shyalika, 2019). A key advantage of GA is the flexibility to handle diverse varieties of optimization, regardless of the objective function been, linear or nonlinear, continuous or discontinuous, stationary or nonstationary, or with random noise. (Gandomi, et al 2013).

Artun et al (2008) used GA to develop a hybrid neuro-genetic methodology for optimization of design scenarios to maximize efficiency for cyclic pressure pulsing in depleted, naturally fractured reservoirs in Eastern Kentucky Big Andy Field. Combining the optimization tool with neural network models to estimate the feasibility of cyclic pressure pulsing in the reservoir per design criteria. Earlier, Bybee (2004) used GA to achieve global optimized displacement efficiency in a production/injection operation system (PIOS) for a particular oil field by linking reservoir, injection, and production performance. Maschio et al (2008) used GA for the optimization of production strategies in a realistic reservoir model. With a varying number of population individuals and generations to evaluate the algorithm efficiency, a quality map was included to aid reservoir management by locating wells and reducing randomness. GA has been used for the reproduction of permeability measurements on a face of Antolini sandstone (Sen et al 1995). Their study, showed GA performance relies highly on population size and the crossover, update, and mutation probabilities and requiring several trials.

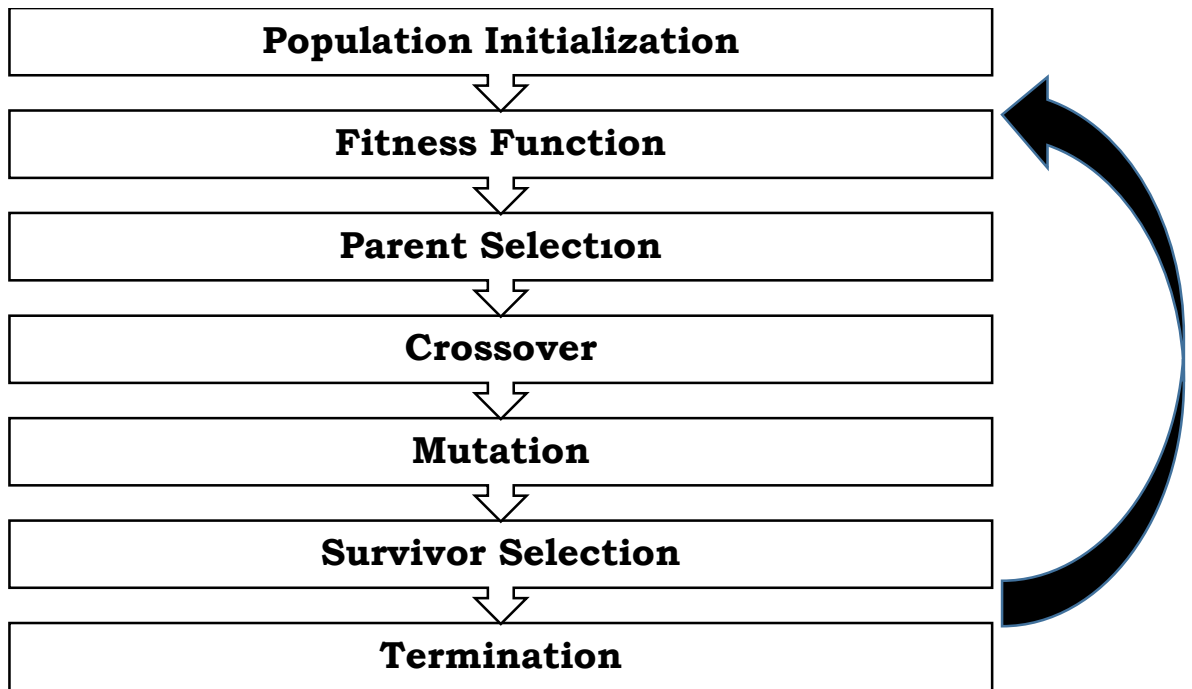


Figure 2.18 Flow path of Genetic algorithm optimization

Emera and Sarma (2005) used G.A to estimate minimum miscibility pressure between flue gas and oil in flue gas injection design; showing effectiveness and much lesser errors compared to other correlations. Emera and Sarma (2006) presented a GA model to the predict interaction of GHG-oil parameters (density, viscosity, solubility, and oil swelling factor) in geosequestration applications. Their optimization, models parameters as functions of saturation pressure, temperature, oil specific gravity, GHG critical properties, GHG liquefaction pressure, oil, and GHG compositions. Emera and Sarma (2008) used GA optimization to develop correlation to estimate the key parameters which affect CO₂-oil physical properties estimates to predict CO₂-oil mixture solubility, density, oil swelling factor, and viscosity contents of dead and live oils. Results showed the GA correlations display better performance in regards to high accuracy and wider ranges of data coverage. Chaari et al (2020) combine GA with a neural network to model a two-phase steady-state pressure drop in pipes. They used GA to predict the optimal combination of inputs subset, with this combination showing superior accuracy prediction.

The reviewed studies show the availability of several options for the generation of steam for industrial applications, as well as methods for modifying and modeling tools in terms of technical applicability of required options. To add with, studies show favorable implementation solar-steam technology for EOR applications focused on precise locations with different reservoir and especially solar radiation characteristics. However, there is no methodological model or tool for attaining an understanding of both the technical and economic feasibility of solar-steam for EOR application for any given location. Also, studies show that the applicability of GA to several applications for process optimization and data analysis facilitates smart data usage and swift decision making; thus, improving operational performance with fewer demands in terms of computational and manpower resources.

In a bid to develop a tool that can predict the optimal steam design parameters and identify the feasibility of solar-steam generation as a viable candidate for EOR applications in a given area. It is paramount to investigate the modeling of solar systems for direct steam generation and understand the parameters that affect the applicability and performance of solar systems in a certain location. And analyze how best GA can be combined with ANN to achieve an optimized solution for steam design in EOR.

CHAPTER 3

PROBLEM STATEMENT

To develop a screening tool that fosters efficient and quick decisions making in the feasibility assessment in terms of the technical and economic viability of solar-steam generation and optimal CSI; it is imperative to identify the parameters for optimum steam design and efficient steam generation systems. The primary objective of this study is to develop a robust tool to aid a fast assessment of the potential and feasibility of solar-steam application for CSI-EOR for heavy oil reservoirs in a given location, provided characteristics of the reservoir and solar resource of the given location. It is desired to develop a tool that permits the input of the characteristics of the reservoir of interests and provides corresponding outputs. To this end the tool would have the following characteristics:

- The GA optimization model for steam design parameters is constructed. Several previously trained ANN models for CSI-EOR, from a previous thesis study, are optimized to predict steam design parameters and estimate the efficiency of the CSI process. The optimized steam design parameters are steam temperature, steam injection rate, injection time, soaking time, quality, and oil economic rate limit.
- Location-based direct steam solar collector model is developed to estimate annual steam and thermal energy production potential. Coupled with an optimized steam design model to indicate the technical feasibility of the procedure.
- Economic indicator analysis tool with basic net present value (NPV) routine calculations considering the investment, injection schemes, and incomes to predict economic feasibility.

CHAPTER 4

METHODOLOGY

To obtain the objective of developing a screening tool that facilitates the feasibility analysis of solar to steam for EOR via CSI technique, the following approaches are taken and completed.

- i. Optimization of the cyclic-steam design parameters
 - GA optimization is used to optimized 5 previously trained ANN models for CSI-EOR. Each ANN for years 2,4,6,8 and 10 of CSI.
 - With different trials for each optimized parameter, population, and generation size constraint.
 - The effects of an optimized steam parameter are analyzed by changing it keeping other parameters constants.
- ii. Solar model construction
 - A solar model is constructed with NREL, SAM software for direct steam production with solar collectors.
- iii. Combination of solar and optimized steam injection model
 - Solar and optimized CSI models are integrated.
 - To permit communication and possible match search between both models.
- iv. Economic feasibility study
 - An NPV calculation routine is incorporated into the combined models for economic calculations.
- v. Analysis
 - Results of the optimization, solar models, Integration of CSI and Solar model, economic analysis are expanded on.

Fig 4.1 further illustrates the process workflow of this study.

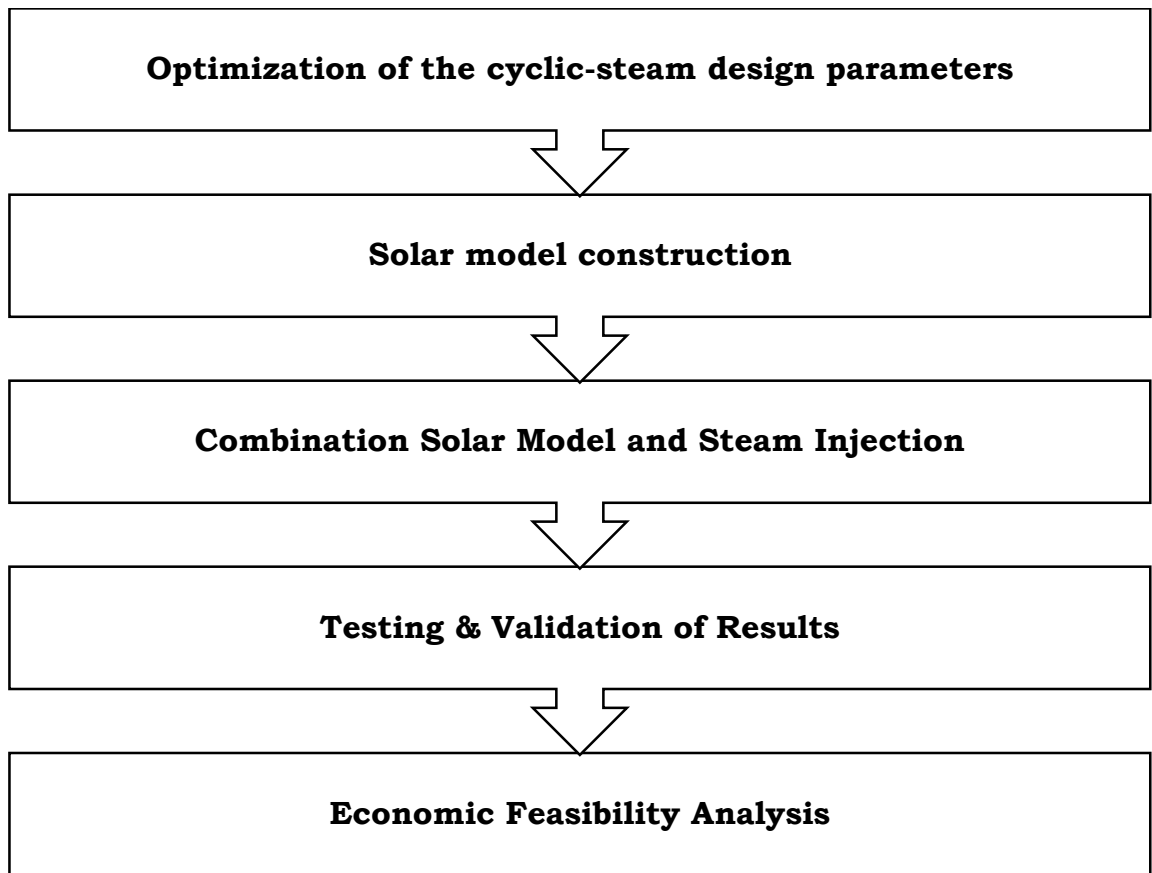


Figure 4.1 Workflow summary

4.1 Screening Model for the Cyclic Steam Injection (CSI) Process (Yalgin 2018).

A numerical model was used to study the CSI process. Using various parameters and scenarios of different combinations of the aforementioned parameters with statistical distributions and ranges. Results were used for a 10-year analysis for improved recovery with a 2-year time step. The numerical model and statistical studies were assembled with 5 ANN models (each for a 2-year. time step over a 10-year period). The result was a CSI screening tool to estimate the efficiency and performance of CSI procedures over a 10-year period. The ANN models use 5964 cases of 36 input parameters, and efficiencies in a neural network train, validate and testing sequence to predict efficiency for each ANN Model. The cases were generated using a numerical simulator run with Computer Modeling Group (CMG) numerical simulator software.

4.2 Optimization Tool Development

A genetic algorithm (GA) is adopted for modeling the optimization process in the feasibility tool. Thus, the CSI process efficiencies are maximized by the minimum objective function value. The objective function is a function of the efficiencies from the individual solution space given by Equation 4.1

$$f = \frac{1}{eff+2} \quad (4.1)$$

where *eff* represents the CSI efficiency of the GA optimized solution space; via the optimization of the operational design parameters for the steam injection. An *eff* value of -1 would yield the best fitness value of chromosomes for the optimization process and *eff* value of 1 would represent the least performing fitness value of chromosomes. Each steam injection parameter is set between lower bounds and upper bounds of [-1,1] for the optimization. This normalization was required to maintain consistency with the ANN. Several trials were made to determine the correct GA options to apply for the optimization process.

To correctly estimate and analyze CSI performance for a reservoir, using the actual properties of that reservoir is the best line of approach, as was the case in this study. Two, case studies of different fields in Amal, Oman and Ikiztepe, Turkey were carried out to investigate CSI performance in these fields as per their respective reservoir properties. Table 4.1 show the reservoir properties used for both fields. Formation thermal conductivity and heat capacity of Amal field were estimated by taking the average of several core sample analyses from the Amal field by Popov et al. (2014); the formation thermal conductivity and heat capacity were calculated to be 34.07 BTU/ft.day.F and 27.49 BTU/ft³.F respectively.

According, to Al-Hinai et al (2012) Amal-West field is estimated to have a low anisotropy (k_v/k_h) value for the field as well, with a value of 0.05 due to the fields' estimated low vertical permeability (21 md) and moderate horizontal permeability (700mD). Viscosity coefficients (A and B) were modified to match the reservoir data. The viscosity range for the screening tool is between the interval of 100-10,000 cp, and the viscosity coefficients range are (0.01-0.05)

and (5,000-6,500) for viscosity coefficients A and B respectively. With these set intervals achieving the estimated viscosity values as found in the literature for Amal field, is an impossible to difficult task. Hence the need for adjustments to coefficients values (A and B) to achieve the required viscosity value range consistent with screening tool range. The viscosity is calculated using Andrade's oil viscosity correlation (Yalgin,2018); based on reservoir temperature and aforementioned viscosity coefficients A and B as shown in Equation 4.2.

$$\mu_{oil} = A + e^{\frac{B}{T_{res}+460}} \quad (4.2)$$

where T_{res} denotes the reservoir temperature, A and B denote the viscosity coefficients and μ_{oil} denotes oil viscosity. Other reservoir parameters for the optimization were calculated from the obtained field data or by taking the averages of input data for 8910 scenarios from the previous study by Yalgin (2018) as listed in Table 4.2 and Table 4.3 respectively. All reservoir parameters were normalized between bounds of [-1, 1] to fit in the ANN generated workspace. Afterwards, the optimization was initiated to estimate CSI recovery efficiency and the required optimized steam design parameters.

Table 4.1 Obtained reservoir properties of Amal and Ikiztepe fields

Property	Unit	Amal	Ikiztepe
Thickness	ft.	500 ⁽²⁾	410 ⁽⁴⁾
Porosity	fraction	0.25 ⁽²⁾	0.20 ⁽⁴⁾
Permeability	md	700 ⁽³⁾	225 ⁽⁴⁾
Anisotropy (k_v/k_h)		0.03 ⁽³⁾	-
Viscosity ⁽¹⁾	cp	2000 ⁽³⁾	745 ⁽⁴⁾
Initial Reservoir Pressure ⁽²⁾	psia	1765 ^(1,3)	1856 ⁽⁴⁾
API Gravity	°API	20 ⁽²⁾	11 ⁽⁴⁾
Depth	ft.	3000 ⁽²⁾	4430 ⁽⁴⁾
Initial Oil Saturation	fraction	0.68 ⁽²⁾	-
Irreducible Water Saturation	fraction	-	0.155 ⁽⁴⁾

(Nandyal et al, 1983)¹, (Rice,1991)², (Al-Hinai et al, 2012)³, (Sarma et al, 1995)⁴

Table 4.2 Calculated reservoir data for both fields

Property	Unit	Amal	Ikiztepe
Specific Gravity	fraction	0.934	0.986
Oil thermal conductivity	BTU/ft.day.F	1.668	1.572
Oil heat capacity	BTU/ft ³ .F	151.9	149.2
Viscosity Coefficient A	cp	0.05	0.05
Viscosity Coefficient B	°F	4430	3990
Reservoir Temperature	°F	122.9	143.3
Initial water Saturation	fraction	0.32	-
Density	lb/ft ³	58.3	61.5

Table 4.2 Average values of reservoir parameters for optimization

Parameter	Values
Area	18.37
Anisotropy of Permeability (kv/kh)	0.509
Formation Compressibility	6.69E-06
Formation Heat Capacity	76.66
Formation Thermal Conductivity	49.86
Gas Thermal Conductivity	1.642
Shale Heat Capacity	0.648
Shale Thermal Conductivity	43.54
Molecular Weight of Oil	400.8
Viscosity Coefficient A	0.0284
Viscosity Coefficient B	5652.6
Residual Oil Saturation	0.1966
Irreducible Water Saturation	0.2
Relative Permeability Exponent (1-4)	2.998
	2.973
	2.978
	2.984
Capillary Pressure Coefficient Oil	2.486
Capillary Pressure Coefficient Gas	0.2
Initial Water Saturation	0.321
Initial Oil Saturation	0.679
Lorenz Coefficient	0.557

A convergence test was performed with ample population and generation size, to observe and prevent premature convergence of the GA optimization. Although, GAs are proven optimization methods, population and generation size trials were carried out. This was done to examine how population and generation size affects the speed and consistency of the optimization process and results. First, the optimization was performed for changing population sizes of 1, 10, 50, 100, 1000, and 10000, with a constant generation size of 1000. In addition, generation sizes of 300 and 500 for a population sizes of 10 and 100 were used to analyze the GA converge and solution difference. Finally, trials for the influence of each steam design parameters on the GA was performed by varying the value for each parameter. Thus, from these changes, we can picture the best design parameters combination to obtain the best efficiency or optimal results for a given period.

4.3 SAM Solar Model

The solar steam model was designed to best meet the GlassPoint 7MWt solar-steam pilot plant of suspended lightweight parabolic troughs enclosed in a glasshouse, similar to agricultural greenhouse industry type glasshouses in the Amal West oil field, Oman (Bierman 2013). Since the application for solar is identified as a sort of top-down approach used for designing the solar model to estimate the solar steam potential capacity for a given location. The solar field footprint of the model spans a land area of 17280 m². IPH and DSLF models were created to predict the steam temperature and flow rate given the solar resource and concentrator parameters for a once-through steam flow solar field. Coupling annual hourly simulation of quasi-steady-state calculations reliant on instantaneous weather data with plant conditions of a prior time step. Weather data are typical meteorological year data set of (TMY, TM2, TM3, or EPW) formats permit transient calculations. The modeling process would be illustrated in the remaining sections of this chapter.

Location Weather Data: Typical meteorological year data for Thumrait, Oman from 1981 to 2015 were collated. Some elements in typical weather data are shown in Table 4.1.

Table 4.4 Typical Meteorological Year data for a location

Data Type	Units
Global horizontal irradiance (GHI)	W/m ²
Diffuse horizontal irradiance (DHI)	W/m ²
Direct normal irradiance (DNI)	W/m ²
Dry and wet bulb temperatures	°C
Wind speed and direction	(m/s),deg
Dew point temperature	°C
Pressure	Millibar
Relative humidity	%
Snow depth	cm
Albedo	Fraction
Extraterrestrial Radiation	W/m ²

These data were collated in hourly, daily, and monthly order for different years over the 35-year period for Oman. However, for location performance comparisons, weather data for the year 2014 was collected for Adiyaman and Batman in the Southeastern regions of Turkey. All weather data were obtained from climate.onebuilding.org.

A SAM enabled resource file checker was used to check for errors or required missing data as follows:

An irradiation component check is performed, to ensure at least two components of irradiance are fully specified, if all three are specified and for consistency. SAM simulator calculates the sun's position, and estimate global horizontal irradiance given the beam and diffuse. A difference no more than 20% for $GHI > 500 \text{ W/m}^2$ between calculated global and specified global and no more than 50% different for 200 W/m^2 is maintained. It was also ensured the beam irradiance is between 0 and 1500 W/m^2 . Next check is for global and diffuse irradiance, to ensure values are between 0 and $IRRMAX \text{ W/m}^2$. Where $IRRMAX = 1.5 \cdot (EXTRA+150)$, and EXTRA is the extraterrestrial irradiance estimate for any time of day. Others checks performed include:

wind speed range between 0 and 30 m/s, wind direction between 0 and 360 degrees, temperatures (dry bulb, wet bulb, and dew point) are between -60 and 60 C, relative humidity values between 2 and 100 % and pressures between 700 and 1100 millibar. Upon completion of the checks for all weather data, weather data was mostly consistent, just the wind speed records which exceed the 30 m/s (31.9 and 37 m/s) for two yearly hours for Oman were found and corrected. Figure 4.1– 4.6 illustrates profiles of TMY weather data for all 3 locations.

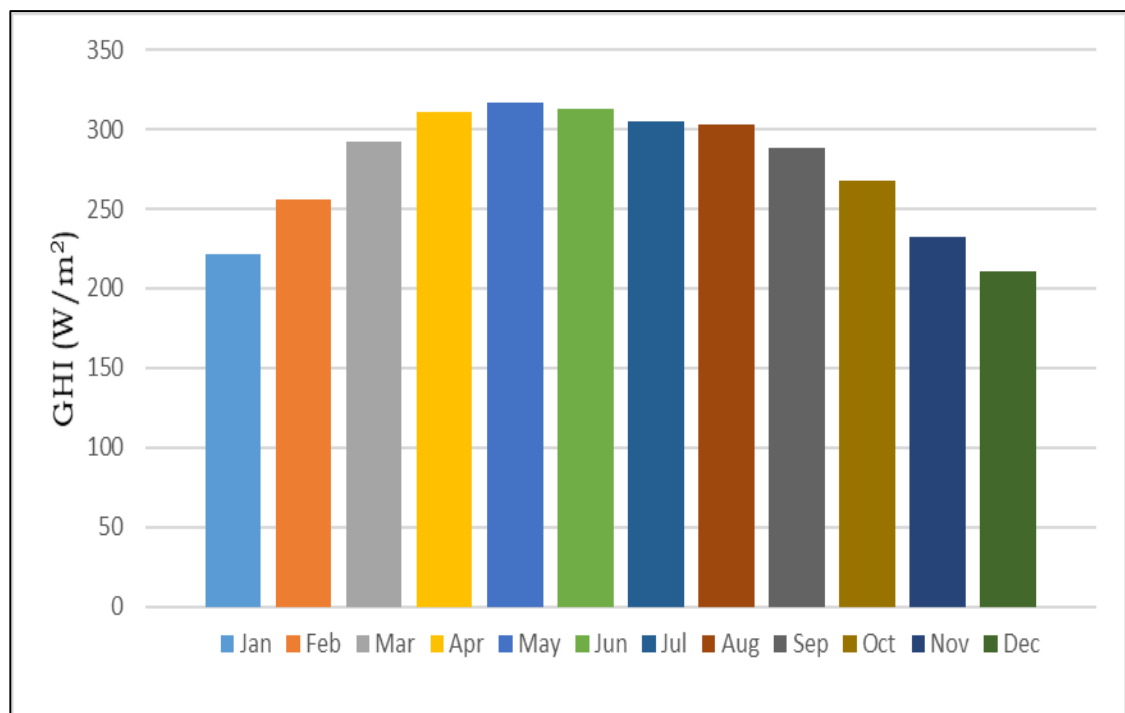


Figure 4.1 Monthly global horizontal radiation for Thumrait, Oman

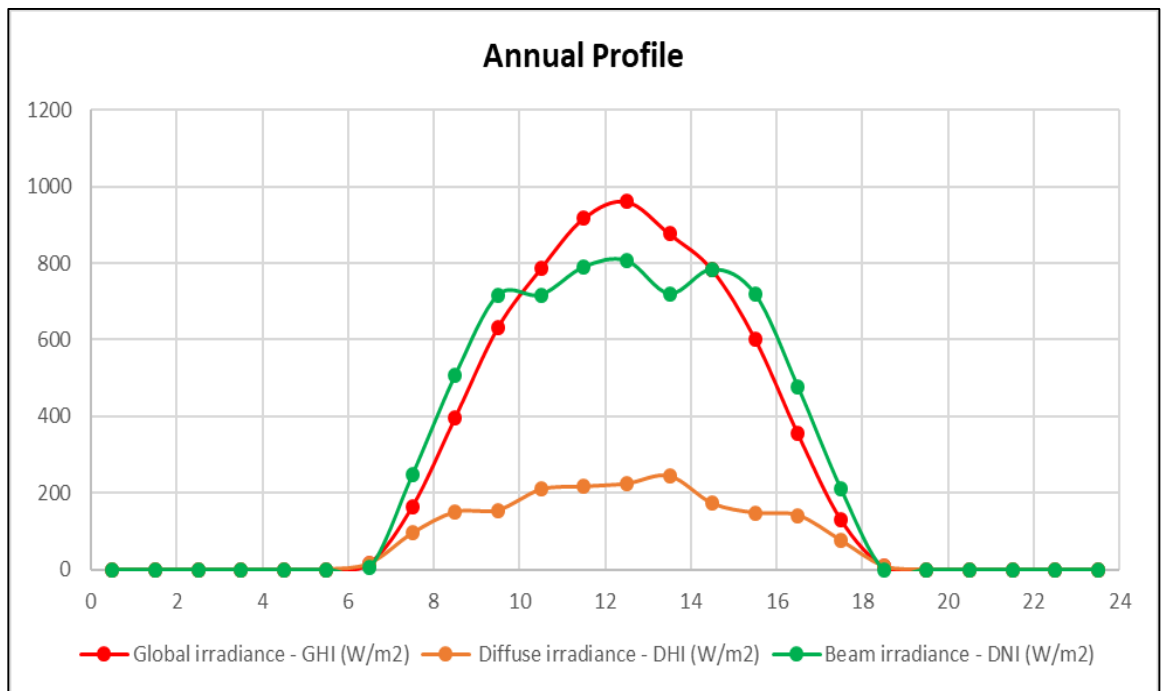


Figure 4.2 Annual profile of GHI, DHI, and DNI in Thumrait, Oman

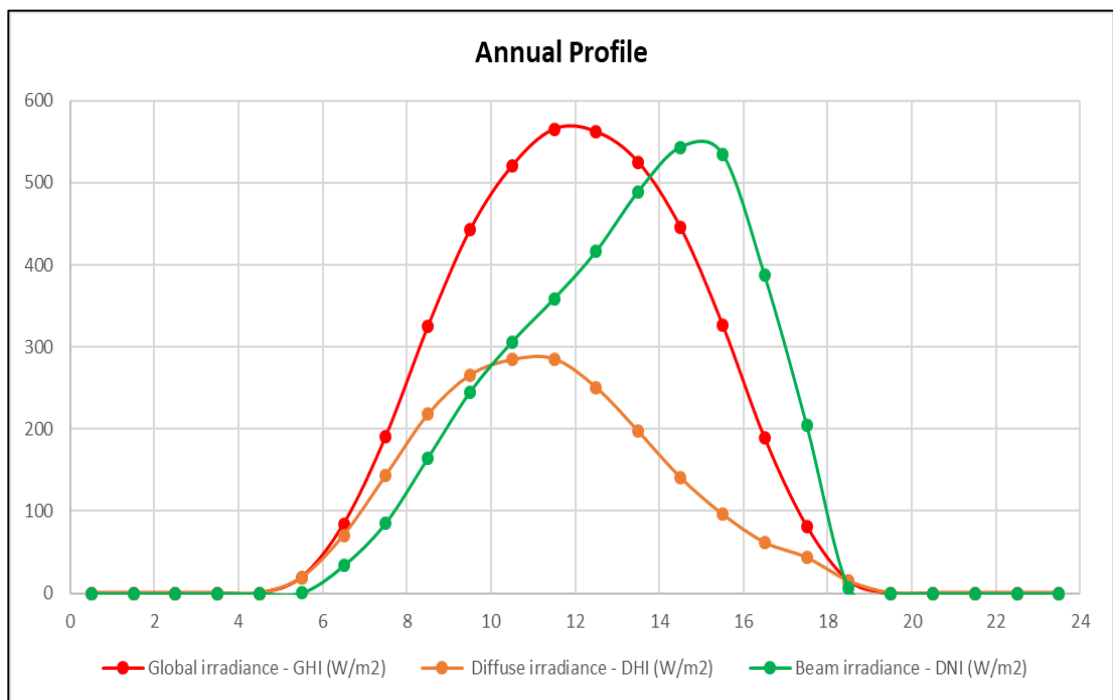


Figure 4.3 Annual profile of GHI, DHI, and DNI in Adiyaman, Turkey

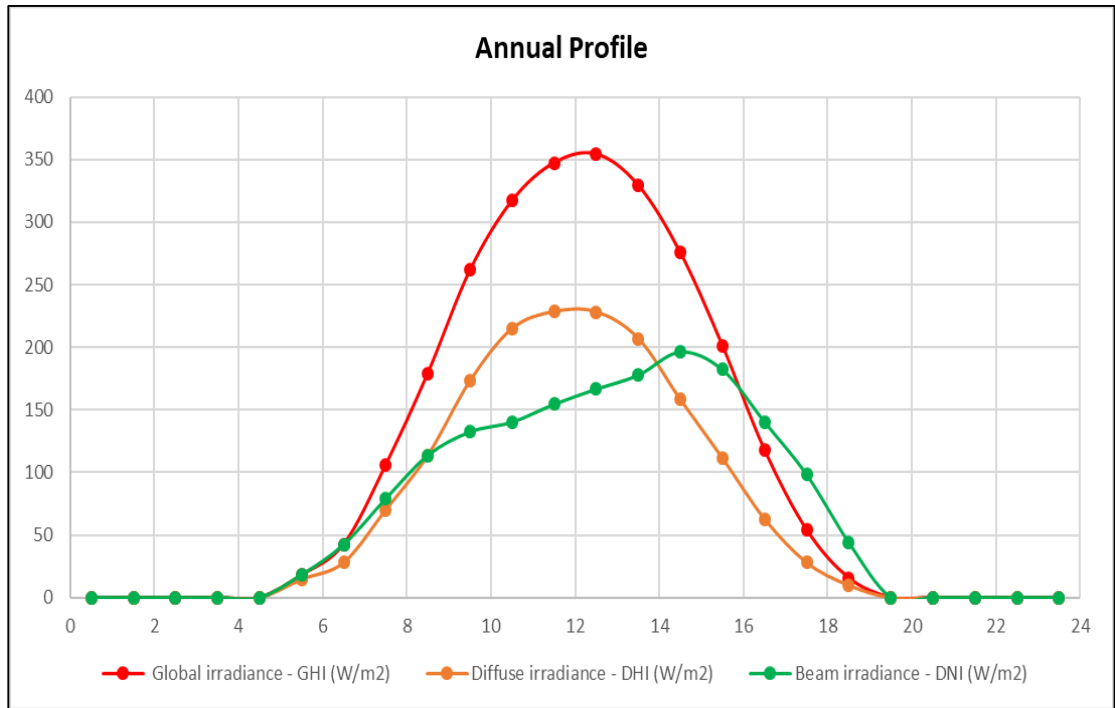


Figure 4.4 Annual profile of GHI, DHI, and DNI in Batman, Turkey

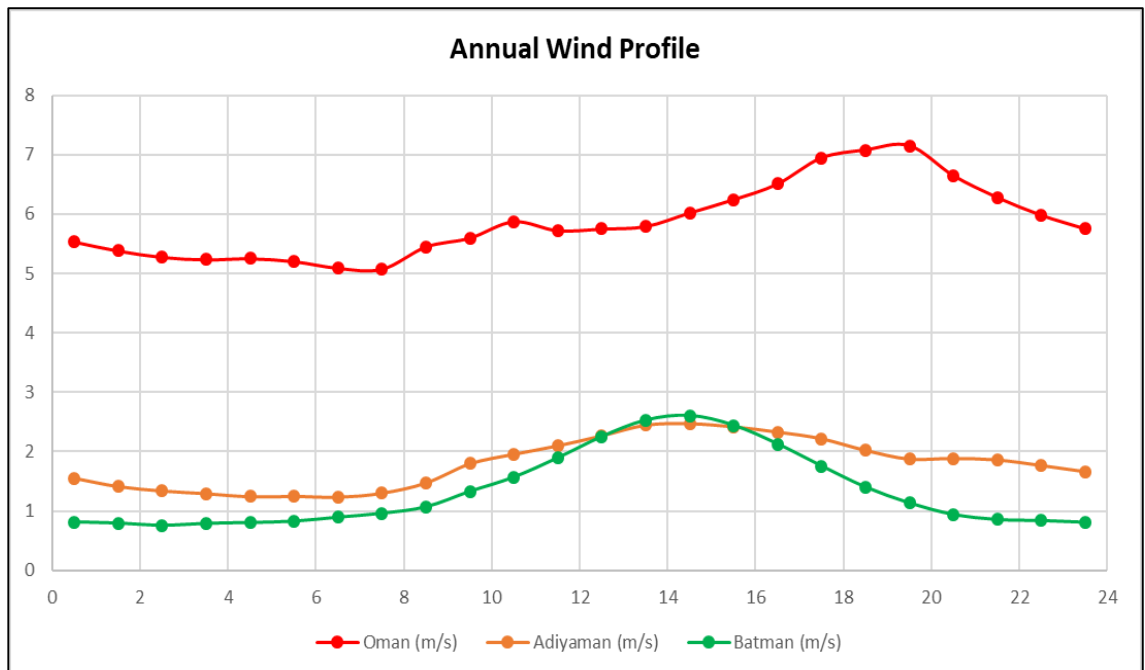


Figure 4.5 Annual wind profile for Thumrait, Oman; Batman, and Adiyaman, Turkey

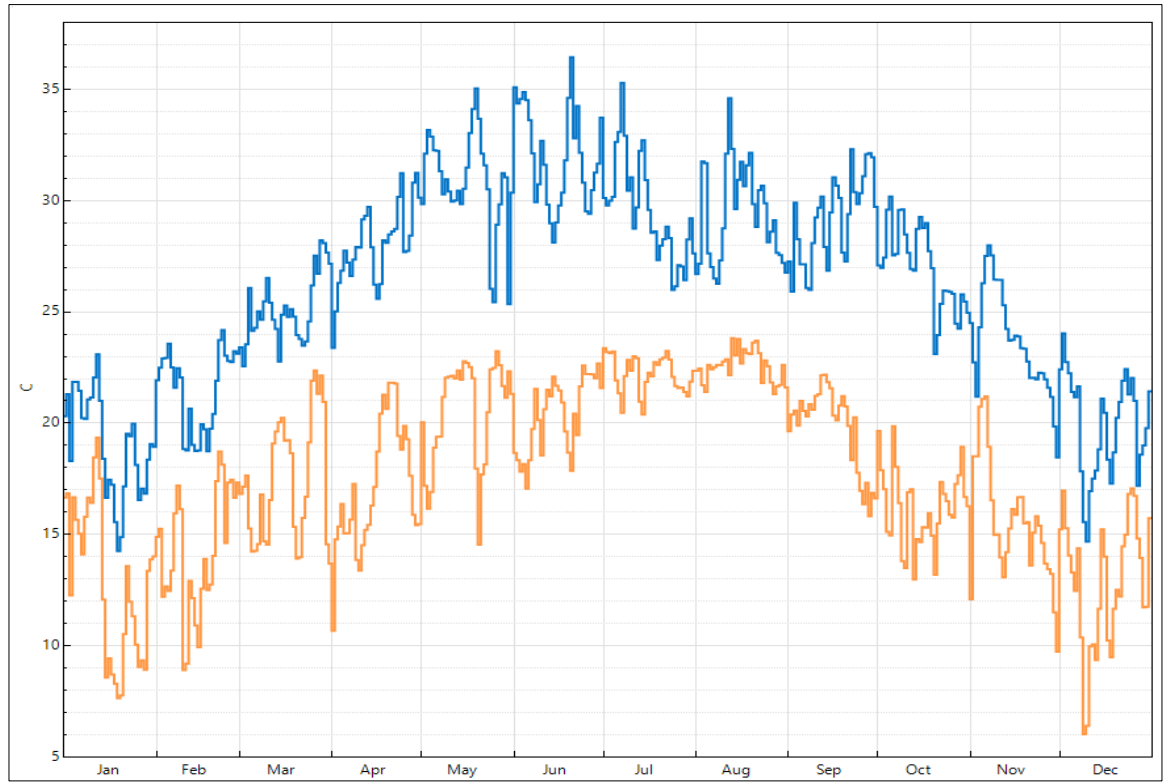


Figure 4.6 Oman yearly temperature variation and differences for Dry bulb (Upper curve) and Wet bulb (Lower curve)

4.4 Optical Performance Analysis

Solar optical performance is a key cornerstone of any solar system as it in large part determines how effective the solar system operates. Hence, this section explains the optical performance model for the solar-CSI model. Typically, LFR optical performance depends on longitudinal and transversal incidence angles, illustrated in Figure 4.7. The optical performance of the LFR of the solar model used for the case study is based on IAM polynomials, which determines the final optical efficiency modifier for the system by taking the product of longitudinal and transversal incidence angle modifier (Wagner and Zhu, 2012). Thus, with these parameters the solar model constantly estimates optical efficiency modifier as it tracks incidences angle changes of the collector with respect to the sun (i.e. sun zenith and azimuth angles). Equations 4.3 - 4.6 illustrates the common relationship between longitudinal incidence angle Φ_L , transversal incidence angle Φ_T , solar azimuth angle γ_s ,

solar height α_s , and zenith angle θ_z for calculating incidence angle modifier IAM.

$$\alpha_s = 90^\circ - \theta_z \quad (4.3)$$

$$\tan(\Phi_T) = \frac{\sin(\gamma_s)}{\tan(\alpha_s)} \quad (4.4)$$

$$\tan(\Phi_L) = \cos(\gamma_s) \times \cos(\theta_z) \quad (4.5)$$

$$\text{IAM}(\Phi_T, \Phi_L) = \text{IAM}(\Phi_T, 0) \times \text{IAM}(0, \Phi_L) \quad (4.6)$$

Using this relationship and incidence angle modifier polynomials, the LFR optical performance can be modeled based on equations 4.7 & 4.8.

$$\text{IAM}(0, \Phi_L) = C_0 + C_1 \Phi_L + C_2 \Phi_L^2 + C_3 \Phi_L^3 + C_4 \Phi_L^4 \quad (4.7)$$

$$\text{IAM}(\Phi_T, 0) = C_0 + C_1 \Phi_T + C_2 \Phi_T^2 + C_3 \Phi_T^3 + C_4 \Phi_T^4 \quad (4.8)$$

IAM Coefficients for C_0 through C_4 are shown in Table 4.5.

Table 4.5 Incidence angle modifier coefficients for Φ_T and Φ_L directions

	C_0	C_1	C_2	C_3	C_4
$\text{IAM}(\Phi_T)$	0.9896	0.44	-0.0721	-0.2327	0
$\text{IAM}(\Phi_L)$	1.0031	-0.2259	0.5368	-1.6434	0.7222

It should be noted that while the default simulator coefficients are used in this study, in reality coefficients are location specific and would vary depending on the location of the solar field. However, in the screening tool user can model the solar optical performance with other options like solar position table or collector incidence angle table.

4.5 Thermal Performance Analysis

To evaluated the thermal performance of the solar-CSI model, receiver thermal losses were modeled using a polynomial heat loss model. The model incorporates steam temperature adjustment $f_{hl}(\Delta T_{local})$ and wind velocity adjustment $f_{hl}(V_{wind})$ factors to calculate the final thermal loss coefficient q'_{hl}

(W/m). Which is used to analyze receiver and overall solar system thermal performance. SAM simulator examines thermal losses at each collector loop as function of temperature difference between the steam and dry bulb temperatures using the following equations.

$$f_{hl}(\Delta T) = C_0 + C_1 \Delta T_{local} + C_2 \Delta T_{local}^2 + C_3 \Delta T_{local}^3 + C_4 \Delta T_{local}^4 \quad (4.9)$$

$$f_{hl}(V_{wind}) = C_0 + C_1 V_{wind} + C_2 V_{wind}^2 + C_3 V_{wind}^3 + C_4 V_{wind}^4 \quad (4.10)$$

$$q'_{hl} = \sum_{i=1}^{N_{modules}} q'_{hl,i} = \sum_{i=1}^{N_{modules}} f_{hl,i}(\Delta T) \times f_{hl}(V_{wind}) \quad (4.11)$$

$$\Delta T_{local} = \frac{T_{field\ outlet} + T_{field\ inlet}}{2} - T_{ambient} \quad (4.12)$$

Equation coefficients (C₀-C₄) depends on the heat loss characteristics of a particular receiver design. SAM's default values are for the Novatec Solar Boiler and shown in Tables 4.6 and 4.7. Therefore, with the aforementioned equations receiver heat losses, outlet steam temperature, heat gain, loop thermal efficiency, overall collector efficiency and as well as calculating the actual field thermal output and area of the solar model.

Table 4.6 Coefficients for steam temperature adjustment heat loss polynomial

C ₀ (W/m)	C ₁ (W/(m-K))	C ₂ (W/(m-K ²))	C ₃ (W/(m-K ³))	C ₄ (W/(m-K ⁴))
0	0.672	0.002556	0	0

Table 4.7 Coefficients for wind velocity adjustment heat loss polynomial

C ₀	C ₁ (1/(m/s))	C ₂ (1/(m/s) ²)	C ₃ (1/(m/s) ³)	C ₄ (1/(m/s) ⁴)
1	0	0	0	0

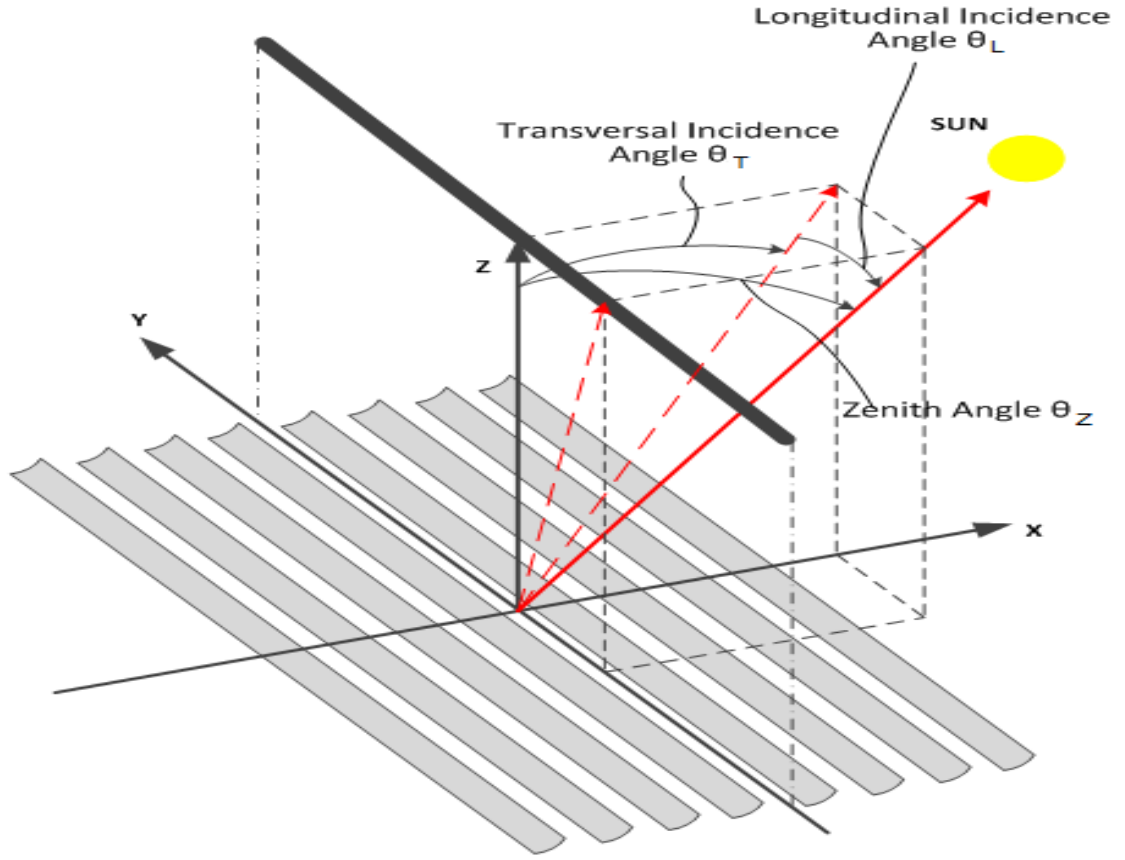


Figure 4.7 Illustration of LFR Solar positions, zenith and incidence angles (NREL, SAM)

4.6 Solar Field Design

This section elucidates on how the solar field size areal extent was modeled using SAM simulator. For a solar system design, with thermal input Q_{input} (DSLRF) or target power rating Q_{target} (IPH) the solar field output is related by the required total area (TRA) for a solar multiple (SM) = 1 and total loop conversion efficiency $\eta_{\text{loop, total}}$. The power output (MWt) can be related by:

$$Q_{\text{input}} = \frac{\text{Gross Output}}{\eta_{\text{design}}} \quad (4.13)$$

Where gross output is the DSLRF plant design power cycle's output, without parasitic losses. η_{design} is the rated cycle efficiency for the conversion of thermal energy to electricity.

Since steam injection is the primary interest and not power generation the power cycle was modified. To minimized power cycle effects on solar model performance of the DSLF solar model, modifications as suggested by Turchi and Neises (2015) to reduced power cycle effects were made and are shown in Table 4.8.

$$Q_{\text{target}} = \text{Heat sink power} \times \text{Target Solar Multiple} \quad (4.14)$$

$$Q_{\text{thermal}} = Q_{\text{target}} = Q_{\text{input}} \quad (4.15)$$

Q_{thermal} denotes the required receiver thermal power to meet the design thermal load. Heat sink power is the IPH capacity or thermal load of the field in thermal megawatts. Target solar multiple for this study was taken as 1.

$$\text{TRA} = \frac{Q_{\text{thermal}}}{\eta_{\text{design}} \times \text{DNI}_{\text{design}} \times \eta_{\text{loop, total}}} \quad (4.16)$$

$\text{DNI}_{\text{design}}$ is the design point direct normal irradiation, a DNI value about the highest field incident DNI value is used, to better represent the expected maximum energy levels of the field (Wagner and Gilman 2011).

$$\eta_{\text{loop, total}}(\text{DSLF}) = \eta_{\text{loop, optical}} \times \eta_{\text{loop, thermal}} \times \eta_{\text{piping, thermal}} \quad (4.17)$$

$$\eta_{\text{loop, total}}(\text{IPH}) = \eta_{\text{loop, optical}} \eta_{\text{loop, thermal}} \quad (4.18)$$

Where f_{tracking} , f_{geometry} , $f_{\text{reflectivity}}$, f_{soiling} , and $f_{\text{opticalerr}}$ indicates the collector optical factors: tracking error, geometry effects, mirror reflectivity, mirror soiling and optical error respectively. The loop optical efficiency can be estimated as follows:

$$\eta_{\text{loop, optical}} = f_{\text{tracking}} \times f_{\text{geometry}} \times f_{\text{reflectivity}} \times f_{\text{soiling}} \times f_{\text{opticalerr}} \quad (4.19)$$

$$\eta_{\text{loop, thermal}} = 1 - \frac{L_{\text{collector}} \times q'_{hl}}{\text{DNI}_{\text{design}} \times \text{RFA}} \quad (4.20)$$

Where $L_{\text{collector}}$ is the length of the collector module (m)

$$\eta_{\text{piping, thermal}} = 1 - \frac{T_{\text{sf, avg}} \times q'_{hl}}{\text{DNI}_{\text{design}}} \quad (4.21)$$

$$T_{\text{sf, average}} = \frac{T_{\text{field out}} - T_{\text{field in}}}{2} \quad (4.22)$$

$T_{\text{field, in}}$, $T_{\text{field, out}}$ and $T_{\text{sf, average}}$, are the inlet, outlet and difference average solar field temperatures.

For total reflective aperture area of a collector unit, RFA (m^2), and a number of boilers units n_{boiler} . The single loop aperture SLA, solar field area A_{SF} , the

required number of loops at solar multiple SM of 1 RNL_{SM1} , number of loops n_{Loops} , and the solar field thermal output for design conditions Q_{SF} is expressed as:

$$SLA = RFA \times n_{boiler} \quad (4.23)$$

$$RNL_{SM1} = \frac{TRA}{SLA} \quad (4.24)$$

$$A_{SF} = SLA \times n_{Loops} \quad (4.25)$$

$$SM = \frac{A_{SF}}{TRA} = \frac{Q_{SF}}{Q_{thermal}} \quad (4.26)$$

$$n_{Loops} = SM \times RNL \quad (4.27)$$

$$Q_{SF} = DNI_{design} \times A_{SF} \times \eta_{loop,total} \text{ (system)} = SM \times \frac{Q_{input}}{\eta_{design}} \quad (4.28)$$

Input solar field design parameters and their values are listed in Table 4.9. For IPH models the required field outlet temperature is obtained by calculating the corresponding saturation pressure with a simplified model proposed by Affandi et al (2013) Equation 4.27, based on the heat sink inlet pressure and the constant values of a-e shown in Table 4.10.

$$\ln(P) = a + b \ln(Tr) + c [\ln(Tr)]^2 + d [\ln(Tr)]^3 + e [\ln(Tr)]^4 \quad (4.29)$$

T_r is the reduced temperature, defined by T/T_{cr} . T_{cr} is the critical temperature; 647.096 K for steam. Equation 6.27 is best applicable within the range of (0.61-22038.9 kPa) and (0-370) °C.

Table 4.8 Power cycle inputs modifications to minimize power cycle influence over the solar model performance (Turchi and Neises 2015)

Power Cycle Input	SAM Default Value	Modifications
Design gross output	111	Equal to thermal power rating of solar field
Estimated gross-net conversion factor	0.9	No change
Availability and Curtailment inputs	Various	No change

Rated cycle conversion efficiency	0.371	1
Boiler operating pressure	100	Saturated steam pressure at field outlet temperature
Steam cycle blowdown fraction	0.02	No change
Fossil backup boiler LHV efficiency	0.9	No change
Aux heater outlet set temperature	391	Field outlet temperature
Fossil dispatch mode	Min backup level	
Low resource standby period	2	No change
Fraction of thermal power needed for startup	0.2	0
Power block startup time	0.5	0
Minimum required startup temp	300	Field inlet temperature
Max turbine over design operation	1.05	2
Min turbine operation	0.25	0.02
Turbine inlet pressure control	Fixed Pressure	
Cooling System inputs	Various	No change

Table 4.9 Design input parameters for Solar field design

Name	IPH	DSLFF	Unit
Design point DNI	950	950	W/m ²
Target solar multiple	1	-	
Heat sink/Turbine inlet pressure	115	100	bar
Field inlet temperature	40	50	°C
Field outlet temperature	-	310	°C
Number of modules per section	24	24	
Collector azimuth angle	0		degree
Ambient temperature	35	35	°C
Min Single loop flow rate	-	0.5	kg/s
Field pump efficiency	0.85	0.85	

Reflective aperture area	720	720	m ²
Length of collector module	44.8	44.8	m
Tracking error	0.9	0.9	fraction
Geometry effects	0.7	0.7	fraction
Mirror reflectivity	0.9	0.9	fraction
Mirror soiling	0.9	0.9	fraction
General optical error	0.9	0.9	fraction

Table 4.10 Constant values for saturation pressure simplified model

a	b	c	d	e
9.56756	5.39806	-6.16183	1.49572	0.4330

4.7 Integration of Optimized CSI and Solar Models

To combine the CSI and solar model a criteria matching scheme was employed to estimate a solar fraction of steam obtainable from the solar field. Since the optimization prescribes the optimum steam parameters to achieve peak performance for CSI operations. The criteria matching scheme checks if a certain criterion is met and if not how to meet such a criterion. Basically, the two key sets of parameters used for the criteria checks are, the steam temperature and flowrate from the optimized steam injection design and the potential output steam temperature and flow rate of the solar model. If the solar model at the very least fit meets or better yet can surpass the target design parameters for each criterion. Thus, a technical feasibility of using solar to sustainably generate steam for CSI would be achieved. To do this the following method was adopted.

Results of hourly data for each criterion from the solar model is converted to daily data for the required steam flowrate and temperature parameters. Annual daily average sun hours $\text{hrs}_{\text{sun, daily}}$ for a location are determined based on historical trends of the average daily hours of solar irradiance. Coupled with the annual hourly data from SAM, daily sun hours are averaged for every 24 hours for 365 days of a year. The hourly data of steam mass flow rate kg/s

is totaled for the entire daily sun hours, while the temperature over the same period is averaged to obtain both daily steam flowrate and temperatures. Daily sun hours were used as these were the period the solar model mostly generates steam that meets the temperature criterion for a given optimized steam temperature for CSI.

If L is a lower bound that indicates (00:00 hrs) and U is an upper bound that indicates (23:00 hrs) for a data duration of 8760 hours we can obtain daily data as follow:

$$L = 24 (t-1) + 1 \quad (4.30)$$

$$U = 24 (t-1) + 24 \quad (4.31)$$

If t denotes each day of the year, we can calculate the daily steam flow q_{steam} and temperature T_{steam} from the first day of a year ($t=1$) till the last day of a year ($t=365$). By taking the sum of q_{steam} and mean of T_{steam} for the duration of daily average sun hours, $hrs_{\text{sun, daily}} = 8$ hrs (i.e. taking the sum of steam flow rate and mean of Temperatures for 8hrs daily over a 365-day period). Furthermore, this is coupled with the injection schedule to developed a target q_{steam} and T_{steam} required over a successive number of days (injection time t_{inj}) to estimate a maximum annual availability factor. This annual availability factor determines the solar fraction of steam f_{solar} usable for the solar-EOR in a CSI procedure.

4.8 Economic Analysis

A classic economic analysis is always a good indicator of the viability and feasibility of a project been considered “go ahead” or “hold still”. This typically entails weighing capital investment costs and project returns. Several economic indicators or analyses are performed. A common method is the net present value NPV; which considers the net of all expenses versus revenues. An NPV calculation routine is also performed considering the capital investment (Capex) of the solar panels, injection costs, and income from improved recovery (i.e. additional production from solar-steam CSI) to give a

better indications of the project feasibility. This performed with following procedures.

Capital Investment Cost: Capital investment accounts for direct project costs for solar collector field costs of mirrors receivers, tracking, cleaning systems, support structures, glasshouse cost and construction costs. Also indirect cost for balance of plant, total engineering costs, project development, and management costs, EPC costs, and overhead costs (O'Donnell et al 2017). Using the SAM financial cost estimates for LFR and International Energy Agency (IRENA,2010) the direct investment cost is estimated. To mirror standard NPV analysis for oil projects, costs have been divided into tangible and intangible. With a salvage value of 10% applied for the overall tangible costs. To add with, the inclusion of a glasshouse structure could reduce the cost of solar collector system PTC or LFR tremendously to the tune of 32% and 50% respectively (ESMAP nd).

Operation and Maintenance Cost: This mainly accounts for the replacement of system parts, water costs, and remedial costs. In common LFR systems, the washing costs are eliminated due to the availability of easily acquired automated cleaning systems for mirrors or glasshouses. Escalation is accounted for in operating cost analysis at a rate of 5%.

Straight-line and sum of year digit depreciation methods were applied, and the depletion considered the costs, gross, and net depletion. With the higher present value of either depreciation and depletion techniques applied for economic analysis. An investment tax credit (ITC) of 25%, insurance cost (0.5-1) percent of capex. A carbon cost for emission savings or cost analysis for GHG emitting boiler resources alternatives (natural gas, gasoline, coal etc.).

The efficiency of the CSI is calculated in terms of present values of cumulative steam volume injected ($PV_{S,inj}$) and resulting cumulative improved recovery (PV_{NP}) as shown in Equations 4.32-4.33. The number of discounting years is denoted by j and i denotes the interest rate, an interest rate of 10%. is used in this study.

$$EFF_n = \frac{PV_{NP}}{PV_{S, inj}} \quad (4.32)$$

$$PV_x = \sum_{j=1}^n \frac{X}{(1+i)^j} \quad (4.33)$$

For a given number cycle the cumulative steam injected S_{inj} is estimated by:

$$S_{inj} = \text{number of cycle} \times q_{\text{steam}} \times t_{inj} \quad (4.34)$$

The recommended number of cycles for economic viability should be between (6-7) and not more than 10 (Mahdavi, and Zebarjad 2018).

For the solar-steam generation, the product of (S_{inj} , f_{solar} , and EFF_n) gives the fraction solar improved recovery.

$$S_{inj} = \text{number of cycle} \times q_{\text{steam}} \times t_{inj} \times f_{solar} \quad (4.35)$$

$$PV_{NP} = EFF_n \times PV_{S, inj} \quad (4.36)$$

$$PV_{NP} = \sum_{j=1}^n \frac{N_p}{(1+i)^j} \quad (4.37)$$

$$N_p = PV_n - PV_{n-j} (1+i)^n \quad (4.38)$$

$$NPV = \text{Discounted (Revenues - Expenses)} \quad (4.39)$$

Period Net Cash Flow = Revenues – Total Capital investment

Total Capital investment = (Tangible + Intangible) Capital Investment

Most prices or costs for the economic parameters have been gathered and adjusted for LFR solar systems from several sources IRENA reports (2012, 2017); (Robbins, 2010); (Molchanov, 2011); (Chaar et al, 2015); (Kurup and Turchi, 2015); (Bierman et al, 2018); GlassPoint 2017, ESMAP World Bank Report, and SAM, NREL

Table 4.11 Economic Parameters for NPV analysis

Economic parameters			
Capital investment		Taxes and Other rates	
Item Unit	Cost	Item Unit	Cost
Solar Field System Unit Cost \$/m ²	\$100	Working Interest	100%
Site Improvements Cost (\$/m ²)	\$20	Oil price per STB	\$50

Solar Field Area (m ²)	17280	Tax Rate	30%
Balance of Plant costs (%Direct costs)	5.00%	Nominal Discount Rate	10%
Non-Solar Land Area Factor	1.00	CO ₂ Emission rate per ton	\$40.00
Salvage Rate	10%	Project life (years)	10
Insurance (CAP) 0.5-1%	1%	Investment Tax Credit	25%
EPC & Indirect Cost Surcharge for engineering, EPC, project management (%Direct costs)	20.00%	Glasshouse rate (\$/m ²)	\$20
Cleaning System	\$50,000	Escalation rate	5%
VOM \$/kW	1.00	FOM \$/kW	10.00

N.B: Costs might not be exact are from estimates of various sources: IRENA reports (2012, 2017); (Robbins, 2010); (Molchanov, 2011); (Chaar et al, 2015); (Kurup and Turchi, 2015); (Bierman et al, 2018); GlassPoint 2017, ESMAP World Bank Report, and SAM, NREL.

CHAPTER 5

RESULTS AND DISCUSSION

5.1 Optimization Performance and Results

Trials on the effects of population and generation size on optimization results showed that for large population and generation sizes there is hardly any change in the optimization result but the performance can be greatly slowed down. However, if the population size is very small and generation size is large there are differences in the yearly optimization results, even if the performance is faster than for large population and generation sizes. Figure 5.1. shows these effects on the optimization performed for changing population sizes of 1, 10,50,100,100, and 10000 and constant generation size of 1000. As observed earlier for a population size of 1 there are noticeable differences in the results of the other population sizes. Further trials for population sizes from the previous case with similar performance up to a population size of 1000 showed that, for smaller generation sizes, there are noticeable differences in the optimization results for efficiencies or steam design parameters. However, with an increase in population size for the same generation size, there is a better similarity in the results of both efficiencies and steam design parameters. These observations are illustrated in Table 5.1 and 5.2 showing results for GA optimization population and generation size tests performed for years 2 and 10. These show a consistent agreement with studies that state population sizes to have a larger effect on the optimization process in attaining optimal solution. However, the difference is quite minute on the recovery efficiency but can be ample amongst other steam design parameters. Convergence tests performed indicated the solution converges to an optimal solution but not prematurely as evidently illustrated in Figure 5.2, 5.3, and 5.4 respectively for a generation size of 300. It can be observed that the GA runs and converges just past half the generation size in Figure 5.2 for a population size of 10. But converges at about half or less the stated generation size in Figure 5.3 and 5.4 for years 2 and 10 for a population size of 100.

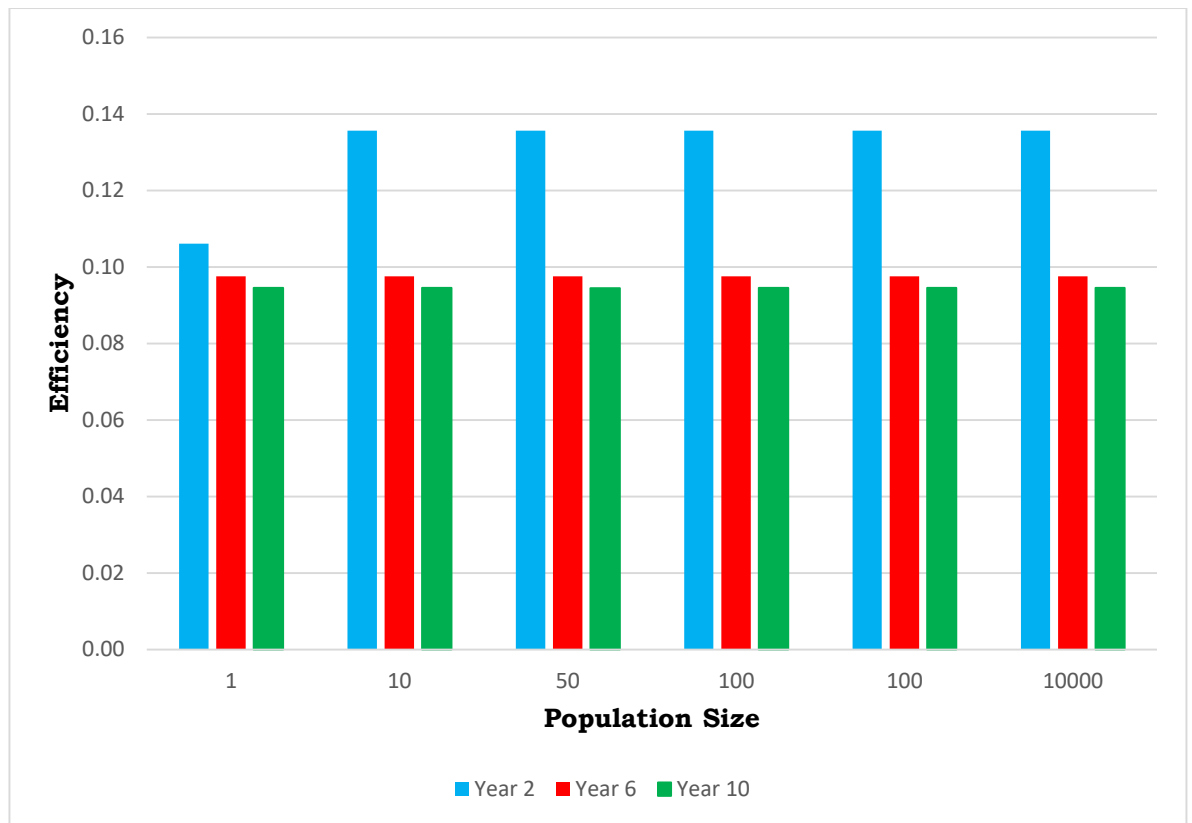


Figure 5.1 Optimized CSI Efficiency per population of 1,10,50,100,500,1000 and 10000

Table 5.1 Results from Population and Generation Trial for Year 2

Year 2						
Population	Units	10		100		1000
Generation		300	500	300	500	500
CSI Efficiency	Fraction	0.11	0.11	0.136	0.136	0.136
Injection time	days	10	10	10	10	10
Injection rate	bbl/day	1105	504	500	500	500
Quality	Fraction	1	1	0.7	0.7	0.7
Temperature	°F	700	529	450	450	450
Economic Rate Limit	bbl/day	5	8	5	5	5
Soaking Time	days	10	24.8	23	23	23

Table 5.2 Results from Population and Generation Trial for Year 10

Year 10						
Population	Units	10		100		1000
Generation		300	500	300	500	500
CSI Efficiency	Fraction	0.0945	0.0935	0.0945	0.0945	0.0945
Injection time	days	10	10.08	10	10	10
Injection rate	bbl/day	500.6	1672	500	500	500
Quality	Fraction	1	1	1	1	1
Temperature	°F	700	586	700	700	700
Economic Rate Limit	bbl/day	5	25	5	5	5
Soaking Time	days	30	20.9	30	30	30

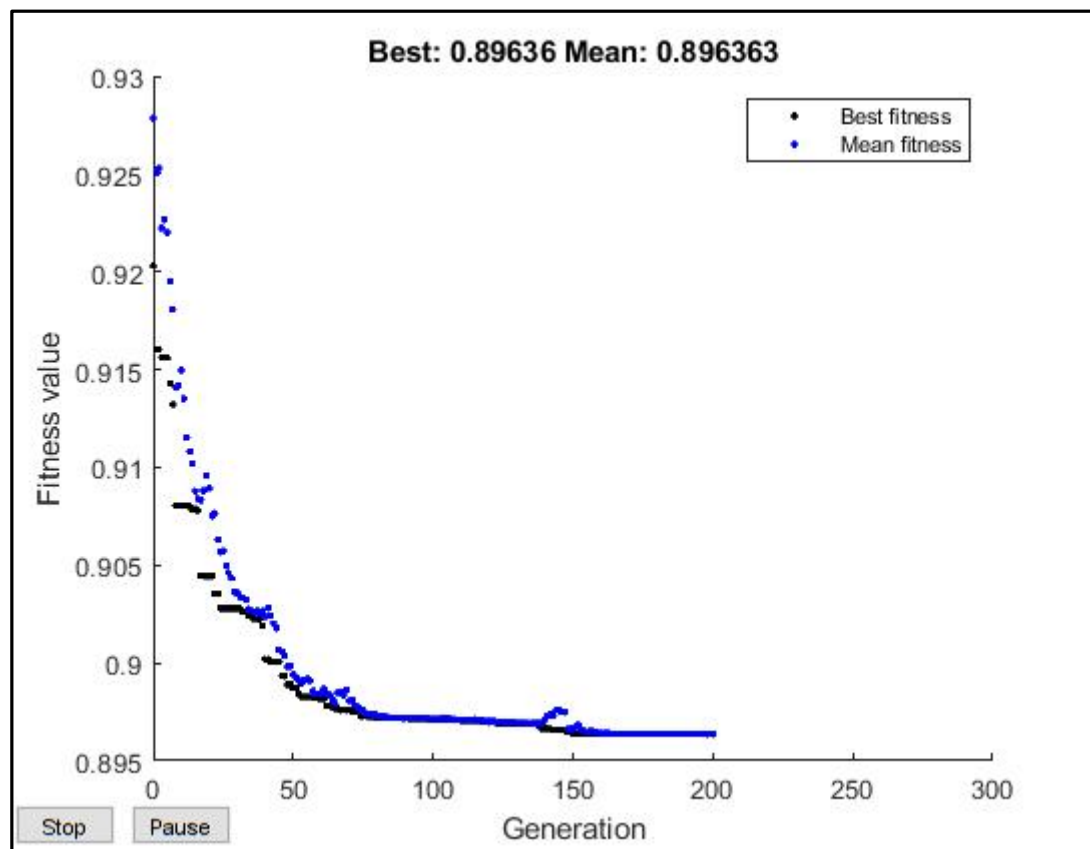


Figure 5.2 Year 2 Fitness Value Evaluation for a population size of 10 and Generation of 300

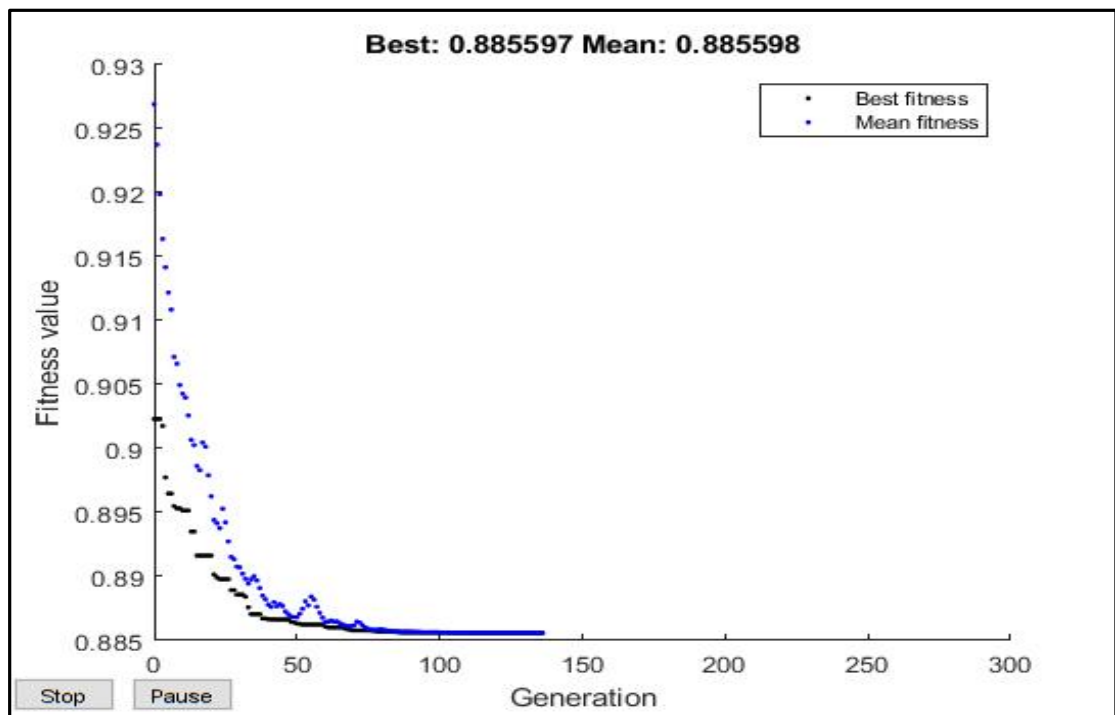


Figure 5.3 Year 2 Fitness Value Evaluation for a population size of 100 and Generation of 300

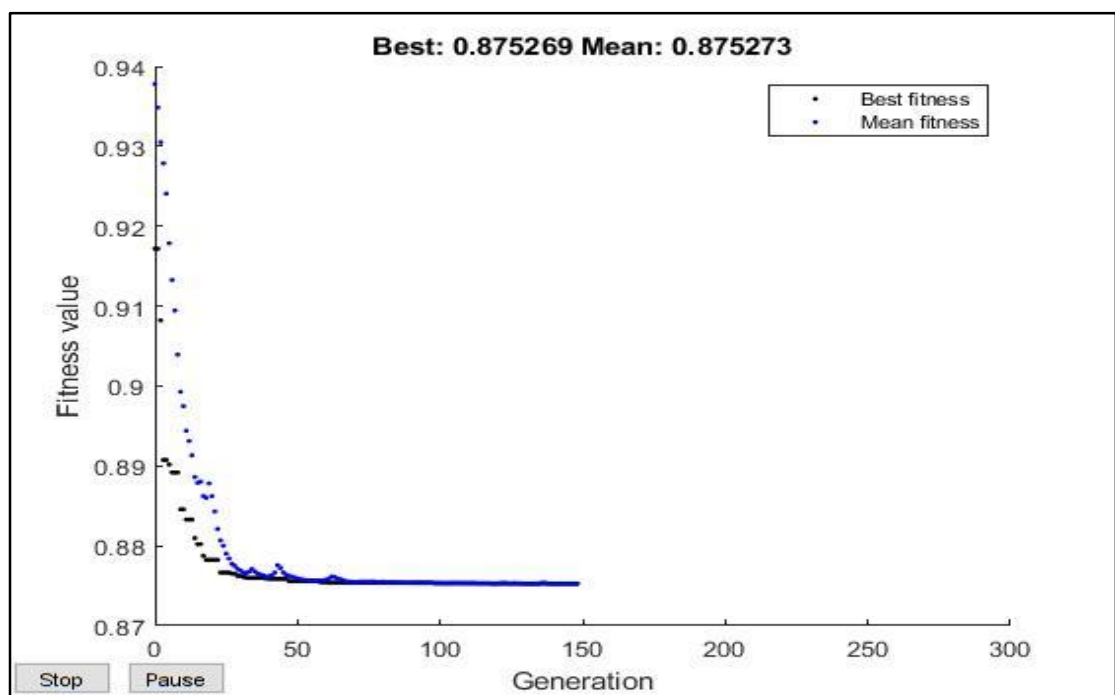


Figure 5.4 Year 10 Fitness Value Evaluation for a population size of 100 and Generation of 300

The conducted parameter variable test; to observe how changing specific design parameters influences the optimization results for a given period highlighted different combination outcomes per steam design parameter test. Also, as observed from Figure 5.5-5.10 the results from the optimized case (i.e. the base case before parameter variation) show the best performance overall compared to any possible variation of the design parameter.

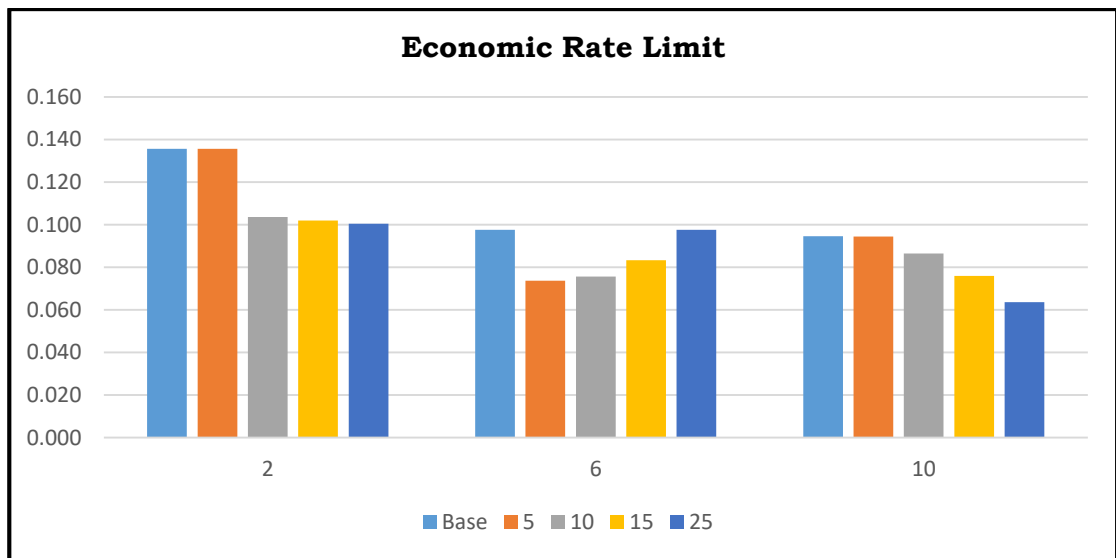


Figure 5.5 Economic rate limit CSI efficiency variation for Year 2-10

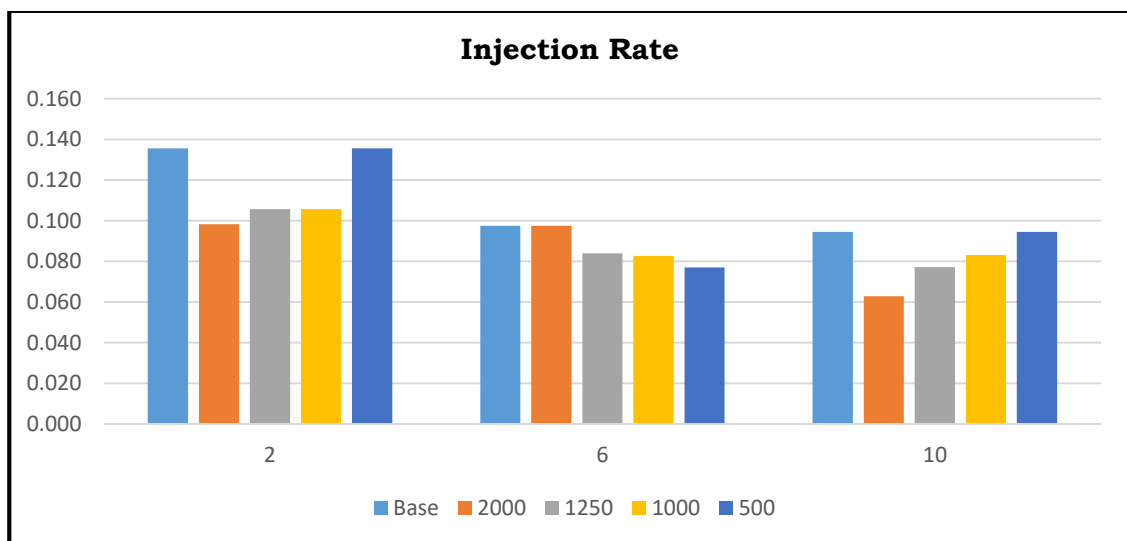


Figure 5.6 Steam injection CSI efficiency variation for Year 2-10

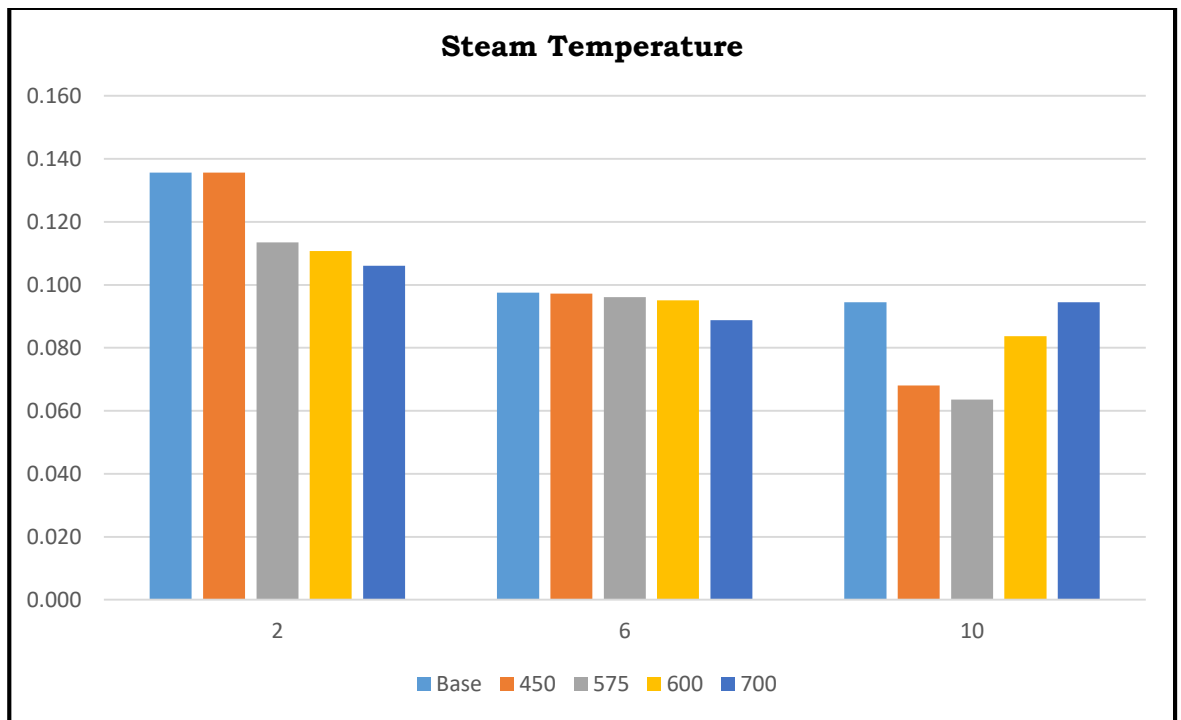


Figure 5.7 Steam temperature CSI efficiency variation for Year 2-10

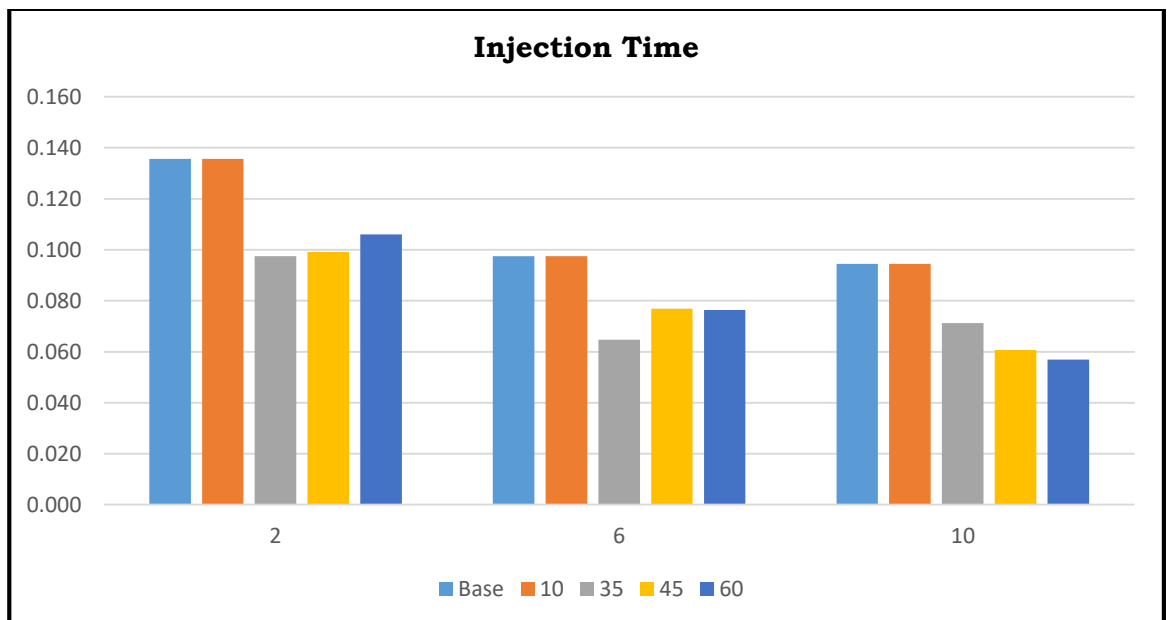


Figure 5.8 Injection time CSI efficiency variation for Year 2-10

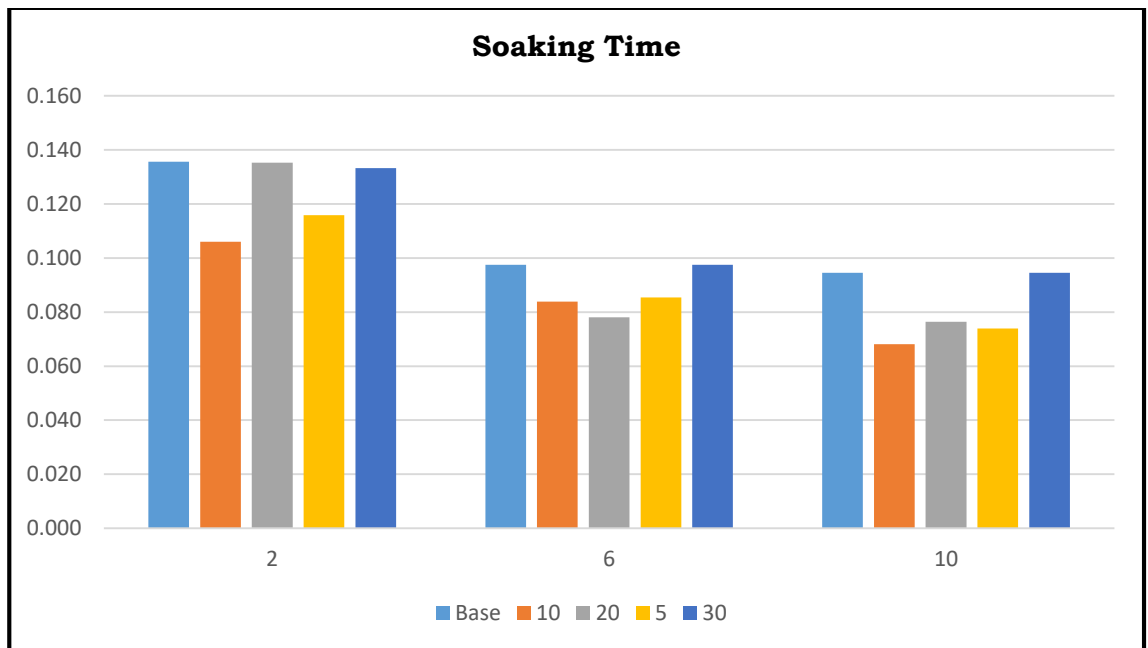


Figure 5.9 Soaking time CSI efficiency variation for Year 2-10

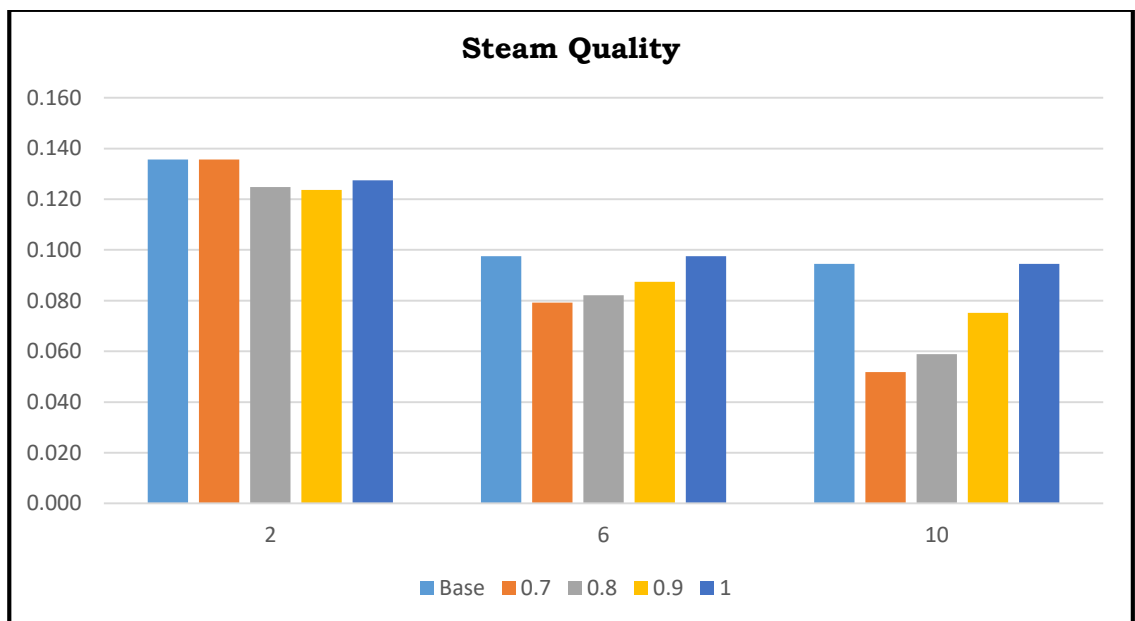


Figure 5.10 Steam CSI quality efficiency variation for Year 2-10

A comparative field analysis for Amal and Ikiztepe fields with the obtained data for the two fields showed a better overall field performance in terms of efficiency of the CSI for Amal field in comparison to Ikiztepe field. With field comparison performed at different values for anisotropy but same Lorenz coefficient. From the optimization results, Amal field requires lesser steam temperatures and higher steam injection rates, while the Ikiztepe field exhibits a contradictory behavior for both parameters. It was also observed that while the above-mentioned behavior holds at high isotropy values, at low isotropy values efficiencies for both fields do not differ gravely. Although the higher steam injection rate behavior for Amal field still holds, other parameters are also comparable. Table 5.3 and 5.4 illustrates these observed behaviors and the ability of the tool to predict optimal CSI steam design parameters and recovery efficiency for a field. The rest of this focuses mainly on the Amal field in solar modeling and economic feasibility analysis.

Table 5.3 Optimized CSI Steam design parameter for Amal field

	Units	Year 2	Year 4	Year 6	Year 8	Year 10
CSI Efficiency	Fraction	0.31	0.50	0.25	0.37	0.66
Temperature	°F	595.89	450.01	568.82	531.49	450.02
Quality	Fraction	0.70	1.00	0.70	1.00	1.00
Injection rate	bbl/day	1999.24	502.09	1999.98	500.08	1479.28
Injection time	days	60.00	10.03	10.04	30.25	13.04
Soaking Time	days	29.99	30.00	30.00	30.00	10.03
Economic Rate Limit	bbl/day	5.03	25.00	8.01	25.00	5.08

Table 5.4 Optimized CSI Steam design parameter for Amal field

	Units	Year 2	Year 4	Year 6	Year 8	Year 10
CSI Efficiency	Fraction	0.23	0.15	0.17	0.13	0.33
Temperature	°F	627.72	450.19	699.97	627.80	700.00
Quality	Fraction	1.00	1.00	0.70	1.00	1.00
Injection rate	bbl/day	502.00	500.87	500.14	1999.79	500.21
Injection time	days	10.05	60.00	27.13	10.07	10.01
Soaking Time	days	10.01	17.75	10.08	24.61	30.00
Economic Rate Limit	bbl/day	5.00	5.00	25.00	25.00	5.00

5.2 Solar Field Performance

With the equations and methods posed to analyze solar field performance, solar models for a location can be created to estimate the steam flow rate, temperature, and steam quality for a given solar field design and the location solar potential. And it is aimed to postulate the feasibility level of this technique both technically and economically. Amal field data and results were used to build a base LFR solar plant of 7MWt modeled to both in terms of area and system rating to best match the sample solar field system. Subsequently, the MATLAB code for both models was generated to aid analysis and calculations outside the SAM user-interface. The standard system control unit of the modular solar boiler to which SAM is modeled after contains 128 primary reflector unit of single loop area (SLA) 513.6 m². But the changes made in Table 5.X were basically to conform the system as best possible to the rating and area of the Amal field solar system. Alongside the aforementioned changes, incidence angle modifiers and polynomial heat loss models are used for the optical characterization and receiver heat loss analysis. No storage systems are accounted for and neither are any heat exchangers. While heat exchangers and storage systems curb the issue of control instability, temperature, and steam availability, the tradeoff here helps to cut costs of an already capital intensive system. Tracking power is set at 0.2 W/m² and Freeze protection at 10°C.

The system output performance analysis focused on the steam content produced primarily in terms of the steam outlet temperature and mass flow rate. The other performance analysis can be sectioned into the solar field collector and receiver in terms of optical and thermal efficiencies. Performance annual profiles for steam mass flow rate, temperature, and collector optical efficiency as depicted in Figure 5.13, 5.14 and 5.15. As observed from the findings of both models, the IPH model has a higher steam mass flow rate performance output. However, annual steam temperature per day and collector efficiencies profiles indicate that higher steam temperatures and collector efficiencies are attainable via the DSLF. Although for the same locational weather resources of Thumrait, Oman, the DSLF model stably

achieved and maintained higher temperatures most times over the year than the IPH model over the same period as shown in Figure 5.16,5.17. Since location weather resources variables are the same for both models; it was observed that for IPH models the periods of high wind speed and to some small extent relative humidity are susceptible to the dips in output even in peak summertime in this region. These factors regardless seem not to have any tremendous effect on the more stable DSLF model which largely maintains steam outlet temperature. The same can be said in regards to the hourly optical efficiency, thermal power of the steam, and thermal power produced by the field. With the same trend observed in the thermal losses for both models, these are depicted in Figure 5.19-5.21.

Table 5.5 Input Values for collector and field

Name	IPH	DSLF	Unit
Design point DNI	950	950	W/m'
Target solar multiple	1	-	
Heat sink/ Boiler operating pressure	115	100	bar
Field inlet temperature	40	50	°C
Field outlet temperature	-	310	°C
Number of modules per section	24	24	
Collector azimuth angle	0		degree
Ambient temperature	35	35	°C
Min Single loop flow rate	-	0.5	kg/s
Field pump efficiency	0.85	0.85	
Reflective aperture area	720	720	m ²
Length of collector module	44.8	44.8	m
Tracking error	0.9	0.9	
Geometry effects	0.7	0.7	
Mirror reflectivity	0.9	0.9	
Mirror soiling	0.9	0.9	
General optical error	0.9	0.9	

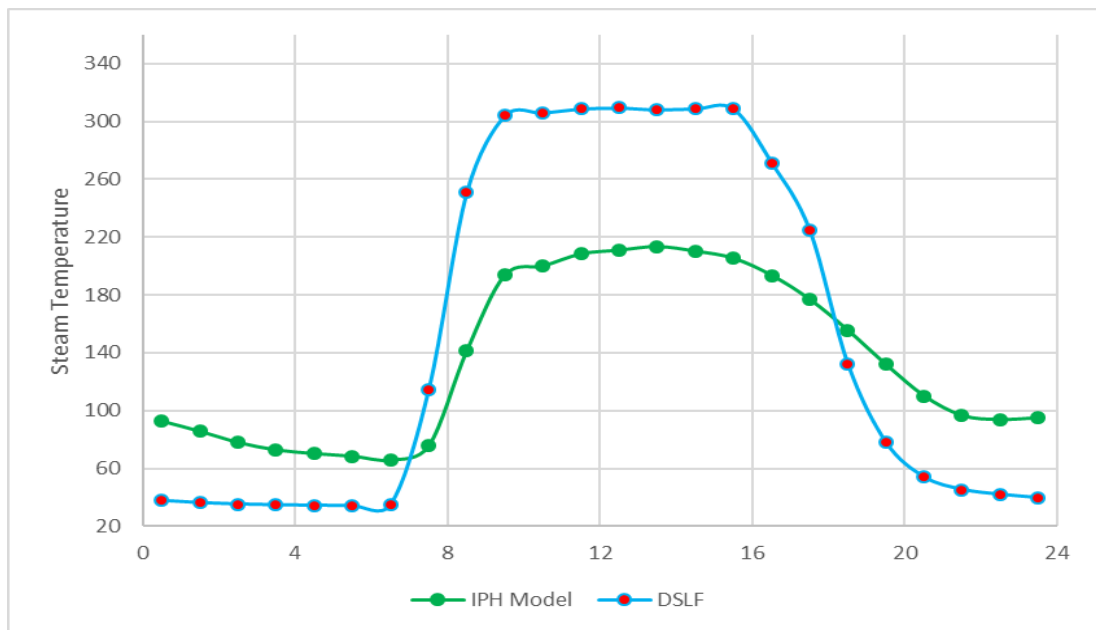


Figure 5.13 Annual daily steam temperature profile for IPH and DSLF models

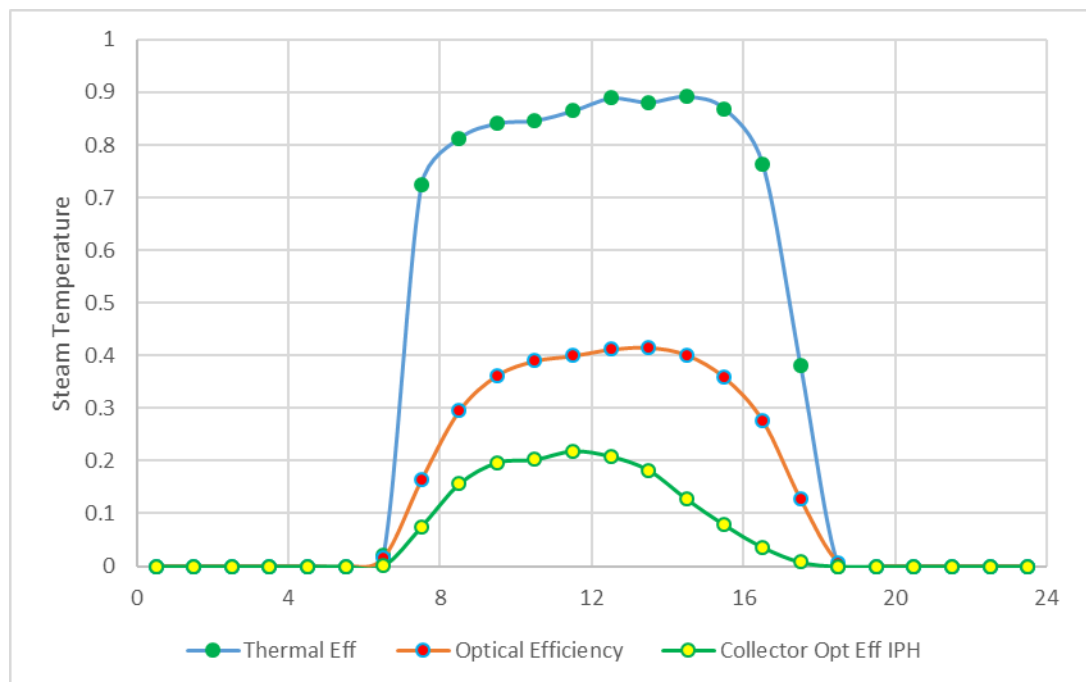


Figure 5.14 Annual Profile of Thermal and Collector optical efficiencies for DSLF and collector efficiency for IPH model

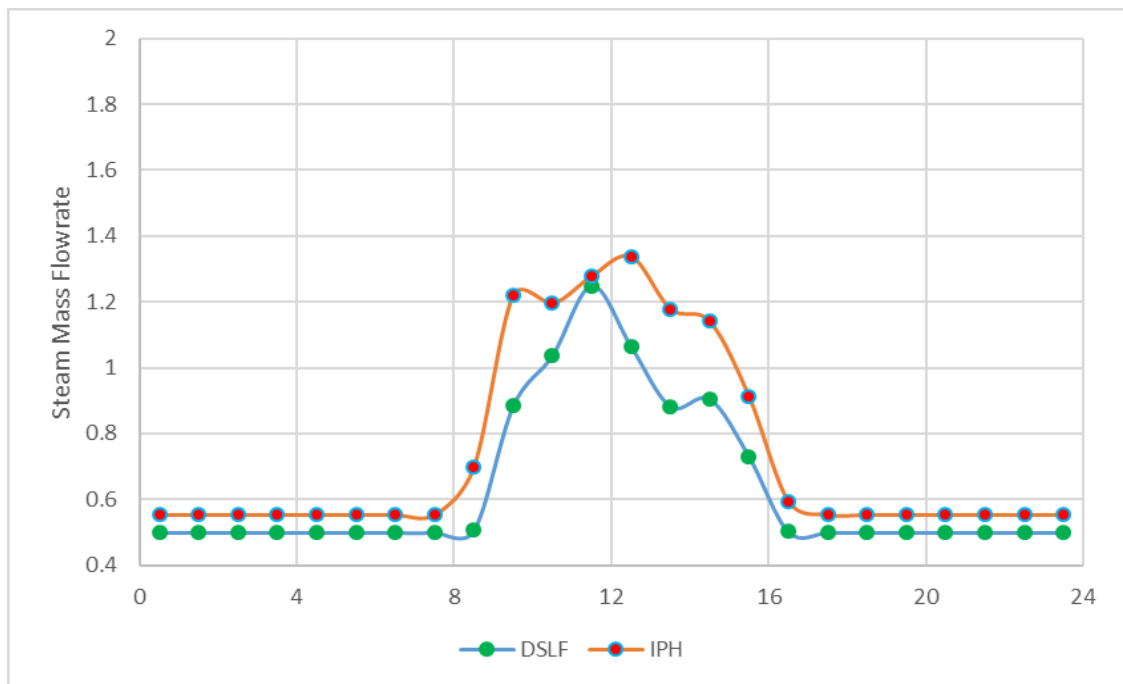


Figure 5.15 Annual steam mass flowrate profile for DSLF and IPH model



Figure 5.16 Hourly wind (top) and field outlet temperature (bottom) for IPH model

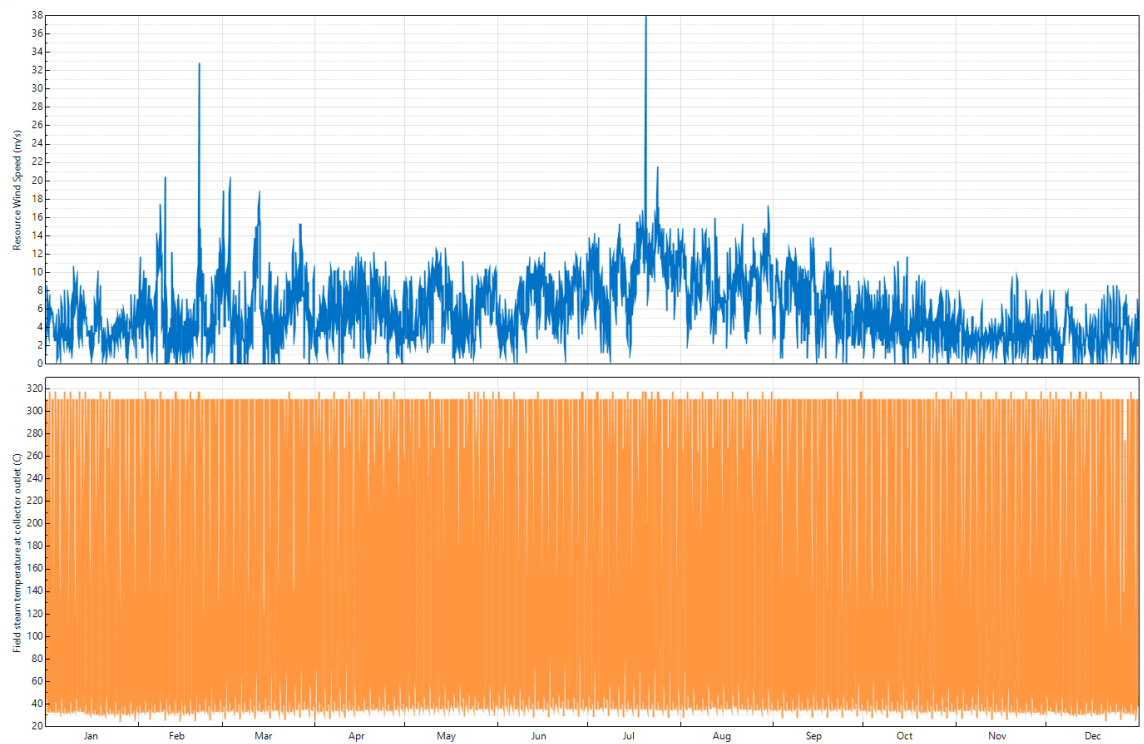


Figure 5.17 Hourly wind (top) and field outlet temperature (bottom) for DSLF model

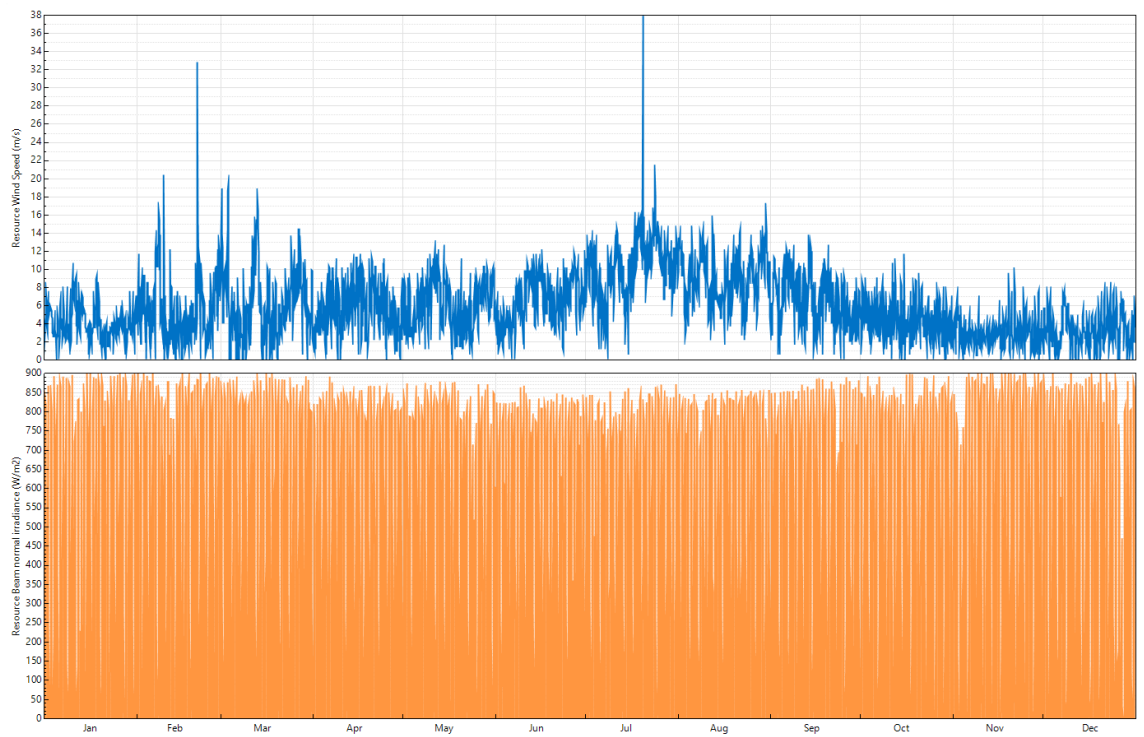


Figure 5.18 Hourly wind (top) and irradiance (bottom) for Both models

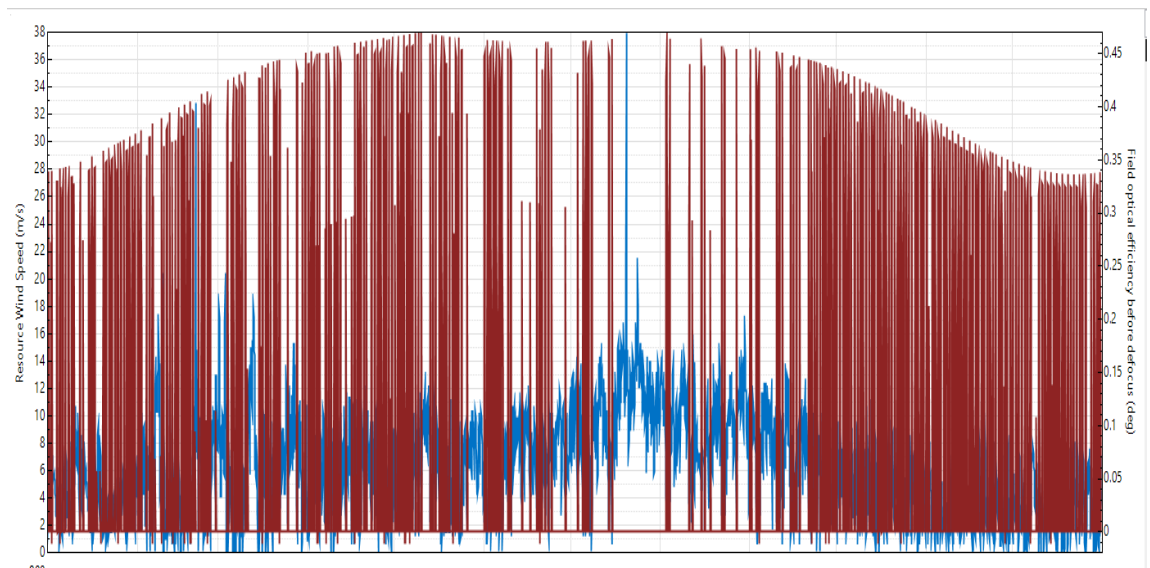


Figure 5.19 Hourly optical efficiency (red) and wind speed (blue) in the IPH model

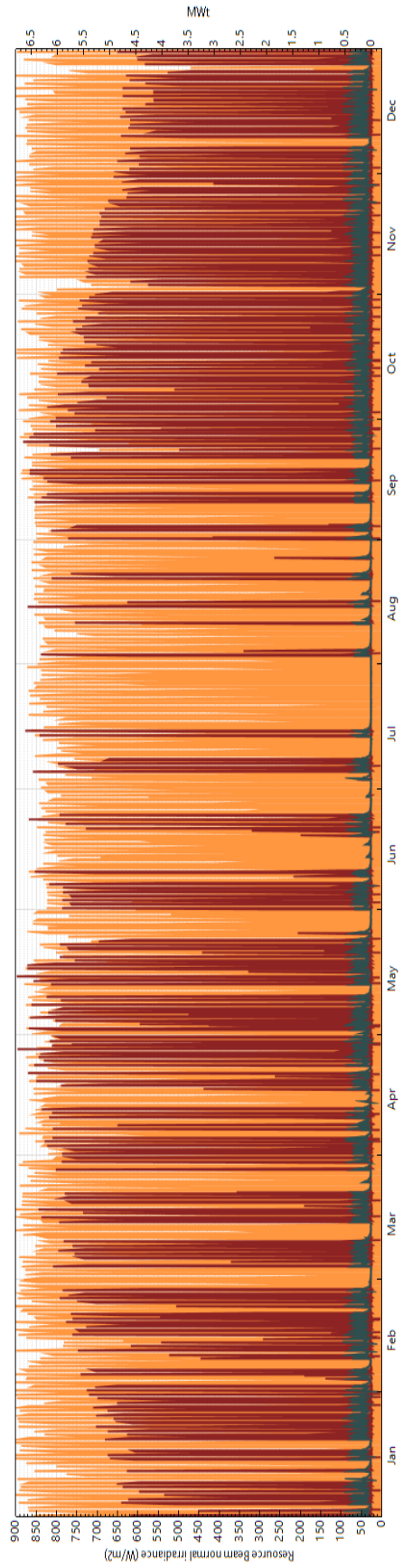


Figure 5.20 IPH Thermal power produced (red) and losses (dark) for available irradiance

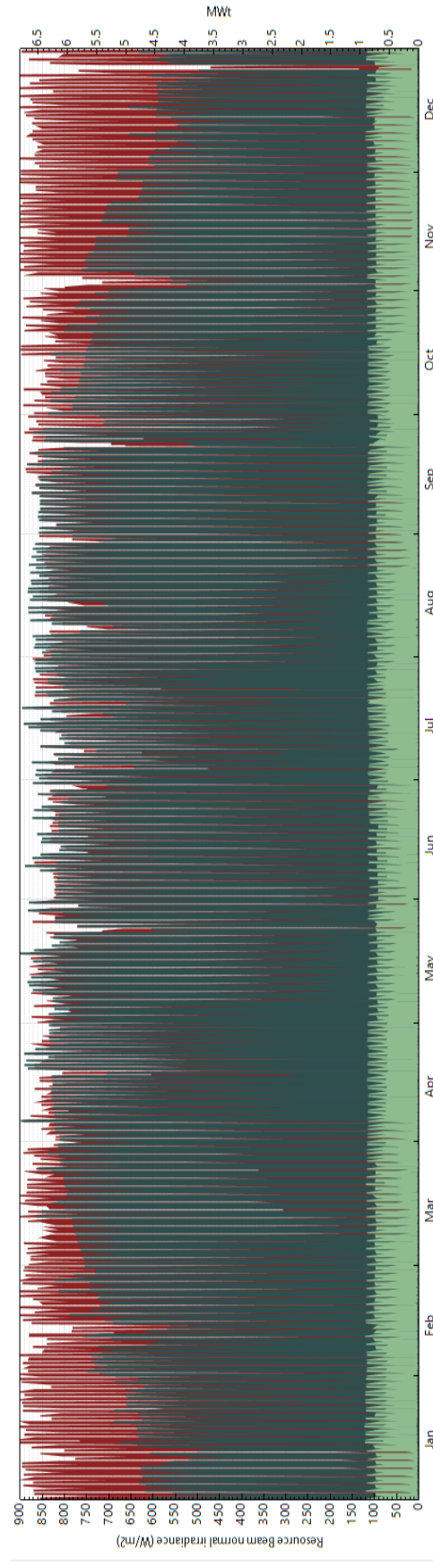


Figure 5.21 DSLF Thermal power produced (dark green) and losses (light green) for available irradiance

SAM was used to perform a parametric analysis was done for both models to observe how design parameters affect the optical and thermal performance of respective models. Given the plethora of inputs required by the model, a few optical and thermal design parameters such as length of collector, collector azimuth angle, heat transfer fluid, saturation pressure, heat loss, and IAM constant. For the IPH model, higher temperatures are attainable with higher saturation pressures to a maximum of 220.5 bar. The collector azimuth angle of 0 (i.e. when the system is oriented in a North-South direction), yields a top overall system performance in terms of annual output; however, it doesn't yield the best optical efficiency as seen in Figure 5.22 and Figure 5.23. for 5 collector azimuth angles (-90, -45, 0, 45, 90). Increasing collector length and heat loss polynomial constants reciprocate an increasing receiver heat loss of the solar system as can be seen in Figure 5.24. A PTC heat exchanger (HXIPH) enabled model was created with generally the same parameters as for the IPH and DSLF models, to see how its performance compares with the IPH and DSLF DSG models. Of the HXIPH heat transfer fluids analyzed included Therminol 59, Therminol 66, Therminol VP-1, and Pressurized Water; indicates Therminol VP-1 commonly used in oilfield practices performs best. While the HXIPH model generally performs it circumvents a keystone of this study that requires direct steam and offsets possible costs from heat exchangers.

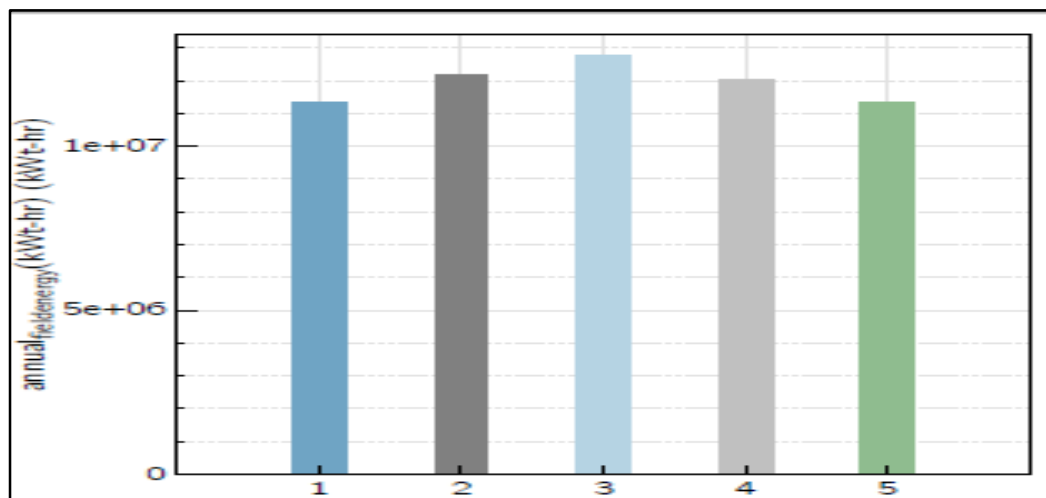


Figure 5.22 Annual output of the IPH model for different collector azimuth angles Left (-90, -45, 0, 45, 90) Right

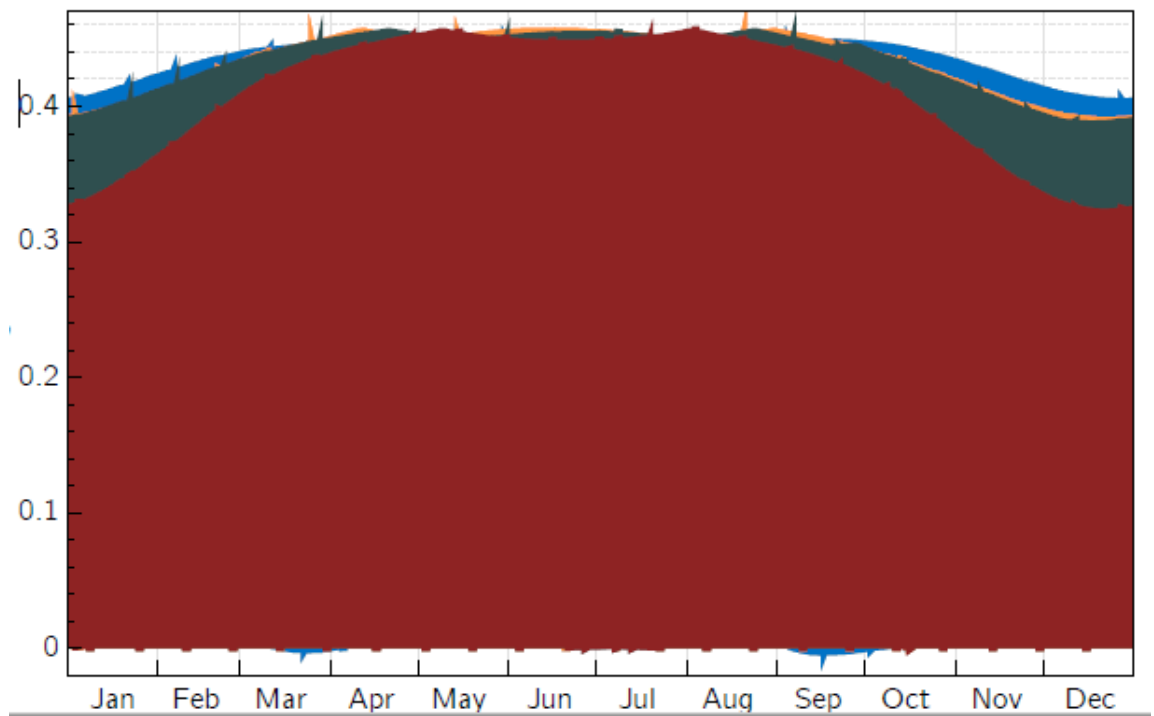


Figure 5.23 Optical efficiency at different collector azimuth angles (-90, -45, 0, 45, 90) (red) collector angle = 0

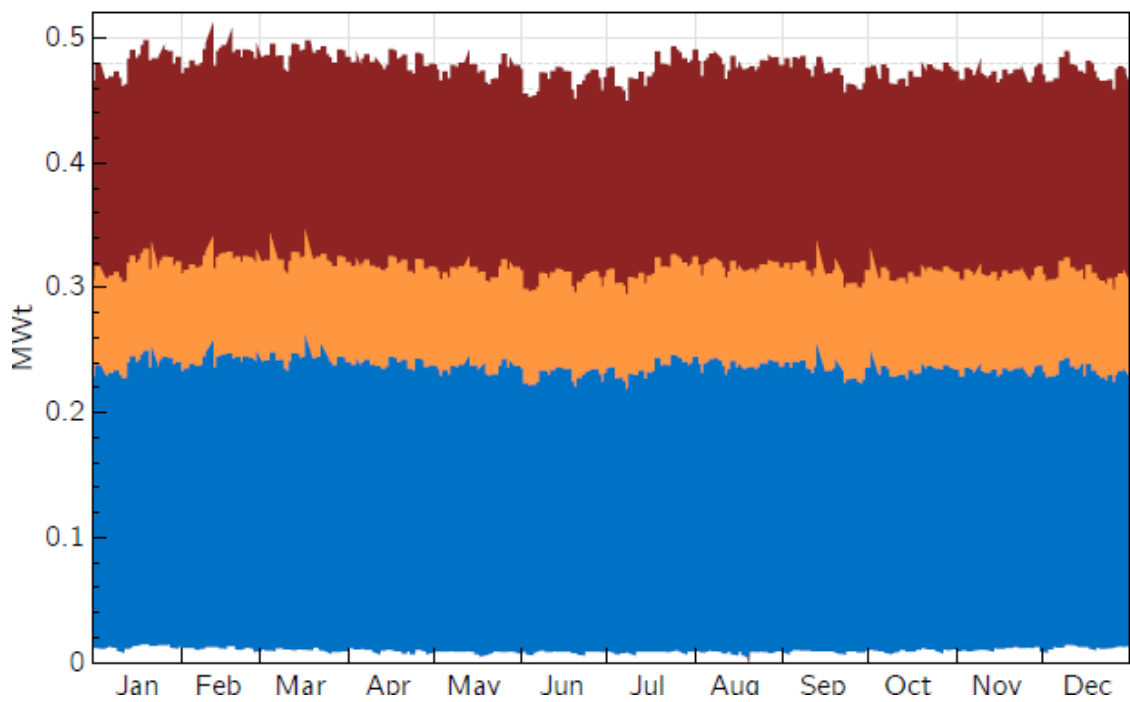


Figure 5.24 Thermal loss performance of the IPH model for varying collector length, longest (red) and shortest (blue)

5.3 Economic Analysis

The optimized steam design parameters for a given reservoir or field obtained via the optimization procedure coupled with the annual solar system temperature and flowrate output calculates the annual availability factor of solar steam. This determines the solar steam fraction f_{solar} available for the CSI. Which is used to analyze the economic feasibility of solar-steam EOR application for an optimum period Year 10 since it has the maximum CSI efficiency Table 5.6 shows the CSI steam solar fraction for years 2-10 for the optimized steam design criteria for Amal field.

Table 5.6 Solar fraction of steam from CSI-SOL combination test for Amal Field

Year	CSI Efficiency	Injection rate (bbl/day)	Steam Temperature (°F)	Q_{avl}	T_{avl}	f_{solar}
2	0.31	1999.24	595.89	100	96	96
4	0.50	502.09	450.01	100	100	96
6	0.25	1999.98	568.82	100	99	96
8	0.37	500.08	531.49	100	99	96
10	0.66	1479.28	450.02	100	100	100

Estimated recovery from the optimized CSI calculated is based on the efficiency, steam injection rate, and injection time for 1 cycle per annum; discounted as previously described for each yearly period, and shown in Table 5.8. And as can be seen the recoveries for each period are not very promising, given the low recovery efficiency values of the CSI procedure. The NPV sensitivity analysis for this project primarily focuses on the oil price and solar field costs for the feasibility analysis since they contribute most to the expenses and revenues. Straight-line depreciation and net allowable depletion techniques were applied for this case since they had higher present values compared to the other depreciation and depletion techniques. Oil prices of (25,50,100) USD, solar field costs (50,100,150) USD, for low mid and high cases respectively, and also site and indirect costs were included in

the sensitivity analysis. Figure 5.25 shows a Tornado plot of the abovementioned parameters and as seen in the plot solar-CSI is most sensitive to the oil price, then solar field cost. Tables 5.7-5.10 show the breakdown of NPV analysis for the MID case with a negative NPV value of - \$157,890, thus the solar-CSI is unfeasible at the MID economic prices, a solar fraction of 100% and optimized efficiency, steam injection rate, temperature, and injection time. The NPV analysis also indicates an oil price of approximately 52.564 USD is required oil price for the project to break-even at the given economic, technical, and field conditions. However, this could change easily, especially if the solar fraction which is another key factor to the economic viability of the project becomes very low. And in such cases given current global oil market trends required prices would be too high. For example, at a solar fraction of 33%, the required oil price to break even is approximately 98.1 USD almost twice the break-even price at a 100% solar fraction, and such prices might be unattainable in the current oil market; thus, making solar-steam more unfeasible in such a case.

Table 5.7 Yearly oil recovery from CSI-SOL and revenues for NPV analysis

Year	10	Solar Fraction	1	Operating and Maintenance Costs
Steam Injection rate (bbl/day)	1479.28	Steam Oil Ratio	1.5	
Injection time	13.04	Cycle	1	
Efficiency	0.66	Incremental Recovery (Np)	Revenues (\$)	
Year	Injected			
1	19289.8	12731.28	636563.8	\$106,611
2	19289.8	12731.28	636563.8	\$110,654
3	19289.8	12731.28	636563.8	\$114,898
4	19289.8	12731.28	636563.8	\$119,355
5	19289.8	12731.28	636563.8	\$124,035
6	19289.8	12731.28	636563.8	\$128,948
7	19289.8	12731.28	636563.8	\$134,108
8	19289.8	12731.28	636563.8	\$139,525
9	19289.8	12731.28	636563.8	\$145,213
10	19289.8	12731.28	636563.8	\$151,186

Table 5.8 Depreciation values for NPV analysis

	Depreciation		Net Revenues After Expenses, Depreciation
Year	Straight-Line	Sum of Year Digits	
0	\$0.00	\$0.00	\$0.00
1	\$284,243	\$516,805	\$289,030
2	\$284,243	\$305,051	\$282,164
3	\$284,243	\$271,156	\$274,954
4	\$284,243	\$237,262	\$267,384
5	\$284,243	\$203,367	\$259,435
6	\$284,243	\$169,473	\$251,089
7	\$284,243	\$135,578	\$242,325
8	\$284,243	\$101,684	\$233,123
9	\$284,243	\$67,789	\$223,462
10	\$284,243	\$33,895	\$213,317
Total	\$2,842,426	\$2,042,058	\$2,536,282

Table 5.9 Depletion values for NPV analysis

Depletion			
Cost	Gross	Net	Allowable
\$0.00	\$0.00	\$0.00	\$0.00
\$44,560	\$127,313	\$122,855.02	\$122,855.02
\$44,560	\$127,313	\$120,833.77	\$120,833.77
\$44,560	\$127,313	\$118,711.46	\$118,711.46
\$44,560	\$127,313	\$116,483.03	\$116,483.03
\$44,560	\$127,313	\$114,143.18	\$114,143.18
\$44,560	\$127,313	\$111,686.34	\$111,686.34
\$44,560	\$127,313	\$109,106.66	\$109,106.66
\$44,560	\$127,313	\$106,397.99	\$106,397.99
\$44,560	\$127,313	\$103,553.89	\$103,553.89
\$44,560	\$127,313	\$100,567.58	\$100,567.58
\$445,600	\$1,273,128	\$1,124,339	\$1,124,339

Table 5.10 Tax and net cash flow after-tax values for NPV analysis

Net Revenues After Expenses, Depreciation, Depletion	Tax	Income Tax	Net Cash Flow (NCF) After Tax
\$0.00	\$0.00	\$36,857	(\$3,108,740)
\$122,855.02	\$36,857	\$36,250	\$493,096
\$120,833.77	\$36,250	\$35,613	\$489,660
\$118,711.46	\$35,613	\$34,945	\$486,052
\$116,483.03	\$34,945	\$34,243	\$482,264
\$114,143.18	\$34,243	\$33,506	\$478,286
\$111,686.34	\$33,506	\$32,732	\$474,109
\$109,106.66	\$32,732	\$31,919	\$469,724
\$106,397.99	\$31,919	\$31,066	\$465,119
\$103,553.89	\$31,066	\$30,170	\$460,284
\$100,567.58	\$30,170	\$337,302	\$455,207
\$1,124,339	\$337,302	\$36,857	\$4,753,802

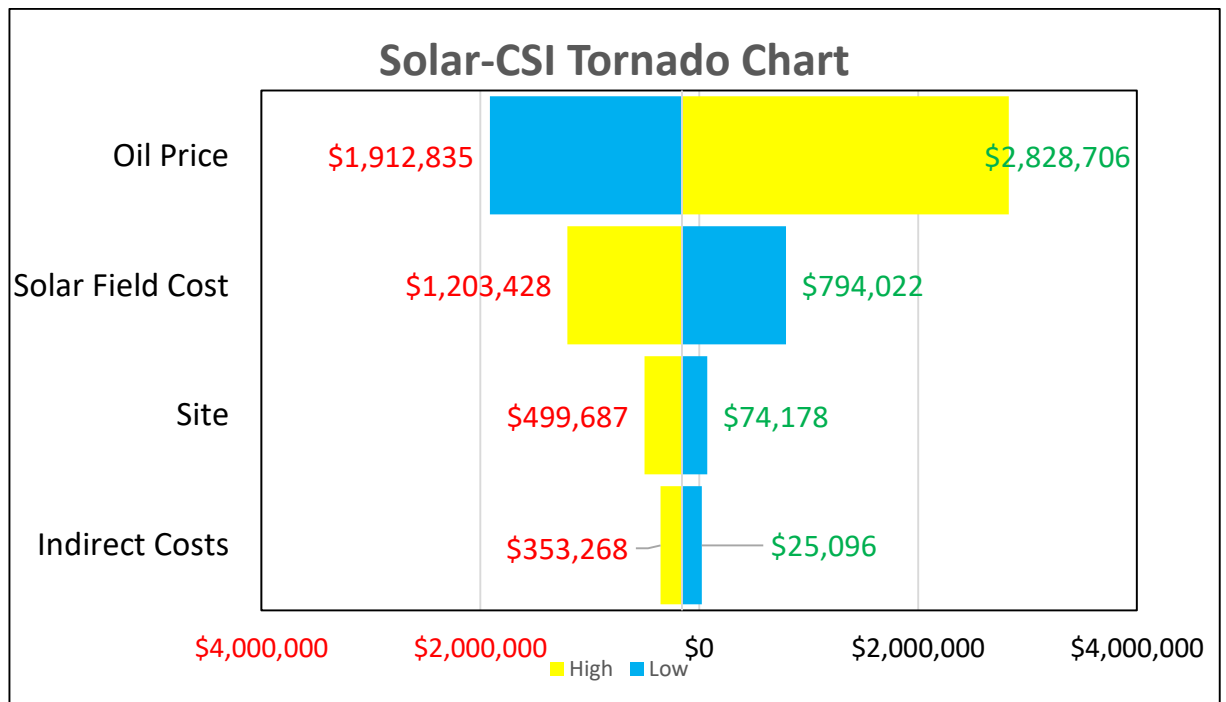


Figure 5.26 Sensitivity analysis of NPV to major economic parameters

Table 5.11 NPV analysis for major economic parameters

Parameter	Low	High	Mid
Indirect Costs	\$25,096	\$353,268	\$157,890
Site	\$74,178	\$499,687	\$157,890
Solar Field Cost	\$794,022	\$1,203,428	\$157,890
Oil Price	\$1,912,835	\$2,828,706	\$157,890

5.4 Sustainability

The business as usual approach of profit maximization by operators of oil firms or integrated oil companies (IOCs), can be a huge deterrent to the sustainability trend and even leave such firms behind as the advancement of the world is towards a long-term approach with environmental considerations coming ahead of maximizing profits. As mentioned above depending on the economic, technical, and field performance the solar-CSI might prove feasible or unfeasible. However, the feasibility analysis of such technical and capital intensive in the current energy climate for energy sources that are anti-polluting or little to no greenhouse gas emissions GHG to combat the issue of global warming, economics, and technical performances cannot be the sole conditions for assessing the feasibility of energy projects or other projects at large. Thus, the inclusivity of other externalities such as environmental pros and cons of a project, the social cost of the project, and for fossils the social cost of carbon becomes a primary requirement for a feasibility study. Such externalities are very broad, sometimes unclear, and problematic to address as seen by several global protocols and agreements. Two forms for accounting for such externalities were used in this study namely: investment tax credit (ITC) and emission savings.

Adopting solar heating applications for oil operations of recovery, exploration, etc. could help move the sustainability in the direction of new paths of profits along with environmental considerations or at best, profit after environmental considerations. Replacing steam generation with solar rather than the normal

gas-fired boiler, is analogous to using your abundant source to replace the obtaining of a scarcer resource by either the same hugely scarce resources or another resource entirely, likely less abundant. This helps alleviate resource usage and direct it towards other necessary or demanding areas of the resource. For example, the 7 MWt Amal solar plant referred to in this study, by the usage of solar for direct steam Oman can save about 80% of its gas presently used for EOR. Also reductions of CO₂ emissions levels by a factor of 238 times (by a ratio of 23.8 g CO₂/MJ with a gas setup to 0.1 g CO₂/MJ with a solar setup) (Islam 2019). Moreover, such systems help to have broad effects, especially when implemented at large scales. Like the 1GW Miraah Project, Oman is estimated to save over 300,000 tons of CO₂ annually, which is equivalent to planting 12.5 million trees annually or 22,00-27,500 acreage of trees. Also the equivalent to removing 63,000 internal combustion engine cars (GlassPoint 2017).

The screening tool adopts an investment tax credit of 25% and calculates the emissions savings from using solar-CSI in place of the alternatives polluting sources. The emissions accrued by the use of carbon-emitting energy sources to generate the steam required for the CSI is calculated using the carbon emission rate (gCO₂/MJ), the energy required per barrel (MJ/bbl) of steam, and carbon costs (\$/Ton). Also with the total emission savings, the tree equivalent and acreage from using solar-CSI are estimated. These analyses were performed using data by Brandt and Unnasch (2010) the energy demand per barrel was estimated as 418 MJ/bbl at 100% quality steam at 500 psia, emission factor of 0.056 kgCO₂/MJ (Hone,2011), and a carbon cost of \$40/ton (Chaar et al, 2015). Tree Equivalent According to Keystone 10 Million Trees Organization the annual carbon per tree is 48 lbCO₂/Tree and an acre contains 436 Trees in 10x10 dimensions (DOE,2010). These environmental gains of using solar-CSI steam generation over fossil fuels can be estimated and weighed against available options by considering the externalities.

As an example, if natural gas was used to produce the annual 19289.8 bbl of steam required for CSI in Amal field the environmental externalities can be calculated as:

Energy Requirement = Steam amount (bbl) × Energy rate (MJ/bbl)

$$= 19,289.8 \times 418 = 8,063,136.4 \text{ MJ}$$

Carbon Emissions = Energy Requirement (MJ) × Emission rate (kgCO₂/MJ)

$$= 8,063,136.4 \times 0.056 = 451535.6 \text{ kgCO}_2$$

Emissions Savings = Carbon Emissions (kgCO₂) × Carbon Cost (\$/ton)

$$= 451535.6/907 \times 40 = \$19913.4$$

Tree Equivalent = Carbon Emissions (kgCO₂) / Tree rate lbCO₂/Tree

$$= (451535.6/2.205) / 48 = 4266.21 \text{ Trees}$$

Tree Acreage = Tree Equivalent / Trees per acre

$$= 4266.21 / 436 = 9.785 \text{ acres}$$

And over the 10-year duration of the CSI procedure these amount sum up to sufficient amount as shown in Table 5.12

Table 5.12 10-year analysis for environmental externalities and considerations to feasibility analysis

Parameter	Value
Energy Requirement (MJ)	8,063,136.4
Carbon Emissions (kgCO ₂)	4,515,356
Emissions Savings (\$)	199,134
Emissions Savings (\$) Discounted (10%)	72,015
Tree Equivalent (Trees)	42,662.1
Tree Acreage (Acres)	97.85

Other social costs that can be considered include the opportunity of using natural gas which least polluting for other industrial purposes. Taking into consideration the availability of the resources itself and using the resource (natural gas) to substitute other more polluting fossils like coal. A complete environmental, economic, technical, and social analysis is not yet fully

encapsulated or applicable in many industrial projects or activities but would serve as the best measure of feasibility of any project with EOR and Solar-EOR nonetheless removed from such standards.

Also, at an ITC of (25-30%) the capital investment for renewable energy sources like solar project deductible from the annual income tax for the project, financial viability might be possible as is the case in this example.

Capital Investment Cost for this Project at given economic prices was estimated at \$3,108,740. Using an ITC of 25% CapEx, the ITC of the project was estimated at \$777,185.00. Deducting the income tax from ITC calculated for the project yields a net cash flow which when discounted solar-CSI turns out to be feasible with an NPV value of \$42,869.06. If emissions saving and ITC are included together in the analysis the NPV = \$114,884.

Table 5.11 Tax and net cash flow after-tax values for NPV analysis considering ITC

Year	Income Tax	Income Tax	Net Cash Flow (NCF) After-Tax without ITC	Net Cash Flow (NCF) After-Tax with ITC
0	\$0.00	\$0.00	(\$3,108,740)	\$529,953
1	\$36,857	\$740,328.49	\$493,096	\$525,910
2	\$36,250	\$704,078.36	\$489,660	\$521,666
3	\$35,613	\$668,464.92	\$486,052	\$517,209
4	\$34,945	\$633,520.01	\$482,264	\$512,529
5	\$34,243	\$599,277.06	\$478,286	\$507,615
6	\$33,506	\$565,771.15	\$474,109	\$502,456
7	\$32,732	\$533,039.16	\$469,724	\$497,039
8	\$31,919	\$501,119.76	\$465,119	\$491,350
9	\$31,066	\$470,053.59	\$460,284	\$485,378
10	\$30,170	\$439,883.32	\$455,207	\$5,091,104
Total	\$337,302		\$4,753,802	\$529,953

5.5 Cyclic Solar Steam Injection (CSSI) Screening Tool

As mentioned earlier, this study aims to develop a tool that can aid investors or engineers to assess the feasibility of using solar energy for steam generation for EOR purposes in a specific region. While the entire process culminates to this target so far it is quite complex following the different models and obtaining results for further analysis. Hence, a graphical user interface (GUI) that incorporates the optimization, solar, and integration models with an NPV analysis was created to provide a user-friendly platform for undertaking the feasibility analysis for solar-CSI. The tool uses a deterministic approach where the user inputs best estimates of each parameter that aptly represents the field, solar design, and resource of the location of interest and other economic parameters for NPV analysis. The tool which is created with MATLAB AppDesigner built-in functions has several sections and this section this chapter sheds some information on the GUI:

Reservoir Tab: Here the user inputs the reservoir parameters that best representative of the reservoir or field. The user can enter porosity, permeability, and total thickness either as 5 separate layers “Layered” or has a “Total/Average”, while other parameters are entered as single input data. Also, while there are 5 separate layered options the user can modify this to account for more layers by taking a pair or more layers as one-layer. All reservoir inputs parameters are within a suggested range; which the user is urged to adhere to as best possible. After entering reservoir inputs the user can click on the Confirm Input; to continue, the tool calculates the other reservoir inputs based on given inputs for other reservoir parameters. This quick process pops the calculated inputs and then the user can enter population and generation size for the optimization process ranging from [10:500] and [10:1000] population and generation respectively. While larger population sizes are recommended for an optimal solution, the user should be aware that larger sizes for both would cause the optimization process to take a longer time to achieve an optimal solution. Thus, sizes of 50 or lesser with several trials are recommended cautiously. After following these steps and not before the user the Start Optimization button or icon. When the

optimization process is done user would see the obtained solutions for each duration in the optimization steam design parameters.

Solar Tab: Firstly, users must select a weather file for the specific area or location. Then select an option for modeling the solar field either for an estimated field area or field rating (system capacity). Selecting trades off control of the other (user can input one or the other). After this, users can input parameters that best represent the solar system of interest. Users can model the optical performance using either solar position or collector incidence angle table or incidence angle modifier. However, users must be aware that the latter is location specific and should be used when the user has such information or data. Users can model the thermal performance by inputting temperature and wind constants for the receiver heat loss polynomial which also may vary according to the type of receiver. Due to simulator restriction, the saturation pressure is limited to 200 bar and an overall pressure of 220.5 bar. After these procedures user can click on the Start Simulation button to initiate the solar model

N.B: To model a solar model enclosed in a glasshouse, the user should set, mirror soiling = 1, and wind effect on receiver and collector performance should be reduced. However, if a solar model enclosed in a glasshouse is not needed, the glasshouse rate should be set equals to zero.

Economics: In this section, the user can integrate the optimization and solar model to achieve this can be done for all years to see how the model performs for each in terms of the solar fraction. Click on the needed Year N or Max Efficiency button then click Integrate to obtain the solar fraction for that set of optimized steam design criteria (steam temperature and steam flowrate) availability. The analysis allows the user to enter Economic parameters (prices, rates, period), and subsequently, click on the Economic-Feasibility Assessment button to make the NPV analysis. Next, the user can select either of the after-tax discounting methods to see how each affects the NPV. The application permits several options for after-tax discounting depreciation, depletion, depreciation & depletion, and none.

Plot Tab: Here the user can see bar plots of income tax, net revenues, optimized efficiency, average monthly temperature, and after-tax discounting calculations.

Appendix F shows an instructional schematic flow and layout for each Tab of the graphical user interface.

CHAPTER 6

CONCLUSION

Previously trained ANN models for CSI-EOR, from a previous thesis study by Yalgin (2018), are fused with GA optimization to predict optimal steam design parameters and estimate the efficiency of the CSI process for a given set of reservoir properties. The optimized steam design parameters are steam temperature, steam injection rate, injection time, soaking time, quality, and oil economic rate limit. The optimized was combined with a simple LFR solar model that was developed in SAM to estimate the fraction of steam deliverable by the solar system for CSI EOR operations. The results indicate a good performance of the optimization and solar combination. The fraction of steam generated is mainly reliant on the optimized steam targets of flowrate and temperature. For very hot (superheated region reaching) temperature target the IPH model struggles to meet the steam requirement as the weather conditions affect the collector efficiency and overall performance of the solar model. Thus in such situations, an auxiliary gas boiler would be required, also a glasshouse structure would be an added plus in locations with severe climatic conditions.

Economic feasibility analysis showed that the Capex intensive nature of solar-to-steam would have a huge effect on the financial performance of such projects. For the case study presented, the NPV analysis showed solar-to-steam would be unfeasible. The solar fraction of the steam is very influential to the extent of which the solar steam option becomes viable. The higher the solar fraction of steam for CSI the better chances of the procedure becoming feasible. This presents avenues towards the integration of solar to oil practice. However, low oil prices would render such avenues of seeking sustainability cumbersome and prolonged and even more so if solar fraction is low. Notwithstanding, economic viability should not be the only motivating reason for implementing such projects and other social and environmental externalities can make such projects promising as observe in when

accounting for ITC in the sample case of this study. While such incentives are not certain to last for long, one might say they are vital for intended developers or firms of the energy production and consumption industries. Since these help to improve their profitability and would pivot towards renewables and from less polluting energy sources. The incentives have to be developed to make renewables even more competitive than it already is with fossils for better sustainability.

CHAPTER 7

RECOMMENDATIONS FOR FUTURE WORK

The findings of this study can be ameliorated via the following:

- Incorporating a probabilistic approach that accounts for uncertainty to better illustrate model performances for solar-CSI
- Further optimization of solar-EOR technologies by comprehensive energy and exergy loss analysis.
- Developing measures suitably solar storage systems for solar-EOR so steady steam from solar can be broached.
- The current DSLF model tries to bypass a power cycle to estimate the solar system annual performance. The model can be improved by having a standalone model for direct steam generation.
- Spatial or areal restriction and integration patterns of the solar steam model in oilfields, to maintain output.
- Investigating the feasibility of combining Solar-CSI with CO₂ injection, heat transfer limitations of CO₂ post injection.

REFERENCES

- Abbas, R., Montes, M. J., Rovira, A., & Martínez-Val, J. M. (2016) "Parabolic Trough Collector or Linear Fresnel Collector? A Comparison of Optical Features Including Thermal Quality Based On Commercial Solutions," *Sol. Energy*, Vol. 124, Pp. 198–215, 2016.
- Abbas, R., Montes, M., Piera, M., & Martinez-Val, J., (2012). "Solar Radiation Concentration Features in Linear Fresnel Reflector Arrays". *Energy Conversion and Management*, 54(1), Feb., Pp. 133–144.
- Abbas, R., Munoz, J., & Martinez-Val, J., (2012). "Steady state Thermal Analysis of an Innovative Receiver for Linear Fresnel Reflectors". *Applied Energy*, 92, Apr., Pp. 503–515
- Abbas, R., Muñoz-Antón, Valdés, J. M. And Martínez-Val, J. M. High Concentration Linear Fresnel Reflectors, *Energy Convers. Management.*, Vol. 72, Pp. 60–68, 2013.
- Affandi M., Mamata, N., Kanafiah, S.N.A.M., & Khalid S.N. (2013). Simplified Equations for Saturated Steam Properties for Simulation Purpose. *Procedia Engineering* Volume 53, 2013, Pages 722-726
- Afsar C. (2018). Solar Generated Steam Injection in Heavy Oil Reservoirs. MS Thesis Graduate School of Natural and Applied Sciences of Middle East Technical University.
- Afsar, C. and Akin, S. (2016). Solar generated steam injection in heavy oil reservoirs: A case study. *Renewable Energy*, Elsevier, vol. 91(C), pages 83-89.
- Agarwal A. & Kovscek A.R. (2013). Solar-Generated Steam for Heavy-Oil Recovery: A Coupled Geomechanical and Reservoir Modeling Analysis. *SPE* 165329
- Agarwal A. Et Al. (2018). Sensitivity Analysis for Solar-Generated Steam for Enhanced Oil Recovery. *SPE-190075-MS*.
- Ali, H.M.K., Hassan, M.A.A. & Alkhider, M.D.M. (2015). Optimization of cyclic steam stimulation (CSS) using (CMG) software to increase the recovery factor. University of Khartoum.
- Ali, S. M. F. (1974). Current status of steam injection as a heavy oil recovery method. *The Journal of Canadian Petroleum Technology*. JCPT74-01-06.
- Anonymous, (2015). Concentrated Solar Linear Fresnel Reflector for power. Retrieved from <https://ellencis.wordpress.com>
- Arpaci, B. (2014). Development of an artificial neural network for cyclic steam stimulation method in naturally fractured reservoirs. Master's Thesis, The Pennsylvania University.

Artun, E., Ertekin, T., Watson, R.W. and J. Miller, J. (2008). Optimized Design of Cyclic Pressure Pulsing in a Depleted, Naturally Fractured Reservoir. Society of Petroleum Engineers. doi:10.2118/117762-MS

Artun, E. (2016). Characterizing reservoir connectivity and forecasting waterflood performance using data-driven and reduced-physics models. SPE 180488. SPE Western Regional Meeting. 24-26 May. Anchorage, Alaska, USA.

Asian Development Bank, (2013). Development of Solar and Wind Power in Karnataka and Tamil Nadu. Chapter 7, Pages 41-57. Retrieved from <https://www.adb.org/sites/default/files/publication/30232/development-solar-and-wind-power.pdf>

Bierman, B., Al-Lawatia, H., DiFilippo, M. and O'Donnell, J. (2018). Deploying enclosed trough for thermal EOR at commercial scale. AIP Conference Proceedings 030002, Issue 2033

Bierman, B., Treynora, C., O'Donnell, J., Lawrence, M., Chandraa, M., Farvera, A., von Behrens, P. and Lindsay, W., (2013). Performance of an Enclosed Trough EOR system in South Oman

BrightSource Energy (2011). Coalinga Project Facts: A BrightSource Energy Concentrating Solar Power Project.

http://www.brightsourceenergy.com/stuff/contentmgr/files/0/ad5d33a2bc493a5079b5dda609724238/folder/bse_coalinga_fact_sheet_033015.pdf

British Petroleum. (2017). BP Statistical Review of World Energy June 2017. London.

Buck R., Bräuning T., Denk T., Pfänder M., Schwarzbözl P., Pitz-Paal R. 2002: Solar-hybrid Gas Turbine-Based Power Tower Systems (REFOS). J. Solar Energy Eng. ASME, 124(1) (2002) 2–9.

Burkholder, F. and Kutscher, C. F. (2009). Heat loss testing of Schott's 2008 PTR70 parabolic trough receiver, NREL Technical Report, 2009.

Bybee, K., (2004). EOR/IOR: Displacement Optimization in Hydrocarbon Reservoirs. Journal of Petroleum Technology January 2004, Volume 56, Issue. 1. <https://doi.org/10.2118/0104-0045-JPT>

Chaar, M., Venetos, M., Dargin, J. and Palmer, D. (2015). Economics of Steam Generation for Thermal Enhanced Oil Recovery. SPE 172004 Presented at The 2014 SPE ADIPEC Abu Dhabi, November 22-25.

Chaari, M., Ben Hmida, J., Seibi, A. C., & Fekih, A. (2020). An Integrated Genetic-Algorithm/Artificial-Neural-Network Approach for Steady-State Modeling of Two-Phase Pressure Drop in Pipes. Society of Petroleum Engineers. Doi:10.2118/201191-PA

Chemisana D., Barrau J., Rosell J. I., Abdel-Mesih B., Souliotis M., and Badia F. (2013). Optical performance of solar reflective concentrators: A

simple method for optical assessment Renewable. Energy. 57 (2013) 120-129.

Chemisana, D., Barrau, J., Rosell, J.I., Abdel-Mesih, B., Souliotis M. F.Badia (2013). Optical Performance of Solar Reflective Concentrators: A Simple Method for Optical Assessment. Renewable Energy Volume 57, September 2013, Pages 120-129

CMG (2017). Computer Modelling Group. Reservoir Simulation Software, Calgary, Alberta, Canada

Conlon, W M, P Johnson, & R Hanson. "Superheated Steam from CLFR Solar Steam Generators." ASME Power Conference. Denver, USA, 2011.

Curry, D. (2005). Energy Systems - Dish Stirling Engine

De Leon, P., Brown, C.K., Margotis, W.J, & Nasr, H.L. (1979). Solar Technology Application to Enhanced Oil Recovery. Chapter 5 (Pages 40 & 43). Solar Energy Research Institute, Midwest Research Institute.

Dersch, J., Schwarzbozl, P., & Richert, T., (2011). "Annual Yield Analysis of Solar Tower Power Plants with GREENIUS". Journal of Solar Energy Engineering, 133(3), P. 031017

Eck, M., Feldhoff, J. F. & Uhlig., R., J. (2010). Thermal Modelling and Simulation of Parabolic Trough Receiver Tubes. Proceedings of the ASME 2010 4th International Conference of Energy Sustainability ES 2010 May 17-22, 2010, Phoenix, Arizona USA. DOI: [https://10.1115/ES2010-90402](https://doi.org/10.1115/ES2010-90402)

Eck, M., Uhlig, R., Mertins, M., Häberle, A., and Lerchenmüller, H (2007). Thermal load of direct steam generating absorber tubes with large diameter in horizontal linear Fresnel collectors." Heat Transfer Engineering 28, no. 1 (2007): 42-48.

Emera, M.K., & Sarma, H.K., (2005) Use of Genetic Algorithm to Predict Minimum Miscibility Pressure (MMP) Between Flue Gases and Oil in Design of Flue Gas Injection Project. SPE Middle East Oil and Gas Show and Conference, 12-15 March, Kingdom of Bahrain 2005. <https://doi.org/10.2118/93478-MS>

Emera, M. K., & Sarma, H. K. (2006). A New Genetic Algorithm (GA) Model Predicts Green-House Gas (GHG) and Reservoir Oil Interaction Parameters More Accurately in Geosequestration Applications. Society of Petroleum Engineers. doi:10.2118/100808-MS

Emera, M.K., & Sarma, H.K., (2008) A Genetic Algorithm-Based Model to Predict CO₂-Oil Physical Properties for Dead and Live Oil. Journal of Canadian Petroleum Technology February 2008, Volume 47, No. 2

Energy Sector Management Assistance Program (ESMAP). Development of Local Supply Chain: The Missing Link for Concentrated Solar Power Projects in India

Facao, J., and Oliveira, A. C., 2009. “Numerical simulation of a linear Fresnel solar collector concentrator”. In 8th International Conference on Sustainable Energy Technologies, no. September, pp. 2–7.

Faergestad, I. M. (2016). Heavy Oil. The Defining Series. Schlumberger-Oilfield Review.

Forristall, R. (2008). Heat Transfer Analysis and Modeling of a Parabolic Trough Solar Receiver Implemented in Engineering Equation Solver", National Renewable Energy Laboratory, 2008.

Gandomi, A.H., Yang, X-S, Talatahari, S., Alavi, A.H., (2013) Metaheuristic Applications In Structures And Infrastructures, Elsevier, 2013, Pages 1-24, ISBN 9780123983640, <https://doi.org/10.1016/B978-0-12-398364-0.00001-2>.

Gandomi, A. H., Yang X., Talatahari, S., & Alavi, A.H., (2013) Metaheuristic Algorithms In Modeling And Optimization,

Genetic Algorithms in Wireless Networking: Techniques, Applications, And Issues - Scientific Figure On Researchgate. Available from: https://www.researchgate.net/figure/illustration-of-examples-of-one-point-two-points-and-uniform-crossover-methods-adapted_fig5_268525551 [Accessed 14 Aug, 2020]

Gharbi, N. E., Derbal, H., Bouaichaoui, S., & Said, N., (2011). “A Comparative Study Between Parabolic Trough Collector and Linear Fresnel Reflector Technologies”. Energy Procedia, 6, Jan., Pp. 565–572.

Giostrì, A., Binotti, M., Silva, P., Macchi, E., & Manzolini, G., (2011). Comparison of Two Linear Collectors in Solar Thermal Plants: Parabolic Trough Vs Fresnel. In Proceedings of The ASME 2011 International Conference On Energy Sustainability.

GlassPoint (2017). Solar Energy for Industry

Goswami, R., Negi, B., Sehgal, H., and Soontha, G., 1990. Optical designs and concentration characteristics of a linear Fresnel reflector solar concentrator with a triangular absorber. Solar Energy Materials, 21(2-3), Dec., pp. 237–251

Haberle, A., Zahler, C., Lerchenmüller, H., Mertins, M., Wittwer, C., Trieb, F., and Dersch, J., 2002. “The Solarmundo line focussing Fresnel collector. Optical and thermal performance and cost calculations”. In Proceedings of the 2002 SolarPACES International Symposium

Hey, T., Tansley, S., and Toole, K. 2009. The Fourth Paradigm (Data-Intensive Scientific Discovery). Microsoft Research, Redmond, Washington.

Huang, F., Li, L., & Huang, W. (2014). Optical Performance of an Azimuth Tracking Linear Fresnel Solar Concentrator,” Sol. Energy, Vol. 108, Pp. 1–12, 2014.

IEA, (2014), World Energy Outlook. International Energy Agency

- IEA, (2018), World Energy Outlook. International Energy Agency
- Irani, M., Temizel, C., Canbaz, C. H., Palabiyik, Y., Moreno, R., Balikcioglu, A., Diaz, J.M., Zhang, G., Wang, J. and Ahmad A. (2018). Technical and Economical Aspects of Use of Solar Energy in Oil & Gas Industry in the Middle East. SPE-193768-MS
- IRENA (2012) (International Renewable Energy Agency). Renewable Energy Technologies: Cost Analysis Series-Concentrating Solar Power. Volume 1: Power Sector (Issue 2/5).
- IRENA (2017) (International Renewable Energy Agency). Renewable Energy Technologies: Renewable Power Generation Costs.
- Islam., M.R (2019). Economically and Environmentally Sustainable Enhanced Oil Recovery, Future Potential of Enhanced Oil Recovery Chapter 6 (Pages: 451-523). First Published:17 December 2019 [Http://Doi.Org//10.1002/9781119479239](http://doi.org/10.1002/9781119479239)
- J. Muñoz, Martinez-Val, J. M., Ramos, A., (2004). "Thermal Regimes in Solar-Thermal Linear Collectors," Solar Energy, Vol. 85, No. 5, May 2011, Pp. 857-870, [Doi.Org/10.1016/J.Solener.2011.02.004](http://doi.org/10.1016/J.Solener.2011.02.004).
- Jenkins, P., Elmnifi, M., Younis, A., Emhamed, A., Amrayid, N., Alshilmany, M., Alsaker M. (2019). Enhanced Oil Recovery by Using Solar Energy:Case Study. Journal of Power and Energy Engineering, 2019, 7, 57-67 <http://www.scirp.org/journal/jpee>
- Jia He, Zhongzhu Qiu Qiming Li Yi Zhang (2012) Optical Design of Linear Fresnel Reflector Solar Concentrators. Energy Procedia Volume 14, 2012, Pages 1960-1966 [https://doi.Org/10.1016/J.Egypro.2011.12.1194](https://doi.org/10.1016/J.Egypro.2011.12.1194)
- Kalogirou, S. A., (2009). "Solar Energy Engineering Processes and Systems", 1st edition, Massachusetts: Elsevier, 2009.
- Kalogirou, S. A., (2014). Solar Energy Engineering Processes and Systems, 2nd Edition, Massachusetts: Elsevier, 2014.
- Kalogirou, S.A. (2009). Solar thermal collectors and applications. Progress in Energy and Combustion Science Issue 30 Pages (231–295)
- Klein, S., 1979. TRNSYS, A Transient System Simulation Program.
- Kulichenko, N., Khanna, N., Subramaniam, C., Khurana, M., Garg, K. and Soni, R. (nd). Development of Local Supply Chain: The Missing Link for Concentrated Solar Power Projects in India. The World Bank: ESMAP (Energy Sector Management Assistance Program).
- Kurup, P. and Turchi, C.S. (2015). Parabolic Trough Collector Cost Update for the System Advisor Model (SAM). National Renewable Energy Laboratory Technical Report NREL/TP-6A20-65228 November 2015.
- Li, Y. Agarwal A. & Kavscek A.R. (2018). Continuous Variable Pressure Steam Injection for Enhanced Oil Recovery. SPE-190100-MS.

Liu, W.-Z., 1997. Steam Injection Technology to Produce Heavy Oils. Petroleum Industry Press, Beijing, China.

Lopez, A., Billy., Donna Heimiller, Nate Blair, And Gian Porro "U.S. Renewable Energy Technical Potentials: A GIS-Based Analysis." Golden, Colorado: National Renewable Energy Laboratory, July 2012. <Http://Www.Nrel.Gov/Docs/Fy12osti/51946.Pdf>.

Lubkoll, M. (2011). A Pre-Feasibility Study of a Concentrating Solar Power System to Offset Electricity Consumption at The Spier Estate. MS Thesis Stellenbosch University

Mahdavi, E., F.S. Zebarjad, Chapter Two - Screening Criteria of Enhanced Oil Recovery Methods, Editor(S): Alireza Bahadori, Fundamentals of Enhanced Oil and Gas Recovery from Conventional and Unconventional Reservoirs, Gulf Professional Publishing, 2018, Pages 41-59, ISBN 9780128130278,

Maschio, C., Nakajima, L., & Schiozer, D.J., (2008). Production Strategy Optimization Using Genetic Algorithm and Quality Map. SPE-113483-MS Society of Petroleum Engineers, Europec/EAGE Conference and Exhibition, 9-12 June 2008, Rome, Italy

Mills, D. R., & Morrison, G. L., (2000). Compact Linear Fresnel Reflector Solar Thermal Power plants. Solar Energy, 68(3), Pp. 263–283.

Mochanov, P. (2011). Can Solar Thermal Technology Transform the Economics of Enhanced Oil Recovery.

Mohaghegh, S. 2011. Reservoir simulation and modeling based on pattern recognition. In SPE Digital Energy Conference and Exhibition Proceedings, SPE-143179-MS. 19-21 April. The Woodlands, Texas. doi:10.2118/143179-MS.

Morin, G., Dersch, J., Platzer, W., Eck, M. & Haberle, A. (2012) "Comparison of Linear Fresnel and Parabolic Collector Power Plants", Solar Energy, Vol. 86, Pp. 1-12, 2012.

Morin, G., Dersch, J., Platzer, W., Eck, M., & Haberle, A., (2011). "Comparison of Linear Fresnel and Parabolic Trough Collector Power Plants". Solar Energy, 86, July, Pp. 1–12.

Morin, G., Dersch, J., Platzer, W., Eck, M., and Haberle, A., (2011). Comparison of Linear Fresnel and Parabolic Trough Collector power plants". Solar Energy, 86, July, pp. 1–12.

Morin, G., Mertins, M., Kirchberger, J., & Selig, M. (2011). Supernova - Construction, Control & Performance of Steam Superheating Linear Fresnel Collector. Solarpaces. Andalucia, 2011.

SAM NREL, National Renewable Energy Laboratory

O'Donnell, J., Heisler, M.A., Chandra, M. (2015). Solar-generated steam for oil recovery: process integration options, net energy fraction, and

carbon market impacts. SPE Western Regional Meeting, 27-30 April, Garden Grove, California. SPE-173996-MS

Palmer, D. and O'Donnell, J. (2014). Construction, Operations and Performance of the First Enclosed Trough Solar Steam Generation Pilot for EOR Applications. SPE-169748-MS.

Palmer, D. and O'Donnell, J. (2015). Solar enhanced oil recovery application to Kuwait's heavy oil fields. SPE Kuwait Oil and Gas Show and Conference, 11-14 October, Mishref, Kuwait. SPE-175290-MS

Kurup, P., Parikh, A., Möllenkamp, J., Beikircher, T., Samoli, A and Turchi, C. (2017). Sam Process Heat Model Development and Validation: Liquid-HTF Trough and Direct Steam Generation Linear Focus Systems. IEA SHC International Conference, ISES Solar World Congress 2017.

Patil, R. G., Kale, D. M., Panse, S. V. & Joshi, J. B. (2014) "Numerical Study of Heat Loss from A Non-Evacuated Receiver of a Solar Collector," Energy Convers. Management., Vol. 78, Pp. 617–626, 2014.

Patil, R. G., Panse, S. V. & Joshi, J. B. (2014) "Optimization of Non-Evacuated Receiver of Solar Collector Having Non-Uniform Temperature Distribution for Minimum Heat Loss," Energy Convers. Management., Vol. 85, Pp. 70–84, 2014.

Pulido-Iparraguirre, D., Valenzuela, L., Fernández-Reche, J.; Galindo, J. and Rodríguez, J. (2019). Design, Manufacturing and characterization of Linear Fresnel Reflector's Facets.

Pye, J. D., 2008. "System Modelling of the Compact Linear Fresnel Reflector". PhD thesis, University of New South Wales.

Ramesh V. K., Chintala, V. and Kumar, S. (2019). Recent Developments, Challenges and Opportunities for Harnessing Solar Renewable Energy for Thermal Enhanced Oil Recovery (EOR). Energy Sources, Part A: Recovery, Utilization, and Environmental Effects.

Ravelli, S., Franchini, G., Perdichizzi, A., Rinaldi S. & V.E. Valcarengh (2016). Modeling of Direct Steam Generation in Concentrating Solar Power Plants. Energy Procedia 101 (2016) 464 – 471

Reynolds, D., 2004. An experimental and computational study of the heat loss characteristics of a trapezoidal cavity absorber. Solar Energy, 76(1-3), Mar., pp. 229–234

Robbins, J. (2010). Starting a Greenhouse Business (Part 1 & 2). University of Arkansas Division of Agriculture <https://www.uaex.edu/>

Rycroft, M., (2017). Linear Fresnel systems: the future for CSP. EE Publishers March 6th, 2017.

SAM (2018). System Advisor Model, National Renewable Energy Laboratory System Advisor Model. Lakewood USA

- Sandler Et Al. (2012). Solar-Generated Steam for Oil Recovery: Reservoir Simulation, Economic Analysis and Life Cycle Assessment. SPE-153806.
- Schlaifer, P. (2012). Performance Calculations and Optimization of a Fresnel Direct Steam Generation CSP Plant with Heat Storage. MS Thesis KTH Industrial Engineering and Management.
- Sen, M.K., Datta-Gupta, A., Stoffa, P.L., Lake, L.W. & Pope, G.A. (1995) Stochastic Reservoir Modeling Using Simulated Annealing And Genetic Algorithms. SPE-24754-PA, Society of Petroleum Engineers. SPE Formation Evaluation Volume 10 Issue 01.
- Shah, A., Fishwick, R., Wood, J., Leeke, G., Rigbyband, S. & Greave, M. (2010). A Review of Novel Techniques for Heavy Oil and Bitumen Extraction and Upgrading. Energy & Environmental Science 2010, Issue 3, pages 700–714. DOI : <https://doi.org/10.1039/b918960b>
- Sheng, J.J. (2013). Enhanced Oil Recovery Field Case Studies. Chapter 16-Cyclic Steam Stimulation, Enhanced Oil Recovery Field Case Studies. Gulf Professional Publishing, 2013, Pages 389-412, ISBN 9780123865458.
- Singh R., (2017). Modelling and Performance Analysis of Linear Fresnel Collector for Process Heat Generation for Ice Cream Factory in Konya. MS Thesis Middle East Technical University
- Singh, P.L., Ganesan S., Yàdav G.C. (1999) Technical Note: Performance Study of a Linear Fresnel Concentrating Solar Device. Renewable Energy Volume 18, Issue 3, November 1999, Pages 409-416. [https://doi.org/10.1016/S0960-1481\(98\)00805-2](https://doi.org/10.1016/S0960-1481(98)00805-2)
- Siva Reddy V. Et Al. (2013). State-Of-The-Art of Solar Thermal Power Plants- A Review. Renewable and Sustainable Energy Review Issue 27. Pp 258-273.
- Song, S., Ma, J., Zhan, Z., and Dai, Y. (2015). Optical Analysis and Optimization of the Linear Fresnel Collector's Mirror Field, International Forum On Energy, Environment Science and Materials, 2015.
- Turchi. C., & Neises T. (2015) Geothermal Risk Reduction Via Geothermal/Solar Hybrid Power Plants. Q2 FY15 Milestone Report: Parabolic Trough Solar-Thermal Output Model. Decoupled from SAM Power Block Assumptions. U.S. Department of Energy – Office of Energy Efficiency and Renewable Energy
- Van Heel, A.P., Van Wunnik, J.N.M., Bntouati, S., Terres, R. (2010). The impact of daily and seasonal cycles in Solar-generated steam on oil recovery. SPE EOR Conference at Oil & Gas West Asia, 11-13 April, Muscat, Oman. SPE-129225-MS
- Vrajitoru D., (2000). Large Population or Many Generations for Genetic Algorithms? Implications in Information Retrieval.
- Walker, G.S. (2013) Development of A Low Cost Linear Fresnel Solar Concentrator. MS Thesis Stellenbosch University 2013.

- Wagner, M.J. and Gilman, P. (2011). Technical Manual for the SAM Physical Trough Model. Technical Report NREL/TP-5500-51825 June 2011
- Wagner, M.J. (2012). Results and Comparison from the SAM Linear Fresnel Technology Performance Model. World Renewable Energy Forum Denver, Colorado, May 13–17, 2012.
- Weiss, W. & Rommel, M. (2008). Process Heat Collectors, State of the Art within Task 33/IV. IEA SHC-Task 33 and SolarPACES-Task IV: Solar Heat for Industrial Processes.
- Wilson, A. (2015). Pilot steam generator uses solar energy successfully for EOR operations in Oman. *Journal of Petroleum Technology*. 67(6):111-113.
- Xenergy. (2001). Statewide Small/Medium Nonresidential Customer Needs and Wants Study. Final Report, December 2001, P1923-0121.
- Yalgin G. (2018). Development of A Screening Model for Cyclic Steam Injection (CSI) Process. MS Thesis Graduate School of Natural and Applied Sciences of Middle East Technical University.
- Yegane, M., Bashtani, F., Tahmasebi, A., Ayatollahi, S. and Al-Wahaibi, Y. (2016). Comparing different scenarios for Thermal Enhanced Oil Recovery in Fractured Reservoirs Using Hybrid (Solar-Gas) Steam Generators, A Simulation Study. SPE Europec featured at 78th EAGE Conference and Exhibition, 30 May-2 June, Vienna, Austria. SPE-180101-MS
- Yen, T.F, Donaldson, E.C. & Chilingarian, G.V. (1989). Enhanced Oil Recovery, II Processes and Operations, 1989.
- Zhu, G., And Wagner, M. J. (2014). A Direct-Steam Linear Fresnel Performance Model for NREL's System Advisor Model. ASME 2012 6th International Conference on Energy Sustainability & 10th Fuel Cell Science, Engineering and Technology Conference ESFuelCell2012 July 23-26, 2012, San Diego, CA, USA
- Zhu, G., Wendelin, T., Wagner, M. J. And Kutscher, C. (2014). "History, Current State, And Future of Linear Fresnel Concentrating Solar Collectors," *Sol. Energy*, Vol. 103, Pp. 639–652, 2014.

APPENDICES

A. Receiver Geometry Calculation and CIAT and SPT Tables

Compound parabola shape of geometry described Figure A.1 for maximum concentration ratio for a receiver of radius r and half acceptance angle θ_c .

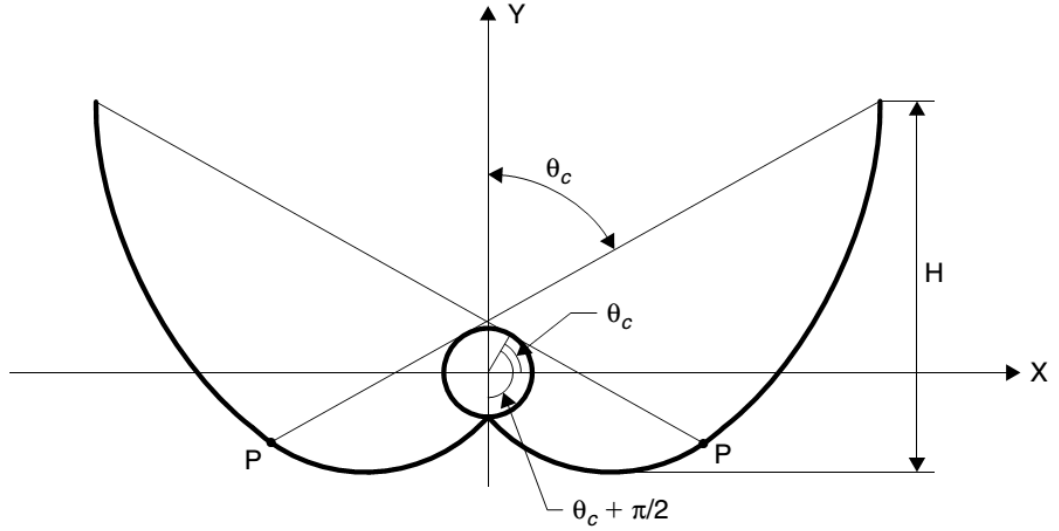


Figure A.1 compound parabola geometry

$$\rho(\theta) = r \theta \text{ for } |\theta| \leq \theta_c + \frac{\pi}{2} \quad \text{A.1}$$

$$\rho(\theta) = r \left[\frac{\theta + \theta_c + \frac{\pi}{2} - \cos(\theta + \theta_c)}{1 + \sin(\theta + \theta_c)} \right] \text{ for } |\theta| \leq \theta_c + \frac{\pi}{2} \leq 0 \leq \frac{3\pi}{2} - \theta_c \quad \text{A.2}$$

Coordinates of point P:

$$X = r \sin(\theta) - \rho \cos(\theta) \quad \text{A.3}$$

$$Y = -r \cos(\theta) - \rho \sin(\theta) \quad \text{A.4}$$

Table A.1 Typical Solar position and CIAT Table (Section A)

0	-180	-160	-140	-120	-100	-80	-60	-40	-20
0	1	1	1	1	1	1	1	1	1
10	0.98	0.974445	0.971976	0.972847	0.97691	0.97691	0.972847	0.971976	0.974445
20	0.93	0.922976	0.92893	0.946005	0.954019	0.954019	0.946005	0.92893	0.922976
30	0.84	0.838618	0.870691	0.913021	0.940911	0.940911	0.913021	0.870691	0.838618
40	0.72	0.729947	0.803687	0.866961	0.900039	0.900039	0.866961	0.803687	0.729947
50	0.55	0.591255	0.707454	0.793509	0.83956	0.83956	0.793509	0.707454	0.591255
60	0.34	0.432178	0.597478	0.664006	0.693511	0.693511	0.664006	0.597478	0.432178
70	0.13	0.265254	0.425586	0.464496	0.477106	0.477106	0.464496	0.425586	0.265254
80	0.01	0.113694	0.20891	0.233255	0.238828	0.238828	0.233255	0.20891	0.113694
90	0	0	0	0	0	0	0	0	0

Table A.2 Typical Solar position and CIAT Table (Section B)

0	20	40	60	80	100	120	140	160	180
1	1	1	1	1	1	1	1	1	1
0.98	0.974445	0.971976	0.972847	0.97691	0.97691	0.972847	0.971976	0.974445	0.98
0.93	0.922976	0.92893	0.946005	0.954019	0.954019	0.946005	0.92893	0.922976	0.93
0.84	0.838618	0.870691	0.913021	0.940911	0.940911	0.913021	0.870691	0.838618	0.84
0.72	0.729947	0.803687	0.866961	0.900039	0.900039	0.866961	0.803687	0.729947	0.72
0.55	0.591255	0.707454	0.793509	0.83956	0.83956	0.793509	0.707454	0.591255	0.55
0.34	0.432178	0.597478	0.664006	0.693511	0.693511	0.664006	0.597478	0.432178	0.34
0.13	0.265254	0.425586	0.464496	0.477106	0.477106	0.464496	0.425586	0.265254	0.13
0.01	0.113694	0.20891	0.233255	0.238828	0.238828	0.233255	0.20891	0.113694	0.01
0	0	0	0	0	0	0	0	0	0

B. Genetic Algorithm Optimization Code

```
tic;
% Fixed Mean Values of reservoir parameters used for optimization
filename = 'avgresprops';
sheet = 1;
resprops = xlsread(filename,sheet,'E2:E40');

i=2;
    load net2;
    clear Rn2;
    genoptrun_years= i;

%%Normalizing Inputs separately %Grid & Reservoir Parameters

    Rn2(1)=mapminmax('apply', resprops(1,:),ps(1,:)); %Area
    Rn2(2)=mapminmax('apply', resprops(2,:),ps(2,:)); %Total
Thickness
    Rn2(3)=mapminmax('apply', resprops(3,:),ps(3,:)); %Reservoir
Depth
    Rn2(4)=mapminmax('apply', resprops(4,:),ps(4,:)); %kv/kh
    Rn2(5)=mapminmax('apply', resprops(5,:),ps(5,:)); %Average
Porosity
    Rn2(6)=mapminmax('apply', resprops(6,:),ps(6,:)); %Average
Permeability
    Rn2(7)=mapminmax('apply', resprops(7,:),ps(7,:)); %Rock
Compressibility
    Rn2(8)=mapminmax('apply', resprops(8,:),ps(8,:)); %Heat
Capacity of Formation
    Rn2(9)=mapminmax('apply', resprops(9,:),ps(9,:)); %Thermal
Conductivity of Formation
    Rn2(10)=mapminmax('apply', resprops(10,:),ps(10,:));
%Thermal Conductivity of Oil
    Rn2(11)=mapminmax('apply', resprops(11,:),ps(11,:));
%Thermal Conductivity of Gas
    Rn2(12)=mapminmax('apply', resprops(12,:),ps(12,:)); %Heat
Capacity of Shale
    Rn2(13)=mapminmax('apply', resprops(13,:),ps(13,:));
%Thermal Conductivity of Shale
%Fluid Parameters
    Rn2(14)=mapminmax('apply', resprops(14,:),ps(14,:)); %Oil
Molecular Weight
    Rn2(15)=mapminmax('apply', resprops(15,:),ps(15,:)); %Oil
Mass Density
    Rn2(16)=mapminmax('apply', resprops(16,:),ps(16,:)); %Oil
Specific Gravity
    Rn2(17)=mapminmax('apply', resprops(17,:),ps(17,:)); %Oil API
Gravity
    Rn2(18)=mapminmax('apply', resprops(18,:),ps(18,:)); %Heat
Capacity of Oil
    Rn2(19)=mapminmax('apply', resprops(19,:),ps(19,:));
%Viscosity Coefficient A
    Rn2(20)=mapminmax('apply', resprops(20,:),ps(20,:));
%Viscosity Coefficient B
%Rock and Fluid Properties
    Rn2(21)=mapminmax('apply', resprops(21,:),ps(21,:));
%Residual Oil Saturation
```

```

Rn2(22)=mapminmax('apply', resprops(22,:),ps(22,:));
%Irreducible Water Saturation
Rn2(23)=mapminmax('apply', resprops(23,:),ps(23,:));
%Relative Permeability Exponent 1
Rn2(24)=mapminmax('apply', resprops(24,:),ps(24,:));
%Relative Permeability Exponent 2
Rn2(25)=mapminmax('apply', resprops(25,:),ps(25,:));
%Relative Permeability Exponent 3
Rn2(26)=mapminmax('apply', resprops(26,:),ps(26,:));
%Relative Permeability Exponent 4
Rn2(27)=mapminmax('apply', resprops(27,:),ps(27,:));
%Capillary Pressure Coefficient for Oil
Rn2(28)=mapminmax('apply', resprops(28,:),ps(28,:));
%Capillary Pressure Coefficient for Gas
%Initial Conditions
Rn2(29)=mapminmax('apply', resprops(29,:),ps(29,:));
%Reservoir Pressure
Rn2(30)=mapminmax('apply', resprops(30,:),ps(30,:));
%Reservoir Temperature
Rn2(31)=mapminmax('apply', resprops(31,:),ps(31,:));
%Initial Water Saturation
Rn2(32)=mapminmax('apply', resprops(32,:),ps(32,:));
%Initial Oil Saturation

Rn2(39)=mapminmax('apply', resprops(39,:),ps(39,:));%Lorenz
Coefficient (h-por-perm)
Rn2 = Rn2';
save Rn2;
%%Optimization section
nvars = 6;
A = [];
b = [];
Aeq = [];
beq = [];
lb = [-1,-1,-1,-1,-1,-1];
ub = [1,1,1,1,1,1];
%Calling Function
fun = @gafitfcn;
options = optimoptions('ga','PopulationSize',50,
'CrossoverFcn',{@crossovertwopoint},'PlotFcn',{@gaplotdistance,@gapl
otrange,@gaplotbestf},'MaxGenerations',20,'Display','iter');
%options = optimoptions(options,'UseVectorized',true);
[x,fval,exitFlag,output] =
ga(fun,nvars,[],[],[],[],lb,ub,[],options);
fval=(1/fval)-2;

%Outputs (reverse)
Efficiency= mapminmax('reverse', fval,ts); %Efficiency
Steam_temp= mapminmax('reverse', x(1),ps(33,:)); %Steam
temperature
Steam_quality= mapminmax('reverse', x(2),ps(34,:)); %Steam
Quality
Steam_Injection_rate = mapminmax('reverse', x(3),ps(35,:));
%Steam Injection rate
Injection_time = mapminmax('reverse', x(4),ps(36,:));
%Injection time
Soaking_time = mapminmax('reverse', x(5),ps(37,:)); %Soaking
time

```

```

        Economic_rate_limit = mapminmax('reverse', x(6),ps(38,:));
%Steam Injection rate
    ga2 =
[Efficiency;Steam_temp;Steam_quality;Steam_Injection_rate;Injection_
time;Soaking_time;Economic_rate_limit];

toc

%%%% GA Optimized Steam design Paramters and Fitness function
% Called after normalization for the optimization

function z = gafitfcn (y)
%load inputs;
load net2;
load Rn2;

%Specifying Steam parameters for optimization
% %Normalizing Steam and Production Parameters Inputs
    Rn2(33)= y(1); %Steam Temperature
    Rn2(34)= y(2); %Steam Quality
    Rn2(35)= y(3); %Steam Injection Rate
    Rn2(36)= y(4); %Injection Time
    Rn2(37)= y(5); %Soaking Time
    Rn2(38)= y(6); %Economic Rate Limit
    eff = sim(net,Rn2);
    z = 1/(eff+2);

end

```

C. Solar Input Generation Code

```

clear;
clc;
location =
'C:/Users/labuser/Desktop/OMN_ZU_Thumrait.AB.413140_TMYx.epw';
tracker = 1;
tilt = 0; %
azimuth = 0; %
field_aperture = 17280; % Field aperture area m^2
eff_cyc = 0.9; % rated cycle efficiency set as 0.9
since we are converting thermal energy to electrical energy
T_in = 50; % Field inlet temperature degree Celsius
T_out = 371; % Field outlet temperature degree
Celsius
Tsfavg = (T_out - T_in)/2; % Average design point solar field
temperature
P_turb = 115; % Turbine/Heat Sink inlet pressure
egn = 1; % Estimated gross to net conversion
factor
dvar = 7; % Design turbine gross output
sys_cap = dvar * egn * 1000; % Nameplate capacity (Watts)/1000 =
MW
DNI_des = 950; % Design point solar irradiation W/m^2
RFA = 720; % Reflective aperture area for per
module m^2
LCM = 44.8; % length of collector module (m)
n_max_nMod_field = field_aperture / RFA; % Max number of module
for a given field aperture
nModBl = 24; % Number of module in boiler section
nModSp = 0; % Number of module in boiler section
SLA = RFA * nModBl + RFA * nModSp; % Single loop area m^2
q_max_out = 7.456; % Field thermal output (MW)
q_des = dvar/eff_cyc; % Design thermal input power
sm = q_max_out / q_des; % Actual solar multiple
x_des = 0.95; % Boiler steam Quality
m_dot = 0.5; % Min single loop flow rate
% Collector and Receiver Section Properties and dimensions
% Parameter Values are in matrices for Boiler and Superheater
Sections
% To maintain consistency with NREL SAM simulator
structure/schematic

% Optical characterization method per section:
% Solar position table SPT: 1
% Collector incidence angle table CIAT: 2
% Incidence angle modifiers IAM. 3
OptType = [ 3 ; 3 ];
IM_T = [ 0.9896 0.044 -0.0721 -0.2327 0 ; 0.9896 0.044
-0.0721 -0.2327 0 ]; % Transverse incidence angle modifier
IM_L = [ 1.0031 -0.2259 0.5368 -1.6434 0.7222 ; 1.0031 -
0.2259 0.5368 -1.6434 0.7222 ]; % Longitudinal incidence angle
modifier
TrEr_Boiler = 0.9; % Boiler Tracking error factor

TrEr_SH = 0; % Superheater Tracking error factor

```

```

TrackinErr=[ TrEr_Boiler ; TrEr_SH ]; % Tracking error Matrix
GmEffctsBoiler = 0.7 ; % Boiler Geometry effects factor
GmEffctsSH = 0 ; % Superheater Geometry effects factor
GeomEffcts =[ GmEffctsBoiler ; GmEffctsSH]; % Geometry effects
Matrix
rho_m_clnBoiler = 0.9 ; % Boiler Mirror reflectivity factor
rho_m_clnSH = 0 ; % Superheater Mirror reflectivity
factor
mirror_cln =[ rho_m_clnBoiler ; rho_m_clnSH ]; % Mirror
reflectivity Matrix
dirt_mirrorBoiler = 0.9; % Boiler Mirror soiling factor
dirt_mirrorSH = 0; % Superheater Mirror soiling factor
dirt_mirrors =[ dirt_mirrorBoiler; dirt_mirrorSH ]; % Mirror
soiling Matrix
gn_opt_errBoiler = 0.9; % Boiler General optical error
gn_opt_errSH = 0; % Superheater General optical error
gn_errors =[gn_opt_errBoiler ; gn_opt_errSH]; % General optical
error Matrix

% Heat loss model Type 1 for Polynomial model (PLM) and 2 for
Evacuated Tube Model (ETM)
% For saturated steam PLM is recommended however receiver design
can be
% similar to ET dimensions.
HLTypeBoiler = 1 ; % Boiler Heat loss model Type
HLTypeSH = 1 ; % Superheater Heat loss model
Type
HLType =[ HLTypeBoiler ; HLTypeSH ];
HL_Tmp =[ 0 0.672 0.002556 0 0 ; 0 0.672 0.002556
0 0 ]; % Heat loss model Temp constants matrix
HL_Wnd =[ 1 0 0 0 0 ; 1 0 0 0 0 ]; % Heat loss
model Wind constants matrix
D_2Boiler = 0.066; % Boiler Absorber tube inner
diameter (m)
D_2SH = 0.066; % Superheater Absorber tube
inner diameter (m)
D2 =[ D_2Boiler ; D_2SH ]; % Absorber tube inner diameter
matrix
D_3Boiler = 0.070; % Boiler Absorber tube Outer
diameter (m)
D_3SH = 0.070; % Superheater Absorber tube
Outer diameter (m)
D3 =[ D_3Boiler ; D_3SH ]; % Absorber tube Outer diameter
matrix
D_4Boiler = 0.1150; % Boiler Glass Envelope inner
diameter (m)
D_4SH = 0.1150; % Superheater Glass Envelope
inner diameter (m)
D4 =[ D_4Boiler ; D_4SH ]; % Glass Envelope inner
diameter matrix
D_5Boiler = 0.12; % Boiler Glass Envelope Outer
diameter (m)
D_5SH = 0.12; % Superheater Glass Envelope
Outer diameter (m)

D5 =[ D_5Boiler ; D_5SH ]; % Glass Envelope Outer diameter
matrix

```

```

D_pBoiler = 0; % Boiler Absorber flow plug
diameter (m)
D_pSH = 0; % Superheater Absorber flow
plug diameter (m)
Dp =[ D_pBoiler ; D_pSH ]; % Absorber flow plug diameter
matrix
rgh_Boiler = 4.500e-05; % Boiler internal surface
roughness
rgh_SH = 4.500e-05; % Superheater internal surface
roughness
Rgh =[ rgh_Boiler ; rgh_SH ]; % internal surface roughness
matrix

% As observed above in other dimensions for Heat loss modeling
% Boiler-Superheater dimensions and info are entered in matrices
% The other HL modeling parameters would be left in matrices
format
% First input(s) in the matrix of each parameter indicate boiler
sections
% Second input(s) in the matrix of each parameter indicate
boiler sections
% Both sections parameters are separated by a semi-colon within
the matrix
% Unless stated otherwise per section indicates both boiler and
superheater sections

% Absorber flow patterns: Tube flow (1) or Annular flow (2) per
section
Flwtype =[ 2 ; 2 ];
% Absorber materials: 304L: 1, 216L: 2, 321H: 3, B42 Copper: 4
per section
AbsrbrMatrl =[ 3 ; 3 ];

eff_pump = 0.850; % Field pump efficiency
lat = 17.67; % Latitude should be equal to latitude
of location & resource (TMY or EPW) file
stowAng = 10; % Solar elevation for collector
nighttime stow
depAng = 10; % Solar elevation for collector
morning deploy

T_frz = 10; % Freeze protection temperature
ColAzmth = 0; % Collector azimuth angle
e_start = 2.700; % Thermal inertia per unit area of
solar field
Tsf_amb = 35; % Solar field Ambient temperature at
design
v_wnd_max = 20; % Stow wind speed
w_per_wash = 0.04; % Water usage per wash
washes_per_yr = 200; % Washes per year

ffrc =[ 0; 0; 0; 0; 0; 0; 0; 0; 0; 0 ]; % Physical trough dispatch
fossil fill fraction array
dfP_hdr_c = 0.01; % Cold header pressure drop fraction
dfP_sf_boil = 0.25; % Boiler pressure drop fraction

dfP_hdr_h= 0.095; % Average design point hot header pressure
drop fraction

```



```

P_boil = 100; % High pressure turbine inlet pressure
P_turb_out = 50; % High pressure turbine outlet
pressure
time_sby = 2; % Low resource standby period
qth_sby_frac = 0.100; % Fraction of thermal power needed for
standby
startup_time = 0.35; % Startup time
startup_frac = 0.35; % Fraction of thermal power needed for
startup
% Fossil dispatch mode: 1= Minimum backup level; 2=Supplemental
Operation; 3 = Topping mode
fossil = 1;
Pipehl_coef = 0.00350; % Piping thermal loss coefficient
Trckpwr = 0.100; % Tracking power
pump_coef = 0;
fixed_par = 0.0055; % Fraction of rated gross power
consumed at all times
% Change just first value, Balance of plant parasitic MW/MWcap
bop_array
bop = [ 0; 1; 0.483; 0.571; 0 ];
% Change just first value, Auxiliary heater, boiler parasitic
MW/MWcap aux_array
aux = [ 0; 1; 0.483; 0.571; 0 ];

dbT = 15; %
Tdew = 10; % Dewpoint temperature
ambPrs = 930.5; % Ambient pressure
windvel = 0; % Ambient windspeed
shft = 0; % Shift in longitude from local
standard meridian
thetaSolarAz_init = 0; % Solar azimuth angle
thetaSolarZen = 0; % Solar zenith angle
Tout_pbinit = 290; % Fluid temperature from the power
block
Tamb_des = Tsf_amb; % Ambient temp at design PC

dT_avg_des_amb = (T_out + T_in)/2 -Tsf_amb; % Average field
temperature at design
dT_avg_Mat =
[dT_avg_des_amb^0;dT_avg_des_amb^1;dT_avg_des_amb^2;dT_avg_des_amb^3
;dT_avg_des_amb^4]; % Average field temperature at design matrix
HL_B_SH = HL_Tmp * dT_avg_Mat; % Heat loss matrix
HL_avg = round (mean (HL_B_SH),2); % Heat loss average
loopeffopt = TrEr_Boiler * GmEffctsBoiler * rho_m_clnBoiler *
dirt_mirrorBoiler * gn_opt_errBoiler; % Loop optical efficiency
loopeffthermal = 1- (LCM * HL_avg)/(DNI_des*RFA); % Loop thermal
efficiency

ppnthrmeff = 1- (Tsfavg*Pipehl_coef)/DNI_des; % Piping
thermal efficiency
total_loop_eff = loopeffopt*loopeffthermal* ppnthrmeff; %Total
loop conversion efficiency
TRA = (q_des*10^6)/(DNI_des*total_loop_eff); % Total
required

```

```
aperture for a solar multiple of 1 (SM = 1)
    RNL = round ((TRA/SLA),3); % required number of loops at SM=1
    RNLmax = ceil (TRA/SLA);   % required number of loops at SM=1
    nLps = ceil (sm*RNL);      % Number of loops for aperture
    save SIF.mat;
```

D. SAM SIPH Function Code

```
function IPH
    function [result] = sscall(action, arg0, arg1, arg2 )
        [pathstr, fn, fext] = fileparts(mfilename('fullpath'));
        ssclibpath = './';
        ssclib = 'ssc';
        if ~libisloaded(ssclib)
            oldFolder = cd(pathstr);

loadlibrary(strcat(ssclibpath,ssclib),strcat(ssclibpath,'sscapi.h'))
;
            cd(oldFolder);
        end
        if strcmp(action,'load')
            if ~libisloaded(ssclib)
                oldFolder = cd(pathstr);

loadlibrary(strcat(ssclibpath,ssclib),strcat(ssclibpath,'../sscapi.h
'));
                cd(oldFolder);
            end
        elseif strcmp(action,'unload')
            if libisloaded(ssclib)
                unloadlibrary(ssclib)
            end
        elseif strcmp(action,'version')
            result = calllib(ssclib,'ssc_version');
        elseif strcmp(action,'build_info')
            result = calllib(ssclib, 'ssc_build_info');
        elseif strcmp(action,'data_create')
            result = calllib(ssclib, 'ssc_data_create');
            if ( isnullpointer(result) )
                result = 0;
            end
        elseif strcmp(action,'data_free')
            result = calllib(ssclib, 'ssc_data_free', arg0);
        elseif strcmp(action,'data_unassign')
            result = calllib(ssclib, 'ssc_data_unassign', arg0, arg1);
        elseif strcmp(action,'data_query')
            result = calllib(ssclib, 'ssc_data_query', arg0, arg1 );
        elseif strcmp(action,'data_first')
            result = calllib(ssclib, 'ssc_data_first', arg0 );
        elseif strcmp(action,'data_next')
            result = calllib(ssclib, 'ssc_data_next', arg0 );
        elseif strcmp(action,'data_set_string')
            result = calllib(ssclib, 'ssc_data_set_string', arg0, arg1,
arg2 );
        elseif strcmp(action,'data_set_number')
            result = calllib(ssclib, 'ssc_data_set_number', arg0, arg1,
single(arg2) );
        elseif strcmp(action,'data_set_array')
            len = length(arg2);
            arr = libpointer( 'singlePtr', arg2 );

            result =
calllib(ssclib,'ssc_data_set_array',arg0,arg1,arr,len);
        elseif strcmp(action,'data_set_matrix')
```

```

[nr nc] = size(arg2);
mat = zeros(nr*nc, 1);
ii = 1;
for r=1:nr
    for c=1:nc
        mat(ii) = arg2(r,c);
        ii=ii+1;
    end
end
arr = libpointer( 'singlePtr', mat );
result =
calllib(ssclib, 'ssc_data_set_matrix', arg0, arg1, arr, nr, nc);
elseif strcmp(action, 'data_set_table')
    result =
calllib(ssclib, 'ssc_data_set_table', arg0, arg1, arg2);
elseif strcmp(action, 'data_get_string')
    result = calllib(ssclib, 'ssc_data_get_string', arg0, arg1);
elseif strcmp(action, 'data_get_number')
    p = libpointer('singlePtr', 0);
    calllib(ssclib, 'ssc_data_get_number', arg0, arg1, p);
    result = get(p, 'Value');
elseif strcmp(action, 'data_get_array')
    p_count = libpointer('int32Ptr', 0);
    [xobj] =
calllib(ssclib, 'ssc_data_get_array', arg0, arg1, p_count);
    setdatatype(xobj, 'int32Ptr', p_count.Value, 1);
    len = p_count.Value;
    result = zeros( len, 1 );
    for i=1:len
        pidx = xobj+(i-1);
        setdatatype(pidx, 'singlePtr', 1, 1);
        result(i) = pidx.Value;
    end
elseif strcmp(action, 'data_get_matrix')
    p_rows = libpointer('int32Ptr', 0);
    p_cols = libpointer('int32Ptr', 0);
    [xobj] =
calllib(ssclib, 'ssc_data_get_matrix', arg0, arg1, p_rows, p_cols);
    setdatatype(xobj, 'int32Ptr', p_rows.Value*p_cols.Value, 1);
    nrows = p_rows.Value;
    ncols = p_cols.Value;
    if ( nrows*ncols > 0 )
        result = zeros( nrows, ncols );
        ii=1;
        for r=1:nrows
            for c=1:ncols
                pidx = xobj+(ii-1);
                setdatatype(pidx, 'singlePtr', 1, 1);
                result(r,c) = pidx.Value;
                ii=ii+1;
            end
        end
    end
elseif strcmp(action, 'data_get_table')
    result = calllib(ssclib, 'ssc_data_get_table', arg0, arg1);
elseif strcmp(action, 'module_entry')
    result = calllib(ssclib, 'ssc_module_entry', arg0);
    if isnullpointer( result )

```

```

        result = 0;
    end
elseif strcmp(action, 'entry_name')
    result = calllib(ssclib, 'ssc_entry_name', arg0);
elseif strcmp(action, 'entry_description')
    result = calllib(ssclib, 'ssc_entry_description', arg0);
elseif strcmp(action, 'entry_version')
    result = calllib(ssclib, 'ssc_entry_version', arg0);
elseif strcmp(action, 'module_var_info')
    result = calllib(ssclib, 'ssc_module_var_info', arg0, arg1);
    if isnullpointer( result )
        result = 0;
    end
elseif strcmp(action, 'info_var_type')
    ty = calllib(ssclib, 'ssc_info_var_type', arg0);
    if (ty == 1)
        result = 'input';
    elseif ( ty==2 )
        result = 'output';
    else
        result = 'inout';
    end
elseif strcmp(action, 'info_data_type')
    dt = calllib(ssclib, 'ssc_info_data_type', arg0);
    if (dt == 1)
        result = 'string';
    elseif (dt == 2)
        result = 'number';
    elseif (dt == 3)
        result = 'array';
    elseif (dt == 4)
        result = 'matrix';
    elseif (dt == 5)
        result = 'table';
    else
        result = 'invalid';
    end
elseif strcmp(action, 'info_name')
    result = calllib(ssclib, 'ssc_info_name', arg0);
elseif strcmp(action, 'info_label')
    result = calllib(ssclib, 'ssc_info_label', arg0);
elseif strcmp(action, 'info_units')
    result = calllib(ssclib, 'ssc_info_units', arg0);
elseif strcmp(action, 'info_meta')
    result = calllib(ssclib, 'ssc_info_meta', arg0);
elseif strcmp(action, 'info_group')
    result = calllib(ssclib, 'ssc_info_group', arg0);
elseif strcmp(action, 'info_required')
    result = calllib(ssclib, 'ssc_info_required', arg0);

elseif strcmp(action, 'info_constraints')
    result = calllib(ssclib, 'ssc_info_constraints', arg0);
elseif strcmp(action, 'info_uihint')
    result = calllib(ssclib, 'ssc_info_uihint', arg0);
elseif strcmp(action, 'exec_simple')
    result = calllib(ssclib, 'ssc_module_exec_simple', arg0, arg1);
elseif strcmp(action, 'exec_simple_nothread')

```

```

        result =
calllib(ssclib, 'ssc_module_exec_simple_nothread', arg0, arg1);
    elseif strcmp(action, 'module_create')
        result = calllib(ssclib, 'ssc_module_create', arg0);
        if ( isnullpointer(result) )
            result = 0;
        end
    elseif strcmp(action, 'module_free')
        result = calllib(ssclib, 'ssc_module_free', arg0);
    elseif strcmp(action, 'module_exec_set_print')
        calllib(ssclib, 'ssc_module_exec_set_print', arg0);
        result = 0;
    elseif strcmp(action, 'module_exec')
        result = calllib(ssclib, 'ssc_module_exec', arg0, arg1);
    elseif strcmp(action, 'module_log')
        p_type = libpointer('int32Ptr', 1);
        p_time = libpointer('singlePtr', 1);
        result = calllib(ssclib, 'ssc_module_log', arg0, arg1,
p_type, p_time);
    elseif strcmp(action, 'module_log_detailed')
        p_type = libpointer('int32Ptr', 1);
        p_time = libpointer('singlePtr', 1);
        text = calllib(ssclib, 'ssc_module_log', arg0, arg1, p_type,
p_time);
        typetext = 'notice';
        if (p_type.Value == 2)
            typetext = 'warning';
        elseif (p_type.Value == 3)
            typetext = 'error';
        end
        if ( strcmp(text, '') )
            result = 0;
        else
            result = {text , typetext , p_time.Value};
        end
    else
        fprintf('ssccall: invalid action %s\n', action) ;
        result = 0;
    end
end
function bb = isnullpointer(p)
bb = false;
try
    setdatatype(p, 'voidPtr', 1, 1);
    deref = get(p);
catch

e = lasterror();
    if strcmp(e.identifier, 'MATLAB:libpointer:ValueNotDefined')
        bb = true;
    end
end
end
clear
SIF = load ('SIF.mat');
ssccall('load');
disp('Current folder = G:/Thesis/SAM Steam Model');

```

```

fprintf('SSC Version = %d\n', sscall('version'));
fprintf('SSC Build Information = %s\n', sscall('build_info'));
ssccall('module_exec_set_print',0);
data = sscall('data_create');
ssccall('data_set_string', data, 'file_name', SIF.location());
ssccall('data_set_number', data, 'I_bn_des', SIF.DNI_des());
ssccall('data_set_number', data, 'T_cold_ref', SIF.T_in());
ssccall('data_set_number', data, 'P_turb_des', SIF.P_turb());
ssccall('data_set_number', data, 'T_hot', SIF.T_out());
ssccall('data_set_number', data, 'x_b_des', SIF.x_des());
ssccall('data_set_number', data, 'q_pb_des', SIF.q_des());
ssccall('data_set_number', data, 'fP_hdr_c',
0.0099999997764825821);
ssccall('data_set_number', data, 'fP_sf_boil',
0.075000002980232239);
ssccall('data_set_number', data, 'fP_hdr_h',
0.02500000037252903);
ssccall('data_set_number', data, 'nModBoil', SIF.nModBl());
ssccall('data_set_number', data, 'nLoops', SIF.nLps());
ssccall('data_set_number', data, 'eta_pump',
0.85000002384185791);
ssccall('data_set_number', data, 'theta_stow', 10);
ssccall('data_set_number', data, 'theta_dep', 10);
ssccall('data_set_number', data, 'T_fp', 10);
ssccall('data_set_number', data, 'Pipe_hl_coef',
0.0035000001080334187);
ssccall('data_set_number', data, 'SCA_drives_elec',
0.20000000298023224);
ssccall('data_set_number', data, 'ColAz', 0);
ssccall('data_set_number', data, 'e_startup',
2.7000000476837158);
ssccall('data_set_number', data, 'T_amb_des_sf',
SIF.Tsf_amb());
ssccall('data_set_number', data, 'V_wind_max', 20);
ssccall('data_set_number', data, 'csp.lf.sf.water_per_wash',
SIF.w_per_wash());
ssccall('data_set_number', data, 'csp.lf.sf.washes_per_year',
SIF.washes_per_yr());
A_aperture=[ SIF.RFA() ; 0 ];
ssccall('data_set_matrix', data, 'A_aperture', A_aperture );
L_col=[ SIF.LCM() ; 0 ];
ssccall('data_set_matrix', data, 'L_col', L_col );
OptCharType=[ 3 ; 0 ];
ssccall('data_set_matrix', data, 'OptCharType', OptCharType );
IAM_T=[ 0.98960000276565552 0.043999999761581421 -
0.072099998593330383 -0.23270000517368317 0 ; 0 0 0 0 0
];
ssccall('data_set_matrix', data, 'IAM_T', IAM_T );

IAM_L=[ 1.0031000375747681 -0.22589999437332153
0.53680002689361572 -1.6433999538421631 0.72219997644424438 ; 0
0 0 0 0 ];
ssccall('data_set_matrix', data, 'IAM_L', IAM_L );
TrackingError = SIF.TrackinErr();
ssccall('data_set_matrix', data, 'TrackingError', TrackingError
);
GeomEffects = SIF.GeomEffcts();
ssccall('data_set_matrix', data, 'GeomEffects', GeomEffects );
rho_mirror_clean = SIF.mirror_cln();

```

```

    sscall( 'data_set_matrix', data, 'rho_mirror_clean',
rho_mirror_clean );
    dirt_mirror = SIF.dirt_mirrors();
    sscall( 'data_set_matrix', data, 'dirt_mirror', dirt_mirror );
    error = SIF.gn_errors();
    sscall( 'data_set_matrix', data, 'error', error );
    HLCharType = [ 1 ; 0 ];
    sscall( 'data_set_matrix', data, 'HLCharType', HLCharType );
    HL_dT = [ 0 0.67199999094009399 0.0025559999048709869 0 0
; 0 0 0 0 0 ];
    sscall( 'data_set_matrix', data, 'HL_dT', HL_dT );
    HL_W = [ 1 0.54 0 0 0 ; 0 0 0 0 0 ];
    sscall( 'data_set_matrix', data, 'HL_W', HL_W );
    D_2 = [ 0.065999999642372131 ; 0 ];
    sscall( 'data_set_matrix', data, 'D_2', D_2 );
    D_3 = [ 0.070000000298023224 ; 0 ];
    sscall( 'data_set_matrix', data, 'D_3', D_3 );
    D_4 = [ 0.11500000208616257 ; 0 ];
    sscall( 'data_set_matrix', data, 'D_4', D_4 );
    D_5 = [ 0.11999999731779099 ; 0 ];
    sscall( 'data_set_matrix', data, 'D_5', D_5 );
    D_p = [ 0 ; 0 ];
    sscall( 'data_set_matrix', data, 'D_p', D_p );
    Rough = [ 4.5000000682193786e-05 ; 0 ];
    sscall( 'data_set_matrix', data, 'Rough', Rough );
    Flow_type = [ 1 ; 0 ];
    sscall( 'data_set_matrix', data, 'Flow_type', Flow_type );
    AbsorberMaterial = [ 1 ; 0 ];
    sscall( 'data_set_matrix', data, 'AbsorberMaterial',
AbsorberMaterial );
    HCE_FieldFrac = [ 0.98500001430511475 0.0099999997764825821
0.004999999888241291 0 ; 0 0 0 0 ];
    sscall( 'data_set_matrix', data, 'HCE_FieldFrac', HCE_FieldFrac
);
    alpha_abs = [ 0.95999997854232788 0.95999997854232788
0.80000001192092896 0 ; 0 0 0 0 ];
    sscall( 'data_set_matrix', data, 'alpha_abs', alpha_abs );
    b_eps_HCE1 = [ 0 ; 0.13840000331401825 ];
    sscall( 'data_set_matrix', data, 'b_eps_HCE1', b_eps_HCE1 );
    b_eps_HCE2 = [ 0 ; 0.64999997615814209 ];
    sscall( 'data_set_matrix', data, 'b_eps_HCE2', b_eps_HCE2 );
    b_eps_HCE3 = [ 0 ; 0.64999997615814209 ];
    sscall( 'data_set_matrix', data, 'b_eps_HCE3', b_eps_HCE3 );
    b_eps_HCE4 = [ 0 ; 0.13840000331401825 ];
    sscall( 'data_set_matrix', data, 'b_eps_HCE4', b_eps_HCE4 );
    sh_eps_HCE1 = [ 0 ; 0 ];

    sscall( 'data_set_matrix', data, 'sh_eps_HCE1', sh_eps_HCE1 );
    sh_eps_HCE2 = [ 0 ; 0 ];
    sscall( 'data_set_matrix', data, 'sh_eps_HCE2', sh_eps_HCE2 );
    sh_eps_HCE3 = [ 0 ; 0 ];
    sscall( 'data_set_matrix', data, 'sh_eps_HCE3', sh_eps_HCE3 );
    sh_eps_HCE4 = [ 0 ; 0 ];
    sscall( 'data_set_matrix', data, 'sh_eps_HCE4', sh_eps_HCE4 );
    alpha_env = [ 0.019999999552965164 0.019999999552965164 0 0
; 0 0 0 0 ];
    sscall( 'data_set_matrix', data, 'alpha_env', alpha_env );

```



```

    EPSILON_4 =[ 0.860000001430511475    0.860000001430511475    1    0 ;
0    0    0    0 ];
    sscall( 'data_set_matrix', data, 'EPSILON_4', EPSILON_4 );
    Tau_envelope =[ 0.96299999952316284    0.96299999952316284    1
0 ; 0    0    0    0 ];
    sscall( 'data_set_matrix', data, 'Tau_envelope', Tau_envelope
);
    GlazingIntactIn =[ 1    1    0    1 ; 0    0    0    0 ];
    sscall( 'data_set_matrix', data, 'GlazingIntactIn',
GlazingIntactIn );
    AnnulusGas =[ 1    1    1    1 ; 0    0    0    0 ];
    sscall( 'data_set_matrix', data, 'AnnulusGas', AnnulusGas );
    P_a =[ 9.9999997473787516e-05    750    750    0 ; 0    0    0    0 ];
    sscall( 'data_set_matrix', data, 'P_a', P_a );
    Design_loss =[ 150    1100    1500    0 ; 0    0    0    0 ];
    sscall( 'data_set_matrix', data, 'Design_loss', Design_loss );
    Shadowing =[ 0.95999997854232788    0.95999997854232788
0.95999997854232788    0 ; 0    0    0    0 ];
    sscall( 'data_set_matrix', data, 'Shadowing', Shadowing );
    Dirt_HCE =[ 0.98000001907348633    0.98000001907348633    1    0 ;
0    0    0    0 ];
    sscall( 'data_set_matrix', data, 'Dirt_HCE', Dirt_HCE );
    b_OpticalTable =[ -180    -160    -140    -120    -100    -80    -60
-40    -20    0    20    40    60    80    100    120    140    160    180    -
999.9000244140625 ; 0    1    1    1    1    1    1    1    1    1    1    1
1    1    1    1    1    1    1    1 ; 10    0.98000001907348633
0.974444498538970947    0.97197598218917847    0.97284698486328125
0.97690999507904053    0.97690999507904053    0.97284698486328125
0.97197598218917847    0.974444498538970947    0.98000001907348633
0.974444498538970947    0.97197598218917847    0.97284698486328125
0.97690999507904053    0.97690999507904053    0.97284698486328125
0.97197598218917847    0.974444498538970947    0.98000001907348633 ; 20
0.93000000715255737    0.92297601699829102    0.92892998456954956
0.94600498676300049    0.95401901006698608    0.95401901006698608
0.94600498676300049    0.92892998456954956    0.92297601699829102
0.93000000715255737    0.92297601699829102    0.92892998456954956
0.94600498676300049    0.95401901006698608    0.95401901006698608
0.94600498676300049    0.92892998456954956    0.92297601699829102
0.93000000715255737 ; 30    0.8399999737739563    0.83861798048019409
0.87069100141525269    0.9130210280418396    0.94091099500656128
0.94091099500656128    0.9130210280418396    0.87069100141525269
0.83861798048019409    0.8399999737739563    0.83861798048019409
0.87069100141525269    0.9130210280418396    0.94091099500656128
0.94091099500656128    0.9130210280418396    0.87069100141525269
0.83861798048019409    0.8399999737739563 ; 40    0.72000002861022949
0.72994697093963623    0.80368697643280029    0.86696100234985352

0.90003901720046997    0.90003901720046997    0.86696100234985352
0.80368697643280029    0.72994697093963623    0.72000002861022949
0.72994697093963623    0.80368697643280029    0.86696100234985352
0.90003901720046997    0.90003901720046997    0.86696100234985352
0.80368697643280029    0.72994697093963623    0.72000002861022949 ; 50
0.55000001192092896    0.59125500917434692    0.70745402574539185
0.79350900650024414    0.83955997228622437    0.83955997228622437
0.79350900650024414    0.70745402574539185    0.59125500917434692
0.55000001192092896    0.59125500917434692    0.70745402574539185
0.79350900650024414    0.83955997228622437    0.83955997228622437
0.79350900650024414    0.70745402574539185    0.59125500917434692
0.55000001192092896 ; 60    0.34000000357627869    0.43217799067497253
0.59747797250747681    0.66400599479675293    0.69351100921630859

```

```

0.69351100921630859    0.66400599479675293    0.59747797250747681
0.43217799067497253    0.34000000357627869    0.43217799067497253
0.59747797250747681    0.66400599479675293    0.69351100921630859
0.69351100921630859    0.66400599479675293    0.59747797250747681
0.43217799067497253    0.34000000357627869 ; 70    0.12999999523162842
0.26525399088859558    0.42558598518371582    0.46449598670005798
0.4771060049533844    0.4771060049533844    0.46449598670005798
0.42558598518371582    0.26525399088859558    0.12999999523162842
0.26525399088859558    0.42558598518371582    0.46449598670005798
0.4771060049533844    0.4771060049533844    0.46449598670005798
0.42558598518371582    0.26525399088859558    0.12999999523162842 ; 80
0.0099999997764825821    0.11369399726390839    0.20891000330448151
0.23325499892234802    0.23882800340652466    0.23882800340652466
0.23325499892234802    0.20891000330448151    0.11369399726390839
0.0099999997764825821    0.11369399726390839    0.20891000330448151
0.23325499892234802    0.23882800340652466    0.23882800340652466
0.23325499892234802    0.20891000330448151    0.11369399726390839
0.0099999997764825821 ; 90    0    0    0    0    0    0    0    0    0    0
0    0    0    0    0    0    0    0    0    0 ] ;
    sscall( 'data_set_matrix', data, 'b_OpticalTable',
b_OpticalTable );
    sh_OpticalTable =[ 0    0 ; 0    0 ];
    sscall( 'data_set_matrix', data, 'sh_OpticalTable',
sh_OpticalTable );
    sscall('data_set_number', data, 'heat_sink_dP_frac',
0.0099999997764825821);
    sscall('data_set_number', data, 'adjust:constant', 4);
    module = sscall('module_create', 'linear_fresnel_dsg_iph');
    ok = sscall('module_exec', module, data);
    if ~ok
        disp('linear_fresnel_dsg_iph errors:');
        ii=0;
        while 1
            err = sscall('module_log', module, ii);
            if strcmp(err, '')
                break;
            end
            disp( err );
            ii=ii+1;
        end
        return
    end

    sscall('module_free', module);
    annual_energy = sscall('data_get_number', data, 'annual_energy'
);
    fprintf('%s = %g\n', 'Annual energy (year 1)', annual_energy);
    annual_field_energy = sscall('data_get_number', data,
'annual_field_energy' );
    fprintf('%s = %g\n', 'Annual field energy (year 1)',
annual_field_energy);
    annual_thermal_consumption = sscall('data_get_number', data,
'annual_thermal_consumption' );
    fprintf('%s = %g\n', 'Annual thermal freeze protection (year
1)', annual_thermal_consumption);
    annual_electricity_consumption = sscall('data_get_number',
data, 'annual_electricity_consumption' );
    fprintf('%s = %g\n', 'Annual electricity load (year 1)',
annual_electricity_consumption);

```

```

        time = sscall('data_get_array', data, 'time_hr' );%Daily Hour
        Temp_in = sscall('data_get_array', data, 'T_field_cold_in' );
%Field Steam Temperature at Header Inlet degC
        %fprintf('%s = %g\n', 'Field steam temperature header
inlet(hourly)', Temp_in);
        Temp_out = sscall('data_get_array', data, 'T_field_hot_out' );
%Field Steam Temperature at Header Outlet degC
        %fprintf('%s = %g\n', 'Field steam temperature header
outlet(hourly)', Temp_out);
        T_loop_out = sscall('data_get_array', data, 'T_rec_hot_out');
%Field Steam Temperature at Receiver degC
        fieldrate = sscall('data_get_array', data, 'm_dot_field' );
%Field Steam Mass Flowrate kg/hr
        looprate = sscall('data_get_array', data, 'm_dot_loop' ); %Loop
Steam Mass Flowrate kg/hr
        quality = sscall('data_get_array', data, 'x_field_hot_out' );
%Field Steam quality
        %Steam_pres_in = sscall('data_get_array', data, 'P_sf_in' );
%Field Steam Inlet Pressure bar
        Field_pres_Drop = sscall('data_get_array', data, 'deltaP_field'
); %Field Steam Pressure Loss bar
        %fprintf('%s = %g\n', 'Field steam pressure loss(hourly)',
field_steam_pres_loss);
        %thermal_eff = sscall('data_get_array', data, 'eta_thermal' );
%Field Thermal Efficiency
        optical_eff = sscall('data_get_array', data, 'eta_opt_ave' );
%Field Optical Efficiency
        %total_eff = sscall('data_get_array', data, 'eta_sf' ); %Field
Optical Efficiency
        save('IPH.mat');

        sscall('data_free', data);
        sscall('unload');
end

```

E. CSI-SAM Combination Code

```
tic;
rhoph = zeros(8760,1); %preallocated vector populated with zeros
qinjph = zeros(365,1); %preallocated vector populated with zeros
Tinjph = zeros(365,1); %preallocated vector populated with zeros
qtonnph = zeros(365,1); %preallocated vector populated with zeros
Qtestph = char(356,1); %preallocated vector populated with zeros
Ttestph = char(356,1); %preallocated vector populated with zeros
run('IPH.m')
load
('IPH.mat','time','Temp_in','Temp_out','T_loop_out','fieldrate');
xlf = load('IPH.mat');
tmp = xlf.Temp_out();
%qlty = xlf.quality();
qph = (xlf.fieldrate()*3600*2.2046);%lb/hr
qtonph = xlf.fieldrate()*3600/1000; %ton/hr
Tsteamph = xlf.Temp_out()*(9/5)+32; %temp/hr
for t = 1:1:8760
rhoph(t,:) = XSteam('rho_pT',100,tmp(t,:))*0.0624; % steam density
lb/cubicft
qsteamph = qph./(rhoph .* 5.615); %IPH solar steam rate per
barrel
end
S = 'Y';
F = 'N';
for i= 1:365
lower = 24*(i-1)+1; %lower bound of iteration
upper = 24*(i-1)+ 24; %upper bound of iteration
tmpQph = qsteamph(lower:upper);
tmpQtonph = qtonph(lower:upper);
tmpTph = Tsteamph(lower:upper);
inter1= tmpQph (10:18);
inter2= tmpTph (10:18);
inter3= tmpQtonph (10:18);
qiph = sum(inter1); %daily steam injection rate calc
qtph = sum(inter3); %daily steam injection rate calc ton/d
Tiph = mean(inter2);%Average daily steam temp calc
qinjph(i,:)= qiph; % Daily rate result
Tinjph(i,:)= Tiph; % Daily Temp result
qtonnph(i,:)= qtph;
steamtonph = sum (qtonnph);
steamaverageph = steamtonph/365;
%round(qinj,4,'significant')
%round(Tinj,3,'significant')
end
for x= 1:356
lb = x; %lower bound of iteration
ub = x+9; %upper bound of iteration
Qtph = qinjph (lb:ub);
Ttph = Tinjph (lb:ub);
if Qtph > 2000
testph = S;
% disp (test)
else

testph = F;
```

```

%         disp (test)

end
    Qtestph(x,:) = testph;
    if Ttph > 700
        tstph = S;
%         disp (tst)
    else
        tstph = F;
%         disp (tst)
    end
    Ttestph (x,:)= tstph;
end
Aph= Qtestph(:)';
numAph = count(Aph,'Y');
Bph= Ttestph(:)';
numBph = count(Bph,'Y');
Qavlph = (numAph/356)*100;
Tavlph = (numBph/356)*100;

toc

```

F. CSSI Graphical Schematic

CSSI

SolarEconomicsPlots

Properties	Values	Units	Range
Area	18.3700	acres	5-30
Reservoir Depth	3000	ft	500-5000
Anisotropy Permeability (kv/kh)	0.5090	frac.	0.01-1
Formation Compressibility	6.6900e-06	1/psi	3E-6 - 1E-5
Formation Heat Capacity	27.4900	Btu/ft ³ .F	25-125
Formation Thermal Conductivity	34.0700	Btu/ft.day.F	10-90
Gas Thermal Conductivity	0.6480	Btu/ft.day.F	0.30-1.00
Shale Heat Capacity	43.5400	Btu/ft ³ .F	33-54
Shale Thermal Conductivity	34.9800	Btu/ft.day.F	10-60
Molecular Weight of Oil	400.8000	lbmole	200-600
API Gravity of Oil	20	API	10-21
Viscosity Coefficient A (avisc)	0.0284	cp	0.01-0.05
Viscosity Coefficient B (bvisc)	4430	R	5000-6500
Residual Oil Saturation (Sor)	0.1956	frac.	0.10 -0.30
Irreducible Water Saturation (...)	0.2000	frac.	0.10 - 0.30
Relative Permeability Exponent 1 (krw)	2.9980	frac.	2.0-4.0
Relative Permeability Expone ...	2.9730	frac.	2.0-4.0
Relative Permeability Expone ...	2.9780	frac.	2.0-4.0
Relative Permeability Expone ...	2.9840	frac.	2.0-4.0
Capillary Pressure Coefficient...	2.4860	frac.	0.5-4.0
Capillary Pressure Coefficient...	0.2000	frac.	0.1-0.3
Reservoir Pressure	1750	psia	500-2000

Confirm Inputs

3

Formation

LAYERED

Total/Average Values

Thickness

Porosity

Permeability

Layered

Porosity

Permeability

52.80

0.252

341.20

52.80

0.252

341.20

52.80

0.252

341.20

52.80

0.252

341.20

52.80

0.252

341.20

66-471

0.10-0.38

21-1648

Total (ft)

Average (frac)

Average (mD)

66-471

0.10-0.38

21-1648

1

Optimization Options


Population

10

Generation

4

Start Optimization



5

Optimization Steam Design Parameters

	Year 2	Year 4	Year 6	Year 8	Year 10
Efficiency (bb/bbl)	0.000	0.000	0.000	0.000	0.000
Temperature (°F)	0.0	0.0	0.0	0.0	0.0
Quality (%)	0.00	0.00	0.00	0.00	0.00
Injection Rate (b/d)	0.0	0.0	0.0	0.0	0.0
Injection Time (days)	0.0	0.0	0.0	0.0	0.0
Soaking Time (days)	0.0	0.0	0.0	0.0	0.0
Economic Rate Limit (b/d)	0.0	0.0	0.0	0.0	0.0

2

Figure F.1 Schematic map of the reservoir tab of the CSSI screening tool graphical user interface

1. Enter reservoir parameters
2. Select layered or Total/Average Value and enter porosity, permeability and thickness data accordingly
3. Confirm Inputs
4. Enter population and generation sizes
5. Start Optimization

CSSI

Reservoir

Solar

Economics

Plots

Field Rating

Field Area

Please Specify Location Weather Resource (TMY,EPW) File

Select File

Location Data

Design Parameters

2

Parameter

Value

Units

Total Available Area

17280.00

m²

Non-Solar Area Factor

1.05

Frac

Design Point Irradiation (DNI)

950.00

W/m²

Tracking Error

1.000

Frac

Mirror Reflectivity

0.935

Frac

Geometry Effects

0.825

Frac

Mirror Soiling

0.950

Frac

General Optical Error

0.995

Frac

Solar Multiple

1.00

Collector/Boiler Per (Section/Module)

12

Integer

Mirror/Reflective Aperture Area

720.00

m²

Field Inlet Temperature

50.00

Celsius

Length of Collector Module

44.80

m

Latitude

17.67

deg

Collector Azimuth Angle

0.00

deg

Ambient Temperature

35.00

Celsius

Estimated Field Rating

4.00

MWt

Water per wash

0.02

Lm²

Number of Yearly Washes

120.00

Boiler Pressure Drop Fraction

0.0750

Frac

Cold Header Pressure Drop Fraction

0.0010

Frac

Hot Header Pressure Drop Fraction

0.0250

Frac

Total Solar Field Pressure Drop

1.00

Bar

Saturation Pressure

20.00

Bar

Total Solar Field Design Point Pressure

0.00

Bar

Total Required Area

0.00

m²

Optimized Steam Injection Temperature

0.00

Fahrenheit

Optimized Steam Quality

0.000

Frac

Optical Characterization Method

4

Solar Position Table

Incidence Angle Modifiers

Collector Incidence Angle Table

Incidence Angle Modifiers

0	-180.0000	-160.0000	-140.0000	-120.0000	-100.0000	-80.0000	-60.0000	-40.0000	-20.00
0	1.0000	1.0000	1.0000	1.0000	1.0000	1.0000	1.0000	1.0000	1.0
10	0.9800	0.9744	0.9720	0.9728	0.9769	0.9769	0.9728	0.9720	0.9
20	0.9300	0.9230	0.9289	0.9460	0.9540	0.9540	0.9460	0.9289	0.9
30	0.8400	0.8386	0.8707	0.9130	0.9409	0.9409	0.9130	0.8707	0.8
40	0.7200	0.7299	0.8037	0.8670	0.9000	0.9000	0.8670	0.8037	0.7
50	0.5500	0.5913	0.7075	0.7935	0.8396	0.8396	0.7935	0.7075	0.5
60	0.3400	0.4322	0.5975	0.6640	0.6935	0.6935	0.6640	0.5975	0.4
70	0.1300	0.2653	0.4256	0.4645	0.4771	0.4771	0.4645	0.4256	0.2
80	0.0100	0.1137	0.2089	0.2333	0.2388	0.2388	0.2333	0.2089	0.1
90	0	0	0	0	0	0	0	0	0

Thermal (Polynomial Heat Loss) Model

5

Steam Temperature Adjustment

0.0000

0.6720

0.002556

0.0000

0.0000

Wind Velocity Adjustment

1.0000

0.0000

0.0000

0.0000

0.0000

C0

C1 (W/(m-K))

C2 (W/(m-K)²)

C3 (W/(m-K)³)

C4 (W/(m-K)⁴)

C0

C1 (1/(m/s))

C2 (1/(m/s)²)

C3 (1/(m/s)³)

C4 (1/(m/s)⁴)

Estimated Field Design and Performance

6

No of loops

0

Daily Field Steam Rate (bb/d)

0

Field Design Output (MWt)

0

Daily Steam Temperature (F)

0

Avg Optical efficiency

0

Actual Saturation Pressure

0

Start Simulation

Figure F.2 Schematic map of the solar tab of the CSSI screening tool graphical user interface

1. Select location weather file
2. Select solar field design option
3. Enter design parameters, collector and receiver parameters
4. Select optical characterization method based on solar position or incidence angles
5. Input receiver design constants
6. Start solar performance simulation

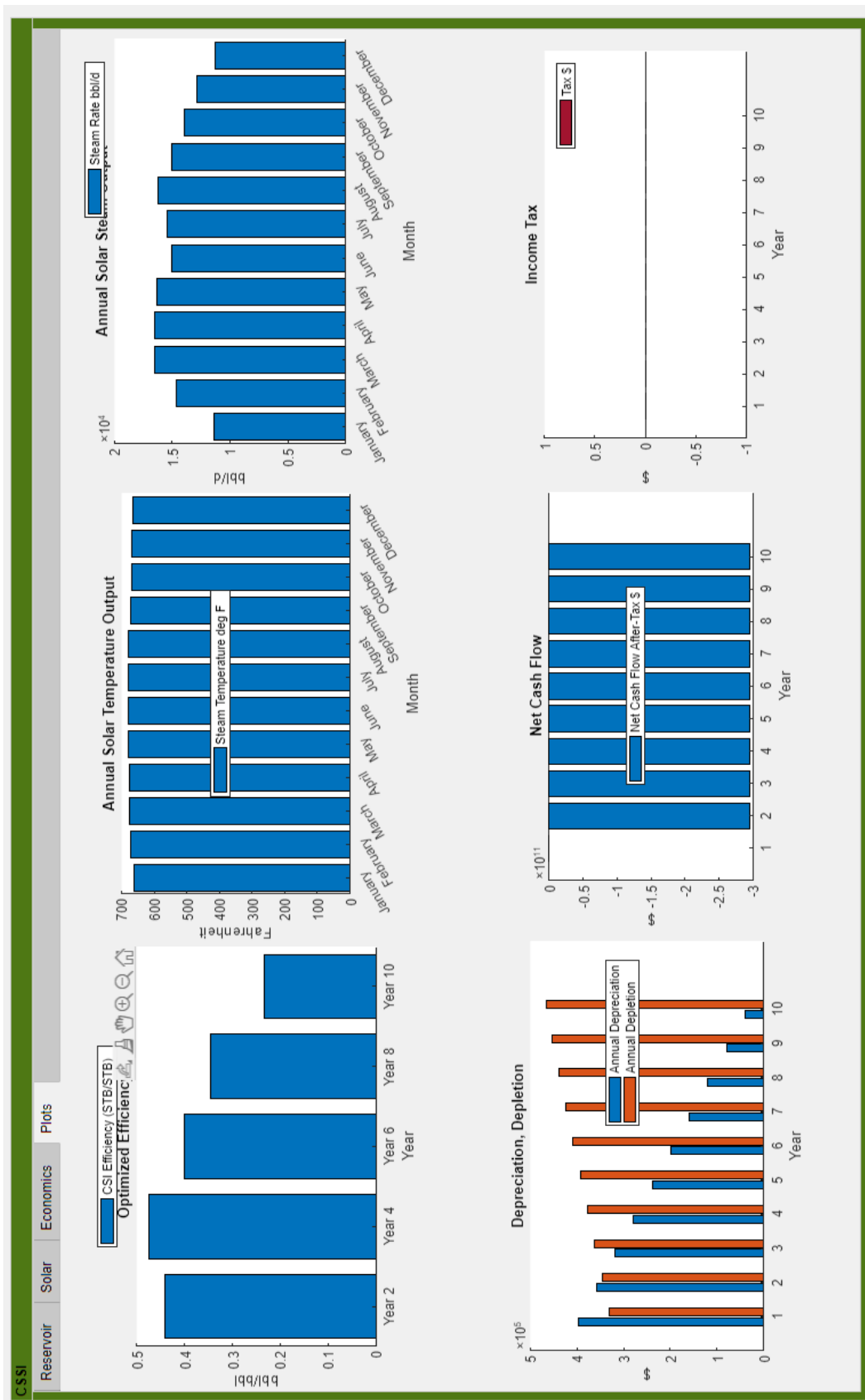


Figure F.4 Layout and plot options of the CSSI screening tool graphical user interface plot tab